

See discussions, stats, and author profiles for this publication at: <https://www.researchgate.net/publication/287498676>

The Western Pansky Tundra layered intrusion, Kola Peninsula: Differentiation mechanism and solidification sequence

Article in *Petrology* · May 2001

CITATIONS

3

READS

57

4 authors, including:



Rais Latypov

University of the Witwatersrand

107 PUBLICATIONS 1,008 CITATIONS

[SEE PROFILE](#)



Vladimir Skiba

Kola Science Centre

26 PUBLICATIONS 126 CITATIONS

[SEE PROFILE](#)

Some of the authors of this publication are also working on these related projects:



Integrated geoscience: cutting edge techniques for understanding complex 3D geological features [View project](#)



Growth of heavily doped LiNbO₃||Zn|| crystals [View project](#)

The Western Pansky Tundra Layered Intrusion, Kola Peninsula: Differentiation Mechanism and Solidification Sequence

R. M. Latypov*, 1, F. P. Mitrofanov*, V. I. Skiba*, and T. T. Alapieti**

* Geological Institute, Kola Research Center, Russian Academy of Sciences,
ul. Fersmana 14, Apatity, Murmansk oblast, 184200 Russia

** Institute of Geosciences, University of Oulu, FIN-90014, Finland

Received October 10, 2000

Abstract—Hypotheses of the genesis of the Western Pansky Tundra layered intrusion differ in the interpretation of some key problems in the petrology of the pluton. These include: (1) whether the pluton is an individual geologic body or a part of the larger Pansky and Fedorovo-Pansky massifs; (2) whether it is a mono- or polyphase pluton; (3) what is the crystallization trend of the parental melt; (4) which processes were responsible for the development of the two critical zones of the intrusion, the Lower and the Upper Layered Unit (LLU and ULU, respectively); and (5) whether the magnetite gabbro is a foreign or syngenetic rock. Based on the analysis of preexisting data, a model was proposed for the evolution of the Western Pansky Tundra intrusion as an individual pluton. The massif is proved to consist of two intrusive phases, the first of which comprises the lower, gabbronorite portion of the massif, from its bottom to the Upper Layered Unit, and the other extends from the Upper Layered Unit to the overlying gabbronorite. The parental melt of the first intrusive phase corresponded to unsaturated tholeiite ($an^L = 65\%$, $f^L = 23\%$). The crystallization of this phase proceeded from bottom to top and, later, when the chamber was divided into a series of smaller reservoirs (subchambers), from their walls to centers. The genesis of the Lower Layered Unit is related to a temporary opening of the chamber and its replenishment with batches of melt whose composition was close to that of the parental magma. The differentiation trend of the parental melt of the first intrusive phase was characterized by the following crystallization succession of minerals: $Pl + Opx$ (norite) \longrightarrow $Pl + Opx + Cpx$ (gabbronorite) \longrightarrow $Pl + Cpx + Opx + Pig$ (gabbronorite with inverted pigeonite) \longrightarrow $Pl + Cpx + Opx + Pig + Mgt$ (magnetite gabbro with inverted pigeonite). The second intrusive phase was produced by a later voluminous melt portion, whose composition was less evolved than that of phase I ($an^L = 75\%$, $f^L = 19\%$). The crystallization of the original melt of phase II started with the coticitic assemblage $Pl + Opx + Cpx$ (gabbronorite). Later, brief disturbances of the differentiation trend occurred at the level of olivine-bearing beds within the Upper Layered Unit because of the injection of melt batches of olivine tholeiite composition. The crystallization succession in these beds was generally as follows: $Pl (\pm Ol)$ (olivine leucogabbro) \longrightarrow $Pl + Ol$ (troctolite) \longrightarrow $Pl + Ol + Opx$ (olivine norite) \longrightarrow $Pl + Opx$ (norite) \longrightarrow $Pl + Opx + Cpx$ (gabbronorite).

INTRODUCTION

The Western Pansky Tundra intrusion is the first massif in Russia determined to contain a number of levels of platiniferous low-sulfide ores, which are in many respects similar to the well-known Merensky and J-M reefs of the Bushveld and Stillwater complexes (Balabonin *et al.*, 1994). The discovery of platiniferous reefs stimulated the active study of various genetic aspects of the intrusion (Krivenko *et al.*, 1989; Abzalov *et al.*, 1993; Mitrofanov *et al.*, 1994; Dokuchaeva, 1994; Korchagin *et al.*, 1994; Orsoev *et al.*, 1997; Latypov, 1994, 1995; Turchenko *et al.*, 1998). Progress was achieved along many research avenues, for example, in PGE mineralogy (Balabonin *et al.*, 1994; Halkoaho *et al.*, 1998). At the same time, the principal petrological problem of the genetic sequence and differentiation mechanism of the intrusion remained explored much

more poorly. However, any attempts to gain insight into the genesis of PGE mineralization can hardly be successive without the resolution of this pivoting problem.

The main difficulty faced by the researchers is the extremely complicated patterns of the cryptic compositional variations of cumulus minerals over the pluton cross section (Borisova *et al.*, 1999). In contrast to other known layered mafite-ultramafite massifs, the Western Pansky Tundra intrusion exhibits no usual evolutionary trend of mineral chemistry either from its bottom to top or from the walls to center of the pluton. Its cryptic layering is of complicated, sinusoidal character with a few well pronounced maxima and minima. The interpretation of such patterns of the cryptic compositional variations of minerals is a challenging task, and, thus, it is little wonder that as many as five principally different hypotheses were proposed as yet for the genesis of the intrusion (Proskuryakov, 1967; Odintsov, 1971; Kozlov, 1973; Dokuchaeva, 1994; Borisova *et al.*, 1999).

¹ Present address: Institute of Geosciences, University of Oulu, P.O. Box 3000, FIN-90014, Finland; e-mail: Rais.Latypov@oulu.fi.

The comparative analysis of these hypotheses led us to outline the most obscure issues in the genesis of the intrusion, which we will critically revise within the guidelines of our new model for the genesis of the Western Pansky Tundra intrusion. Our model is based mainly on the results of our earlier investigations into a broad range of petrologic problems pertaining to the intrusion (Latypov *et al.*, 1999a, 1999b; Latypov and Chistyakova, 2001a, 2001b). This study is a logical completion of a cycle of earlier publications devoted to the Western Pansky Tundra intrusion.

OVERVIEW OF THE GEOLOGIC SETTING AND INNER STRUCTURE OF THE INTRUSION

According to the currently dominating concepts (Dokuchaeva, 1994), the Western Pansky Tundra intrusion is a part of the larger Fedorovo-Pansky Massif, which is exposed at the modern erosion level in the form of a series of large blocks (Fig. 1). The largest of them are the Fedorovo and the Western and Eastern Pansky Tundra blocks (listed in order of their occurrence from west to east). The Western Pansky Tundra intrusion extends northwestward for more than 25 km, is cropped out over an area of approximately 80 km², and dips south-southwest at angles of 30°–35°. The true thickness of the intrusion is 3–4 km. Its structural-tectonic setting is controlled by a junction zone between two large geologic structures of different ages: the Archean Keivy geoblock and the Early Proterozoic Imandra–Varzuga zone. The contacts between the intrusion and the volcano-sedimentary complex of the Imandra–Varzuga zone are obscured by younger tectonic motions and profound rock transformations in both the massif itself and the structurally higher Imandra–Varzuga zone. Structurally, the massif cuts, at an acute angle, the primary structural elements of the volcano-sedimentary rocks of the Kuksha and Seidorechka suites of the Strelna Formation. At its northern contact, the intrusion is bounded over a large distance by the White Tundra alkaline granites (Batieva, 1976). The U–Pb zircon age of the gabbronorite was assayed at 2491 ± 1.5 Ma (Bayanova *et al.*, 1994) and 2501.5 ± 1.4 (Amelin *et al.*, 1995), the anorthosite was dated at 2449 ± 12 Ma (Bayanova *et al.*, 1995), and the ϵ_{Nd} (2487 ± 51) of the intrusion equals –2.1 ± 0.5 (Balashov *et al.*, 1993).

The Western Pansky Tundra intrusion is generally characterized by a relatively simple geologic structure (Figs. 1, 2) and is dominated (90–95%) by rocks of gabbronorite composition, which vary in their proportions of rock-forming minerals, textures, and structures. The cross section of the pluton begins with a zone of taxitic gabbronorite (50–60 m) with abundant mafic pegmatoid segregations and xenoliths of the variably assimilated host gneisses. The unit is overlain by a norite zone (40–50 m), which mostly consists of norite (*Pl*–*Opx* cumulates) with subordinate amounts of plagioclase pyroxenite (*Opx* cumulates with inter-

cumulus *Pl*).² Layers of the latter rocks contain chromite mineralization in the form of small accessory grains of aluminochromite–subferrialuminochromite (Dokuchaeva, 1994). Structurally upward, the chromite zone grades into a gabbronorite zone, which is the thickest in the massif (ca. 3000–4000 m) and predominantly consists of gabbronorite (*Pl*–*Opx*–*Cpx* cumulates) with varying grain sizes, structures, and the qualitative proportions of cumulus minerals. The lower and upper portions of this zone (Fig. 1) are made up of gabbronorite with a pronounced trachytoid structure, whereas its central part is dominated by massive gabbronorite (Kozlov, 1973).

The central part of the gabbronorite zone abounds in magnetite gabbro (*Pl*–*Cpx*–*Opx*–*Pig#*–*Mgt* cumulates), which occurs as layers and lenticular bodies from 20 to 100 m thick and from a few meters to 10 km long. Bodies of magnetite gabbro are grouped at three stratigraphic levels: lower, intermediate, and upper. The surrounding gabbronorite (*Pl*–*Cpx*–*Opx* cumulates) commonly grades into bodies of magnetite gabbro with inverted pigeonite (*Pl*–*Cpx*–*Opx*–*Pig#*–*Mgt* cumulates) through a zone of gabbronorite with inverted pigeonite (*Pl*–*Cpx*–*Opx*–*Pig#* cumulates; Latypov and Chistyakova, 2001a, 2001b).

The relatively monotonous succession of the gabbronorite zone includes two clearly pronounced layered units: upper and lower. The Lower Layered Unit (LLU; 50–100 m thick) visibly differs from the monotonous massive gabbronorite by contrasting intercalations of complementary leucocratic and melanocratic rocks. The former are leucogabbro (*Pl* cumulates with two intercumulus pyroxenes) and anorthosite (*Pl* cumulate), and the latter are gabbronorite, norite, and pyroxenite. The Upper Layered Unit (ULU, 250–300 m thick) differs from the gabbronorite mainly by the appearance of various olivine-bearing rocks. The Upper Layered Unit is subdivided into three subunits of finely layered rocks separated by zones of massive gabbronorite. Subunit I consists of anorthosite and gabbronorite, subunit II is made up of olivine norite (*Pl*–*Ol*–*Opx* cumulates) and gabbronorite (*Pl*–*Cpx*–*Opx*–*Ol* cumulates), olivine leucogabbronorite (*Pl*–cumulate with intercumulus *Ol*, *Cpx*, and *Opx*), anorthosite, and gabronorite; and subunit III comprises troctolite (*Pl*–*Ol* cumulates), anorthosite, and gabbronorite. The Lower Layered and Upper Layered units contain reefs of PGE-enriched low-sulfide mineralization (Balabonin *et al.*, 1994).

² The following abbreviations are used in the text, in tables, and figures: *Pl*—plagioclase, *Ol*—olivine, *Opx*—orthopyroxene, *Cpx*—clinopyroxene, *Pig*—pigeonite, *Pig#*—inverted pigeonite, *Mgt*—magnetite, *Crt*—chromite, *Qz*—quartz, *Am*—amphibole, *Fo*—forsterite, *Fa*—fayalite, *Or*—orthoclase, *Ab*—albite, *An*—anorthite, *Spl*—spinel, *Ap*—apatite, *Ilm*—ilmenite, *Pr*—pyrite, *L*—melt, rock—solid rock, $an^L = 100 \times An/(An + Ab)$ for the normative plagioclase composition in melt, $f^L = Fe/(Fe + Mg)$ for melt iron fraction.

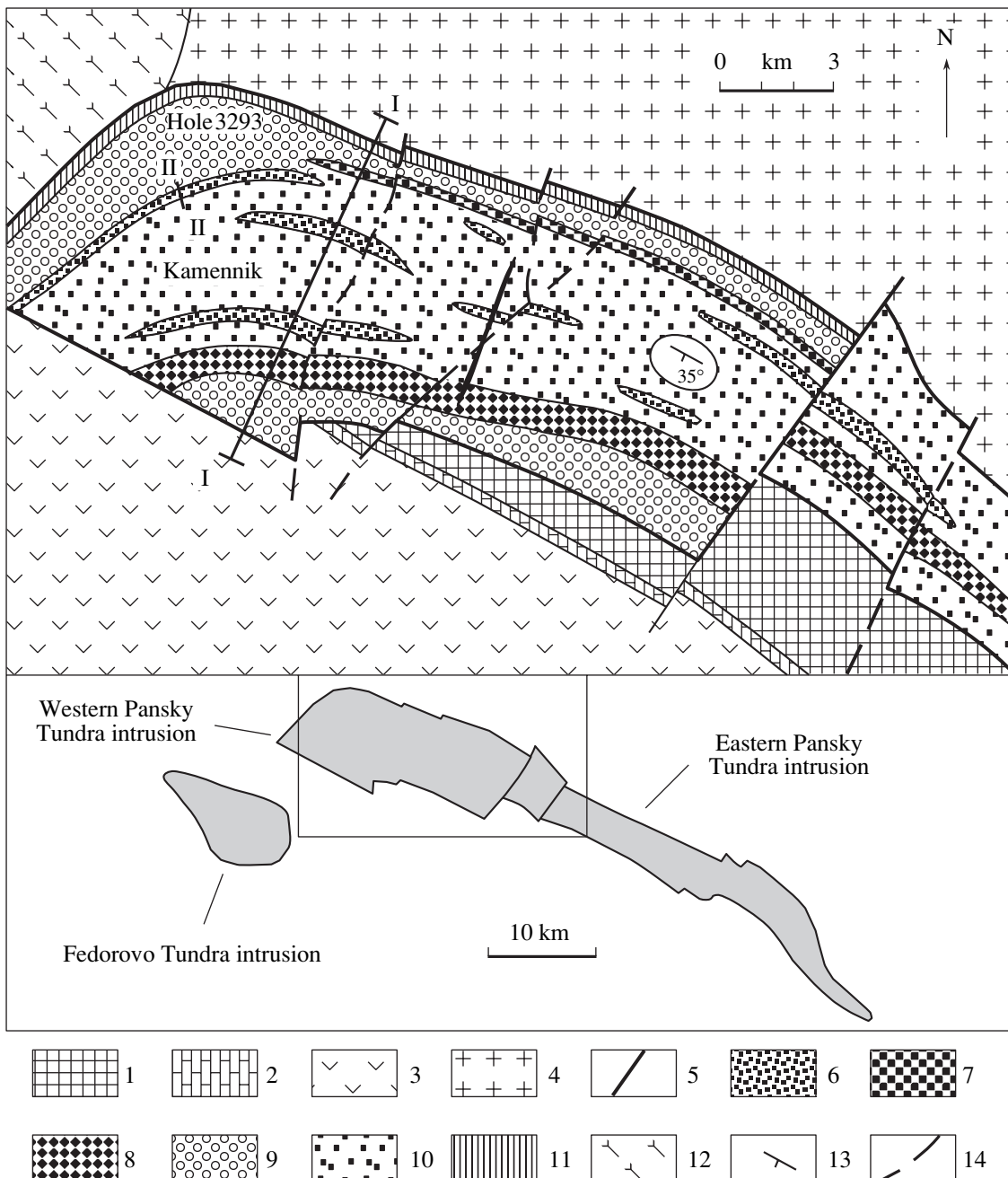


Fig. 1. Schematic geological map of the Early Proterozoic Western Pansky Tundra intrusion (simplified after Odinets, 1971). (1–3) Lower Proterozoic volcano-sedimentary rocks of the Strelna Formation: (1) metaandesite, Seidorechka suite, (2) quartzite, Seidorechka suite, (3) metabasalts, Kuksha suite; (4) White Tundra alkaline granite; (5) gabbro-dolerite and quartz dolerite dikes; (6–11) intrusion: (6) magnetite gabbro, (7) Lower Layered Unit; (8) Upper Layered Unit; (9) trachytoid rocks of the gabbronorite zone; (10) massive rocks of the gabbronorite zone; (11) rocks of the norite zone; (12) Archean granitoids, Keivy block; (13) layering and its dip angle; (14) faults. Line I–I shows the position of a profile across the intrusion (see Figs. 2, 3, and 5), II–II profile across magnetite gabbro (see Fig. 4).

DIFFERENTIATION MECHANISM AND SOLIDIFICATION SEQUENCE OF THE WESTERN PANSKY TUNDRA INTRUSION

In order to explain the genesis of the Western Pansky Tundra intrusion, five models were proposed

(Proskuryakov, 1967; Odinets, 1971; Kozlov, 1973; Dokuchaev, 1994; Borisova *et al.*, 1999). They were developed in different years and are distinct in several principal points, which are summarized in Table 1. The most important problems remaining unresolved as yet include: (1) whether the massif is an individual geo-

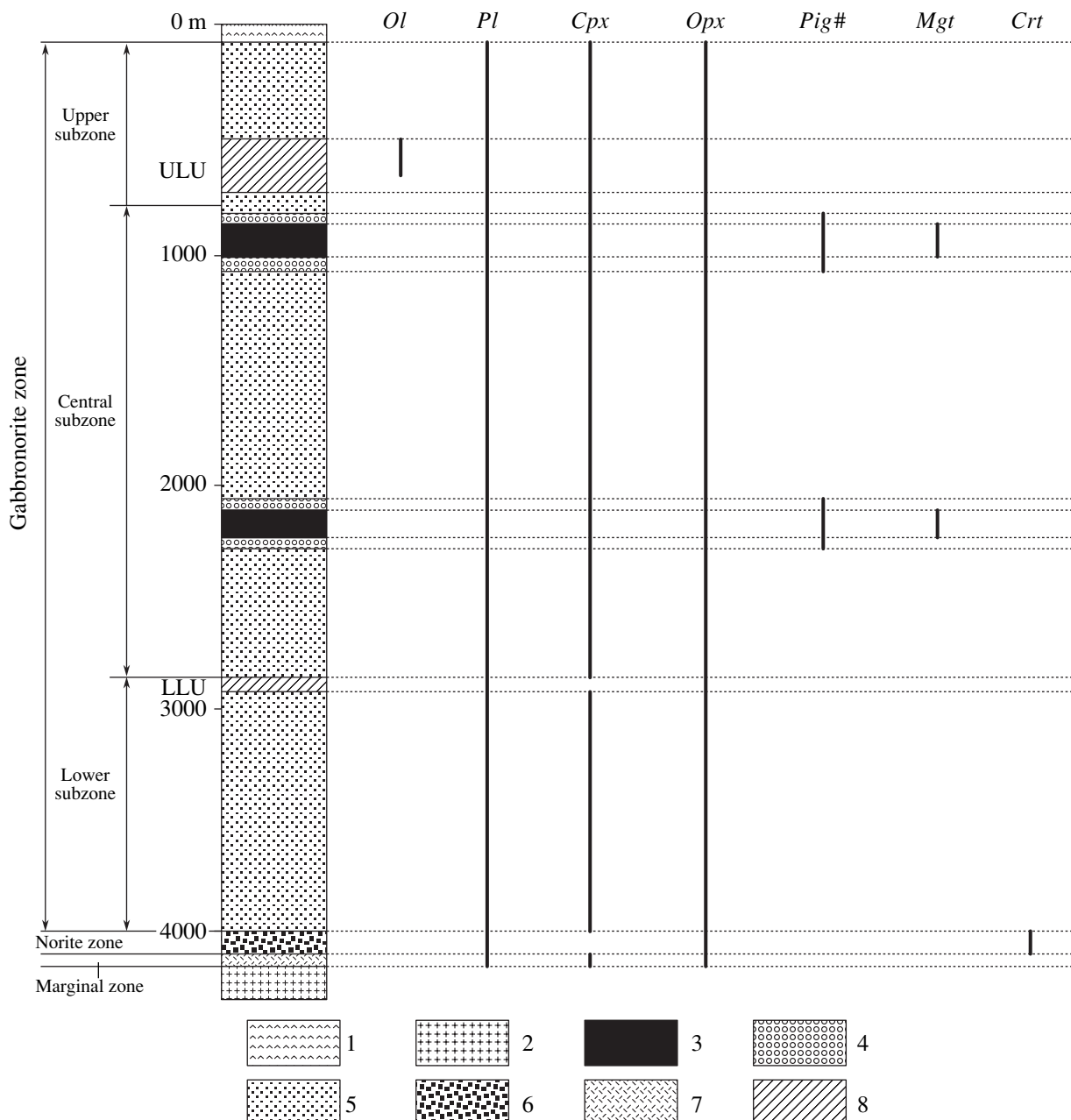


Fig. 2. Stratigraphic column for the Western Pansky Tundra intrusion (line I–I in Fig. 1) with intervals containing cumulus phases. (1) Volcano-sedimentary rocks of the Imandra–Varzuga zone; (2) Archean gneisses and granitoids of the Keivy block; (3–8) rocks of the intrusion: (3) magnetite gabbro with inverted pigeonite ($Pl-Cpx-Opx-Pig\#-Mgt$ cumulates), (4) gabbronorite with inverted pigeonite ($Pl-Cpx-Opx-Pig\#$ cumulates), (5) gabbronorite ($Pl-Cpx-Opx$ cumulates), (6) norite ($Pl-Opx$ cumulates), (7) taxitic gabbronorite ($Pl-Cpx-Opx$ cumulates), (8) layered units: LLU—Lower Layered Unit, ULU—Upper Layered Unit.

logic body or merely a part of the large Pansky and Fedorovo-Pansky massifs; (2) whether it comprises one or more intrusive phases; (3) what was the solidification sequence of the pluton and in which direction did its solidification front advance; (4) what was the settling succession of minerals during the parental melt crystallization; (5) what are the geneses of the two critical units, the Lower and Upper Layered units; and (6) whether the magnetite gabbro is a foreign or syngenetic

rock. Evidently, a model can be considered feasible only if it is able to provide justified explanations of these problems.

The Western Pansky Tundra Intrusion as an Individual Pluton

Originally, the main argument for combining the Eastern and Western Pansky Tundra intrusions into a

Table 1. Comparative analysis of models proposed to account for the genesis of the Western Pansky Tundra intrusion

| Reference | Status of the intrusion | Number of phases | Solidification succession of the intrusion and the direction of the crystallization front advance | Genesis of layered units | Genesis of magnetic gabbro | Crystallization trend |
|--------------------------------------|------------------------------------|------------------|---|---|---|--|
| Proskuryakov (1967) | Part of the Pansky Massif | One | ULU, LLU, then, volumetric crystallization in the whole chamber | In-chamber differentiation | Residual derivatives | $Pl \rightarrow Pl + Ol \rightarrow Pl + Opx + Cpx \rightarrow Pl + Pig + Cpx + Mgt$ |
| Odinets (1971) | Individual pluton | One | From margins to centers | In-chamber differentiation | Residual derivatives | Not discussed |
| Kozlov (1973) | Individual pluton | Three | Phase I: ULU. Phase II: upper and central portions of the massif, including LLU. Phase III: lower part of the intrusion | ULU is an intrusive phase, LLU was produced by in-chamber differentiation | Residual derivatives | First phase: $Pl \rightarrow Pl + Ol$. Second phase: $Pl + Opx + Cpx \rightarrow Pl + Pig + Cpx + Mgt$. Third phase: $Pl + Opx + Cpx + Qtz(?)$ |
| Dokuchaeva (1994) | Part of the Fedorovo-Pansky Massif | One | Successive, from bottom to top, development of 3 megarythms | In-chamber differentiation | Excluded from the succession without discussion | $Ol + SpI \rightarrow Ol + Opx \rightarrow Opx \rightarrow Opx + Pl \rightarrow Opx + Pl + Cpx \rightarrow Opx + Cpx + Pl + Am + Qtz$ |
| Borisova <i>et al.</i> (1999) | Not discussed | Three | Not discussed | LLU was produced by in-chamber differentiation, and ULU resulted from magma replenishment | Transformed xenoliths of metabasalts | $Pl + Opx \rightarrow Pl + Opx + Cpx$ |
| Latypov and Chistyakova (this paper) | Individual pluton | Two | Phase I: lower and central parts of the intrusion | ULU and LLU resulted from magma replenishment | Residual derivatives | First phase: $Pl + Opx \rightarrow Pl + Opx + Cpx + Pig + Mgt \rightarrow Pl + Opx + Cpx + Pig + Mgt$. Second phase: $Pl + Opx + Cpx \rightarrow Pl + Ol \rightarrow Pl + Ol + Opx \rightarrow Pl + Opx + Cpx$. |

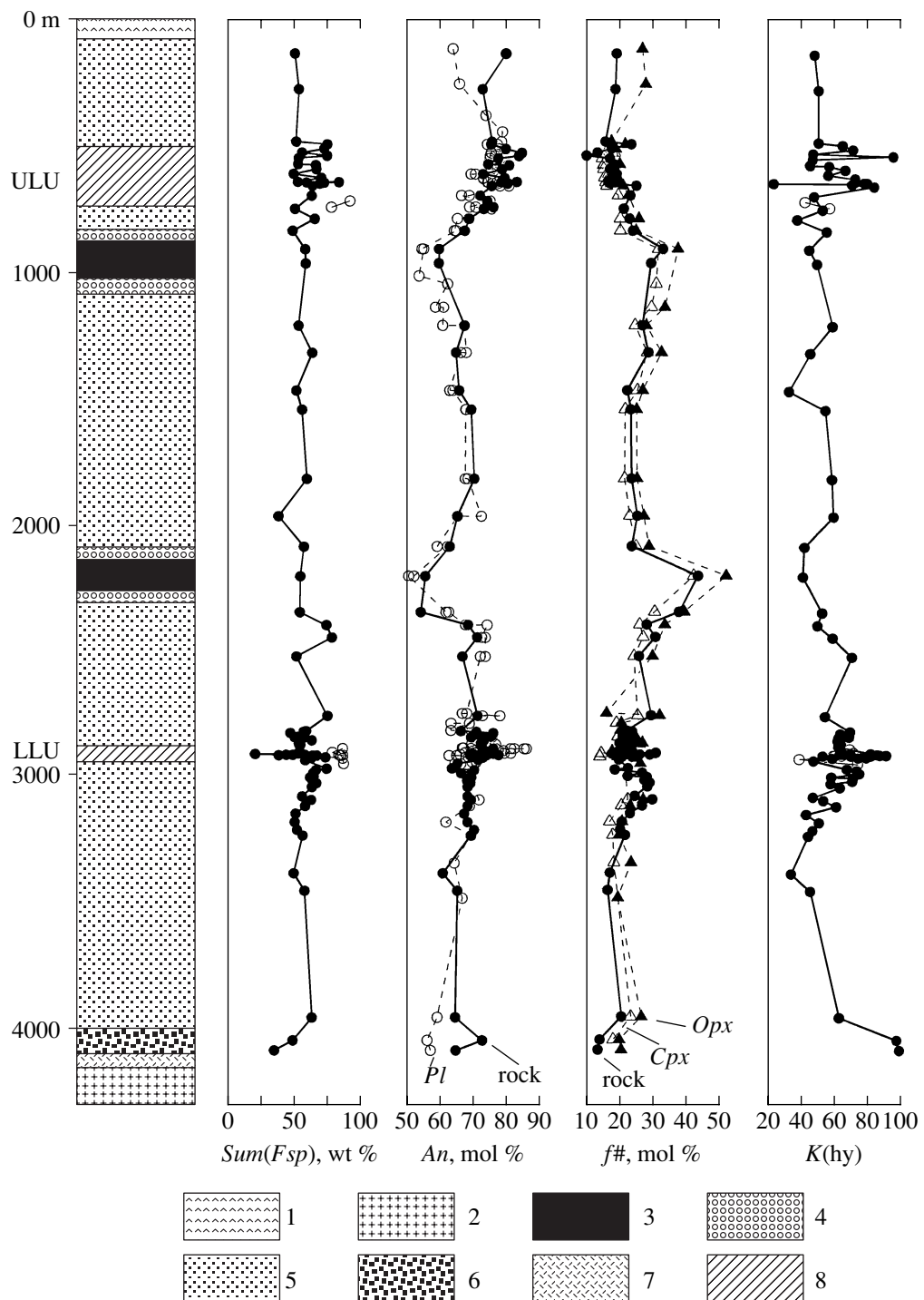


Fig. 3. Compositional variations of rocks and minerals (*Pl*, *Opx*, and *Cpx*) over the vertical section of the intrusion.

See Fig. 1 for the position of line I–I. The gabbronorite zone (which underlies the LLU) and the norite zone are characterized with the use of data on the northwestern part of Mount Kamennik, including Hole 3293 (see Fig. 1).

(1) Volcano-sedimentary rocks of the Imandra–Varzuga zone; (2) Archean granitoids of the Keivy block; (3–8) rocks of the intrusion: (3) magnetite gabbro with inverted pigeonite (*Pl*–*Cpx*–*Opx*–*Pig#*–*Mgt* cumulates), (4) gabbronorite with inverted pigeonite (*Pl*–*Cpx*–*Opx*–*Pig#* cumulates), (5) gabbronorite (*Pl*–*Cpx*–*Opx* cumulates), (6) norite (*Pl*–*Opx* cumulates), (7) taxitic gabbronorite (*Pl*–*Cpx*–*Opx* cumulates), (8) layered units.

$\text{Sum}(Fsp) = \text{Or} + \text{Ab} + \text{An}$, $\text{An} = 100 \times \text{An}/(\text{An} + \text{Ab})$, $f\# = 100 \times \text{Fe}/(\text{Fe} + \text{Mg})$, $K(\text{hy}) = 100 \times \text{Opx}/(\text{Opx} + \text{Cpx})$. Open circles in the $\text{Sum}(Fsp)$ and $K(\text{hy})$ columns show leucogabbro and anorthosite. Data used in the construction of the plot are presented in Tables 2–5. The composition of minerals at various depths are as follows: $\text{An} = 63$, $f\#(\text{Opx}) = 25$ for 112 m; $\text{An} = 65$, $f\#(\text{Opx}) = 27$ for 250 m; $\text{An} = 73$ for 372 m; $\text{An} = 78$ for 435 m; $\text{An} = 53$ for 1000 m; $\text{An} = 58$, $\text{An} = 60.5$, $f\#(\text{Opx}) = 33$; $f\#(\text{Cpx}) = 29$ for 1122 m; $f\#(\text{Opx}) = 20.4$ for 4078 m [borrowed from (Dokuchaeva, 1994; Borisova *et al.*, 1999)].

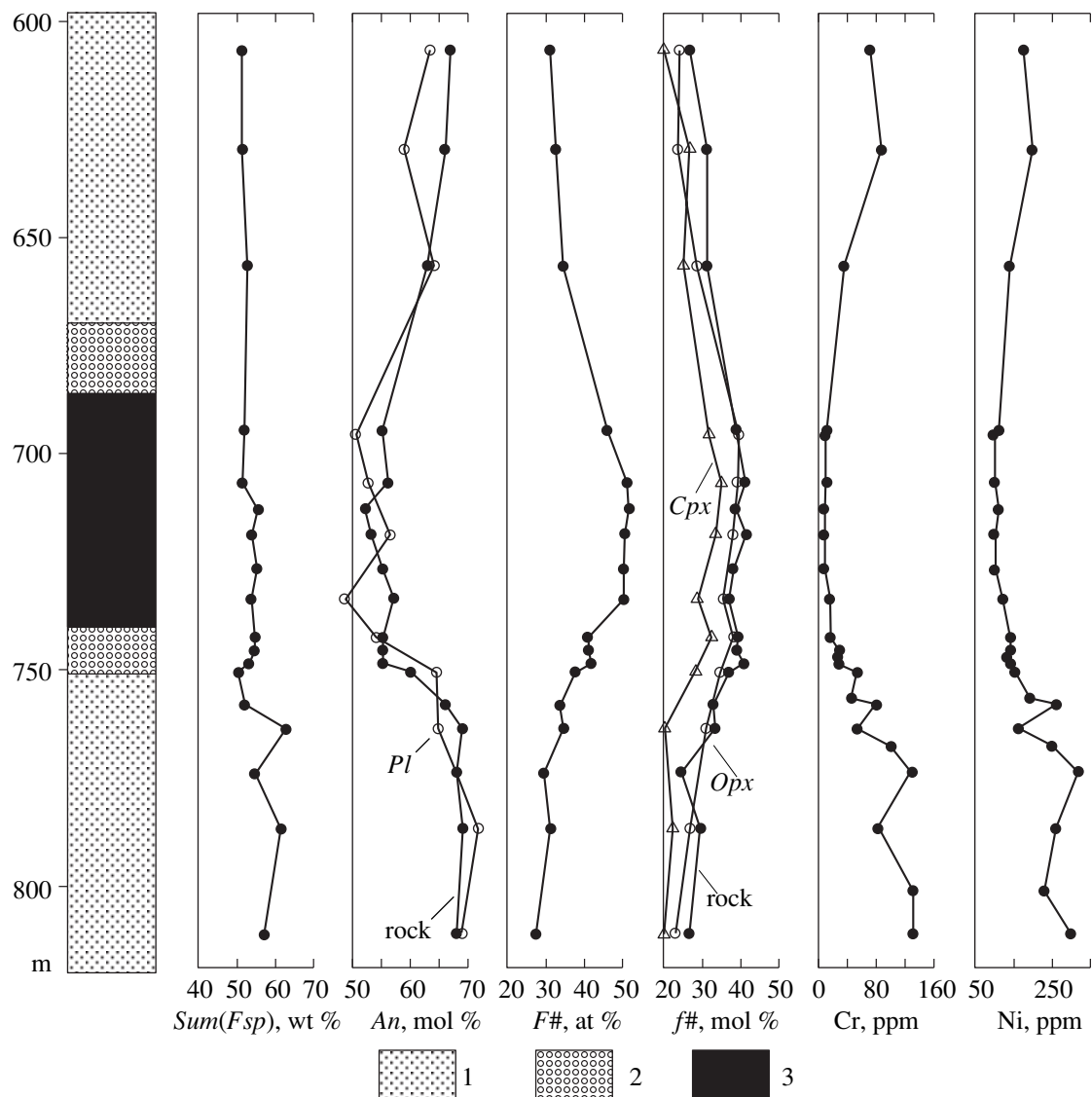


Fig. 4. Compositional variations of rocks and minerals over the vertical section of the magnetite gabbro at the lower level in the northwestern part of Mount Kamennik (Fig. 1, line II-II).

(1) Gabbronorite (*Pl-Cpx-Opx* cumulates); (2) gabbronorite with inverted pigeonite (*Pl-Cpx-Opx-Pig#* cumulates); (3) magnetite gabbro with inverted pigeonite (*Pl-Cpx-Opx-Pig#-Mgt* cumulates).

$\text{Sum}(Fsp) = Ab + Or + An$; $An = 100 \times An/(An + Ab)$; $F\# = 100 \times (\text{Fe}^{2+} + \text{Fe}^{3+})/(\text{Fe}^{2+} + \text{Fe}^{3+} + \text{Mg})$; $f\# = 100 \times Fs/(Fs + En)$.

The plot is based on data from (Latypov and Chistyakova, 2001a).

single body of the Pansky intrusion was the recognition of their “common” olivine unit (Upper Layered Unit) (Proskuryakov, 1967). However, we determined that the Upper Layered Unit, whose thickness attains 200–300 m, includes three subunits of thinly layered rocks. Subunit I is characterized by the presence of anorthosite, subunit II bears olivine norite, olivine leucogabbronorite, and anorthosite, and subunit III contains troctolite and anorthosite (Latypov and Chistyakova, 1999b). The three subunits of ULU are clearly traced throughout the whole massif along its trend, and the 15–20-m-thick troctolite layer, which can be readily discerned in field and rests on the top of

subunit III, serves as a good marker of the upper ULU boundary. No such layers are present in the olivine unit of the Eastern Pansky Tundra intrusion, which contains anorthosite, olivine leucogabbronorite, and troctolite (Proskuryakov, 1967), and its olivine-bearing rocks include only olivine gabbronorite (*Pl-Cpx-Opx-Ol* cumulates). This unit does not display any subunits that can be traced along the strike, and its thickness is normally insignificant (60–70 m). Hence, the olivine units of the two massifs are principally different, cannot be regarded as a “common” unit, and, hence, it seems to be impermissible to combine the two plutons into a single intrusion.

Table 2. Chemical and normative compositions (wt %) of rocks from the Western Pansky Tundra intrusion

| | | p-430* | p-433 | yuk-39 | yuk-40 | yuk-41 | yuk-49a | yuk-48 | yuk-42 | yuk-44 | yuk-43 | yuk-50 | yuk-51 | yuk-31v | yuk-14a | yuk-14v | yuk-45 | yuk-46 | yuk-70 | yuk-47 |
|--------------------------------|--------|--------|--------|--------|--------|--------|---------|--------|--------|--------|--------|--------|--------|---------|---------|---------|--------|--------|--------|--------|
| Com- | ponent | 130** | 270 | 475 | 485 | 502.5 | 518 | 528.5 | 539.5 | 562 | 565.5 | 581 | 600 | 614.5 | 631 | 632 | 633 | 633.5 | 638 | 647 |
| 1 | 2 | 3 | 4 | 5 | 6 | 7 | 8 | 9 | 10 | 11 | 12 | 13 | 14 | 15 | 16 | 17 | 18 | 19 | | |
| SiO ₂ | 50.11 | 51.30 | 51.66 | 50.12 | 45.79 | 42.38 | 43.60 | 51.80 | 51.48 | 50.16 | 49.59 | 52.36 | 49.44 | 46.02 | 47.40 | 47.70 | 43.90 | 47.24 | 50.97 | |
| TiO ₂ | 0.20 | 0.18 | 0.12 | 0.14 | 0.06 | 0.01 | 0.05 | 0.13 | 0.19 | 0.04 | 0.04 | 0.12 | 0.11 | 0.01 | 0.12 | 0.01 | 0.12 | 0.01 | 0.15 | |
| Al ₂ O ₃ | 15.06 | 15.58 | 15.43 | 22.80 | 21.98 | 16.61 | 22.00 | 16.36 | 15.69 | 20.75 | 20.54 | 14.68 | 21.76 | 15.90 | 25.65 | 18.16 | 21.70 | 21.34 | 19.40 | |
| Fe ₂ O ₃ | 0.91 | 1.33 | 1.18 | 0.49 | 1.42 | 2.30 | 2.38 | 0.48 | 1.00 | 0.76 | 0.88 | 0.72 | 1.09 | 1.75 | 1.25 | 1.34 | 1.46 | 1.30 | 0.25 | |
| FeO | 4.83 | 4.79 | 4.16 | 3.54 | 4.28 | 5.48 | 3.17 | 3.98 | 4.37 | 3.56 | 3.68 | 5.04 | 3.64 | 6.05 | 2.98 | 5.34 | 4.88 | 4.36 | 5.62 | |
| MnO | 0.12 | 0.13 | 0.13 | 0.07 | 0.09 | 0.09 | 0.07 | 0.09 | 0.11 | 0.08 | 0.09 | 0.13 | 0.02 | 0.14 | 0.05 | 0.12 | 0.09 | 0.08 | 0.11 | |
| MgO | 10.90 | 10.64 | 11.51 | 6.19 | 10.11 | 17.44 | 11.37 | 10.65 | 10.17 | 8.20 | 9.48 | 11.71 | 8.44 | 15.80 | 5.77 | 14.01 | 10.80 | 10.82 | 9.56 | |
| CaO | 13.92 | 13.18 | 13.50 | 13.10 | 11.73 | 9.98 | 10.88 | 14.25 | 13.79 | 14.01 | 12.78 | 12.39 | 12.80 | 10.10 | 13.06 | 10.40 | 11.62 | 11.9 | 10.78 | |
| Na ₂ O | 1.05 | 1.50 | 1.34 | 2.00 | 1.56 | 0.88 | 1.22 | 1.30 | 1.43 | 1.39 | 1.54 | 1.43 | 1.57 | 0.93 | 1.93 | 1.26 | 1.55 | 1.47 | 1.69 | |
| K ₂ O | 0.15 | 0.20 | 0.06 | 0.14 | 0.09 | 0.08 | 0.44 | 0.05 | 0.08 | 0.07 | 0.09 | 0.07 | 0.10 | 0.08 | 0.15 | 0.07 | 0.12 | 0.08 | 0.11 | |
| H ₂ O ⁻ | 0.03 | 0.10 | 0.20 | 0.20 | 0.49 | 0.44 | 0.38 | 0.17 | 0.22 | 0.17 | 0.23 | 0.21 | 0.25 | 0.46 | 0.27 | 0.25 | 0.34 | 0.25 | 0.21 | |
| LOI | 2.95 | 1.22 | 0.72 | 0.92 | 2.06 | 3.88 | 3.78 | 0.87 | 1.08 | 0.48 | 0.56 | 0.85 | 0.48 | 2.55 | 0.99 | 1.35 | 2.45 | 0.82 | 0.91 | |
| P ₂ O ₅ | | | | | | | | | | | | | | | | | | | | |
| S | Total | 100.23 | 100.15 | 100.01 | 99.71 | 99.66 | 99.57 | 99.34 | 100.13 | 99.61 | 99.67 | 99.50 | 99.71 | 99.70 | 99.79 | 99.62 | 100.01 | 99.03 | 99.74 | 99.76 |
| ap | | | | | | | | | | | | | | | | | | | | |
| <i>Ilm</i> | 0.38 | 0.34 | 0.23 | 0.27 | 0.11 | 0.02 | 0.10 | 0.25 | 0.36 | 0.08 | 0.08 | 0.23 | 0.21 | 0.02 | 0.23 | 0.02 | 0.23 | 0.02 | 0.29 | |
| <i>Mgt</i> | 1.32 | 1.93 | 1.71 | 0.71 | 2.06 | 3.34 | 3.45 | 0.70 | 1.45 | 1.10 | 1.28 | 1.04 | 1.58 | 2.54 | 1.81 | 1.94 | 2.12 | 1.89 | 0.36 | |
| <i>Pr</i> | | | | | | | | | | | | | | | | | | | | |
| <i>Or</i> | 0.89 | 1.18 | 0.35 | 0.83 | 0.54 | 0.48 | 2.60 | 0.30 | 0.47 | 0.41 | 0.54 | 0.41 | 0.59 | 0.44 | 0.89 | 0.41 | 0.71 | 0.46 | 0.65 | |
| <i>ab</i> | 8.88 | 12.69 | 11.33 | 16.91 | 13.19 | 7.44 | 10.32 | 10.99 | 12.09 | 11.76 | 13.02 | 12.09 | 13.28 | 7.87 | 16.32 | 10.66 | 13.11 | 12.43 | 14.29 | |
| <i>an</i> | 35.94 | 35.19 | 35.91 | 52.82 | 52.70 | 41.13 | 53.25 | 38.66 | 36.16 | 50.17 | 48.86 | 33.43 | 52.03 | 38.99 | 60.88 | 43.69 | 51.90 | 51.40 | 45.03 | |
| <i>En</i> | 17.38 | 17.55 | 19.14 | 12.02 | 7.70 | 4.66 | 6.78 | 16.86 | 15.73 | 14.71 | 16.81 | 20.91 | 17.15 | 16.46 | 7.53 | 17.41 | 0.98 | 11.01 | 21.49 | |
| <i>Fs</i> | 5.13 | 5.06 | 4.48 | 4.68 | 2.06 | 0.89 | 0.93 | 4.36 | 4.40 | 4.32 | 4.37 | 6.24 | 4.61 | 4.15 | 2.27 | 4.45 | 0.28 | 2.89 | 9.09 | |
| <i>Di</i> | 21.04 | 19.26 | 20.51 | 7.30 | 3.54 | 5.69 | 0.50 | 20.82 | 20.69 | 12.29 | 9.44 | 17.77 | 7.40 | 7.25 | 2.46 | 5.14 | 3.66 | 5.17 | 4.97 | |
| <i>Hd</i> | 5.41 | 4.84 | 4.19 | 2.47 | 0.83 | 0.95 | 0.06 | 4.70 | 5.05 | 3.14 | 2.14 | 4.63 | 1.73 | 1.59 | 0.65 | 1.14 | 0.92 | 1.18 | 1.83 | |
| <i>Qtz</i> | 0.88 | 0.77 | 1.23 | 0.57 | | | | | 1.45 | 1.91 | 1.03 | 1.89 | | | | | | | 0.63 | |
| <i>Fo</i> | | | | | | | | | | | | | | | | | | | | |
| <i>Fa</i> | | | | | | | | | | | | | | | | | | | | |
| <i>Sum(Fsp)</i> | 47.83 | 50.81 | 49.00 | 72.29 | 69.99 | 53.39 | 72.22 | 50.89 | 50.50 | 63.72 | 64.13 | 47.18 | 67.82 | 50.21 | 81.08 | 56.78 | 70.00 | 66.45 | 61.20 | |
| <i>f#</i> | 18.34 | 18.00 | 15.10 | 22.81 | 16.92 | 12.69 | 9.48 | 16.44 | 17.54 | 18.24 | 16.49 | 18.49 | 16.95 | 16.06 | 18.66 | 16.25 | 17.91 | 16.61 | 24.33 | |
| <i>an(norm)</i> | 79.23 | 72.33 | 74.92 | 74.64 | 79.01 | 83.89 | 82.95 | 76.82 | 73.81 | 80.09 | 77.95 | 72.26 | 78.69 | 82.37 | 77.85 | 79.44 | 78.87 | 79.58 | 74.81 | |
| <i>K(hy)</i> | 45.97 | 48.41 | 48.88 | 63.08 | 69.13 | 45.60 | 93.25 | 45.39 | 43.88 | 55.21 | 64.66 | 54.97 | 70.44 | 69.98 | 75.91 | 77.68 | 21.79 | 68.64 | 81.80 | |

Table 2. (Contd.)

| Component | yuk-55 | yuk-54 | yuk-53 | yuk-52 | yuk-71 | yuk-72 | yuk-73 | yuk-121/5 | yuk-74 | yuk-75 | yuk-76 | yuk-77 | yuk-78 | yuk-79 | yuk-80 | yuk-81 | yuk-82 | yuk-83 | yuk-84 |
|--------------------------------|--------|--------|--------|--------|--------|--------|--------|-----------|--------|--------|--------|--------|--------|--------|--------|--------|--------|--------|--------|
| 685 | 706 | 730 | 737 | 775 | 822 | 894 | 950 | 1194 | 1300 | 1450 | 1525 | 1800 | 1950 | 2072 | 2190 | 2334 | 2384 | 2434 | |
| 20 | 21 | 22 | 23 | 24 | 25 | 26 | 27 | 28 | 29 | 30 | 31 | 32 | 33 | 34 | 35 | 36 | 37 | 38 | |
| SiO ₂ | 51.34 | 50.02 | 49.90 | 51.98 | 52.01 | 52.15 | 50.35 | 51.04 | 51.80 | 51.50 | 52.02 | 51.90 | 51.70 | 50.96 | 52.00 | 47.60 | 53.90 | 52.05 | 50.82 |
| TiO ₂ | 0.12 | 0.14 | 0.12 | 0.20 | 0.18 | 0.37 | 0.49 | 0.18 | 0.18 | 0.20 | 0.28 | 0.16 | 0.18 | 0.26 | 0.23 | 1.36 | 0.38 | 0.29 | 0.25 |
| Al ₂ O ₃ | 18.88 | 28.17 | 23.70 | 14.97 | 19.12 | 14.05 | 15.58 | 15.89 | 15.40 | 18.15 | 14.60 | 16.48 | 17.80 | 10.58 | 16.30 | 13.58 | 14.60 | 21.98 | 23.46 |
| Fe ₂ O ₃ | 0.54 | 0.69 | 0.54 | 0.73 | 0.83 | 0.68 | 3.27 | 2.64 | 0.96 | 1.23 | 1.52 | 0.71 | 0.75 | 2.29 | 1.39 | 5.15 | 0.91 | 0.93 | 0.88 |
| FeO | 4.39 | 1.63 | 3.20 | 5.44 | 3.80 | 6.54 | 7.77 | 6.76 | 6.72 | 5.37 | 5.20 | 5.39 | 5.27 | 8.78 | 5.23 | 11.02 | 8.39 | 3.84 | 3.68 |
| MnO | 0.11 | 0.03 | 0.06 | 0.12 | 0.10 | 0.15 | 0.17 | 0.15 | 0.14 | 0.12 | 0.13 | 0.12 | 0.19 | 0.13 | 0.21 | 0.15 | 0.07 | 0.07 | 0.07 |
| MgO | 7.94 | 1.52 | 4.90 | 10.86 | 6.53 | 11.08 | 7.06 | 7.69 | 9.80 | 6.80 | 8.78 | 9.45 | 9.05 | 12.95 | 8.30 | 5.70 | 7.26 | 4.67 | 4.01 |
| CaO | 13.68 | 14.30 | 13.57 | 12.79 | 13.79 | 12.01 | 11.95 | 11.63 | 11.61 | 12.74 | 14.20 | 12.38 | 12.30 | 10.68 | 13.00 | 11.16 | 10.58 | 12.72 | 12.68 |
| Na ₂ O | 1.90 | 2.59 | 1.99 | 1.44 | 2.18 | 1.69 | 2.43 | 2.44 | 1.85 | 2.38 | 1.84 | 1.83 | 1.90 | 1.36 | 2.26 | 2.36 | 2.60 | 2.51 | 2.40 |
| K ₂ O | 0.14 | 0.21 | 0.32 | 0.09 | 0.18 | 0.08 | 0.05 | 0.09 | 0.10 | 0.12 | 0.18 | 0.10 | 0.14 | 0.09 | 0.12 | 0.14 | 0.31 | 0.23 | 0.27 |
| H ₂ O ⁻ | 0.19 | 0.22 | 0.27 | 0.22 | 0.17 | 0.20 | 0.16 | 0.21 | 0.20 | 0.18 | 0.21 | 0.19 | 0.24 | 0.20 | 0.14 | 0.19 | 0.17 | 0.21 | 0.21 |
| LOI | 0.83 | 0.68 | 1.15 | 0.93 | 0.72 | 0.94 | 0.88 | 1.08 | 0.93 | 0.99 | 1.04 | 0.92 | 0.78 | 1.25 | 0.78 | 1.19 | 1.01 | 0.84 | 0.87 |
| S | | | | | | | <0.01 | | | | | | | | | | | | |
| Total | 100.06 | 100.20 | 99.72 | 99.77 | 99.61 | 99.94 | 100.16 | 99.75 | 99.70 | 99.80 | 99.97 | 99.65 | 100.18 | 99.63 | 99.94 | 99.61 | 100.25 | 100.30 | 99.60 |
| ap | | | | | | | | | | | | | | | | | | | |
| <i>Mgt</i> | 0.23 | 0.27 | 0.23 | 0.34 | 0.70 | 0.93 | 0.34 | 0.38 | 0.53 | 0.38 | 0.34 | 0.30 | 0.34 | 0.49 | 0.44 | 2.58 | 0.72 | 0.55 | 0.48 |
| <i>Mgt</i> | 0.78 | 1.00 | 0.78 | 1.06 | 1.20 | 0.99 | 4.74 | 3.83 | 1.39 | 1.78 | 2.20 | 1.03 | 1.09 | 3.32 | 2.02 | 7.47 | 1.32 | 1.35 | 1.28 |
| <i>Pr</i> | | | | | | | | | | | | | | | | | | | |
| <i>Or</i> | 0.83 | 1.24 | 1.89 | 0.53 | 1.06 | 0.47 | 0.30 | 0.53 | 0.59 | 0.71 | 1.06 | 0.59 | 0.83 | 0.53 | 0.71 | 0.83 | 1.83 | 1.36 | 1.60 |
| <i>ab</i> | 16.07 | 21.90 | 16.83 | 12.18 | 18.44 | 14.29 | 20.55 | 20.64 | 15.65 | 20.13 | 15.56 | 15.48 | 16.07 | 11.50 | 19.11 | 19.96 | 21.99 | 21.23 | 20.30 |
| <i>an</i> | 42.58 | 64.62 | 54.79 | 34.12 | 41.86 | 30.52 | 31.46 | 32.14 | 33.42 | 38.49 | 31.05 | 36.46 | 39.63 | 22.50 | 33.98 | 26.05 | 27.26 | 48.03 | 52.44 |
| <i>En</i> | 12.71 | 2.22 | 8.81 | 18.64 | 8.83 | 19.56 | 10.79 | 12.59 | 17.98 | 10.53 | 10.76 | 16.60 | 6.61 | 23.99 | 12.24 | 8.17 | 12.38 | 7.71 | 7.36 |
| <i>Fs</i> | 4.90 | 1.32 | 3.86 | 6.40 | 3.36 | 7.88 | 6.80 | 6.72 | 8.48 | 5.43 | 3.97 | 6.54 | 6.62 | 10.53 | 4.93 | 8.14 | 9.76 | 3.94 | 4.24 |
| <i>Di</i> | 15.21 | 3.38 | 7.30 | 18.10 | 16.02 | 17.31 | 14.63 | 14.14 | 13.84 | 13.80 | 23.93 | 14.94 | 12.7 | 17.78 | 18.17 | 12.98 | 12.27 | 8.44 | 5.65 |
| <i>Hd</i> | 5.11 | 1.75 | 2.79 | 5.41 | 5.31 | 6.08 | 8.04 | 6.58 | 5.69 | 6.21 | 7.70 | 5.13 | 4.44 | 6.80 | 6.38 | 11.26 | 8.43 | 3.73 | 2.84 |
| <i>Qtz</i> | 0.62 | 1.61 | 1.01 | 1.80 | 2.30 | 1.00 | 0.88 | 1.01 | 1.17 | 1.14 | 1.97 | 1.45 | 0.82 | 0.68 | 0.99 | 0.85 | 3.08 | 2.93 | 2.34 |
| <i>Fo</i> | | | | | | | | | | | | | | | | | | | |
| <i>Fa</i> | | | | | | | | | | | | | | | | | | | |
| <i>Sum(Fsp)</i> | 60.68 | 89.53 | 75.56 | 48.19 | 63.14 | 46.63 | 55.98 | 56.51 | 51.29 | 61.51 | 49.65 | 54.05 | 57.81 | 36.61 | 55.75 | 53.08 | 52.65 | 72.51 | 76.82 |
| <i>f#</i> | 22.62 | 31.09 | 24.97 | 20.68 | 22.41 | 23.44 | 32.37 | 28.87 | 26.41 | 28.20 | 21.94 | 23.07 | 23.28 | 25.04 | 23.45 | 43.10 | 37.50 | 27.97 | 30.46 |
| am(norm) | 71.41 | 73.55 | 75.42 | 72.53 | 68.15 | 66.80 | 59.06 | 66.81 | 64.31 | 65.28 | 68.95 | 70.00 | 64.83 | 62.23 | 55.16 | 53.88 | 68.08 | 70.89 | |
| K(hy) | 46.40 | 40.77 | 55.65 | 51.57 | 36.34 | 53.98 | 43.67 | 48.23 | 57.53 | 44.37 | 31.78 | 53.55 | 57.45 | 41.14 | 40.22 | 51.69 | 48.85 | 57.74 | |

Table 2. (Contd.)

| Component | yuk-85 | yuk-86 | 5v/6.9 | 5v/9.11 | 5v/15 | 18.6a | 5v/28.8 | 5v/43.6 | 5v/56.4 | 5v/61.8 | 5v/65.9 | 5v/76.5 | 5v/91.3 | 5v/95.1 | 5v/95.9 | 5v/96.71 | 5v/97.5 | 5v/99.0B |
|--------------------------------|--------|--------|--------|----------|-------|--------|---------|---------|---------|---------|---------|---------|---------|---------|---------|----------|---------|----------|
| | 2512 | 2750 | 2811.9 | 2814.911 | 2820 | 2823.6 | 2833.8 | 2848.6 | 2861.4 | 2866.8 | 2870.9 | 2881.5 | 2896.3 | 2900.1 | 2900.9 | 2901.71 | 2902.5 | 2904 |
| SiO ₂ | 51.46 | 51.45 | 51.52 | 51.52 | 51.20 | 50.29 | 52.27 | 52.27 | 52.27 | 50.49 | 50.40 | 51.67 | 49.70 | 50.85 | 0.00 | 53.56 | | |
| TiO ₂ | 0.22 | 0.24 | 0.13 | 0.22 | 0.30 | 0.22 | 0.13 | 0.12 | 0.15 | 0.12 | 0.27 | 0.20 | 0.16 | 0.16 | 0.20 | 0.13 | 0.08 | 0.24 |
| Al ₂ O ₃ | 14.88 | 22.68 | 16.93 | 17.00 | 14.27 | 17.00 | 17.16 | 19.18 | 16.10 | 16.53 | 16.19 | 26.74 | 24.18 | 16.47 | 17.59 | 16.24 | 17.34 | 5.81 |
| Fe ₂ O ₃ | 1.22 | 0.62 | 0.67 | 0.87 | 1.06 | 0.87 | 1.09 | 0.83 | 1.06 | 0.95 | 0.98 | 0.95 | 0.80 | 0.82 | 1.01 | 0.66 | 0.62 | 1.86 |
| FeO | 7.33 | 3.76 | 5.61 | 5.92 | 6.36 | 5.92 | 5.35 | 5.41 | 5.25 | 5.27 | 5.42 | 2.53 | 3.85 | 5.82 | 5.96 | 5.59 | 4.76 | 8.80 |
| MnO | 0.16 | 0.07 | 0.12 | 0.11 | 0.14 | 0.11 | 0.13 | 0.10 | 0.11 | 0.10 | 0.11 | 0.04 | 0.07 | 0.14 | 0.11 | 0.11 | 0.10 | 0.21 |
| MgO | 10.98 | 4.52 | 10.54 | 9.90 | 11.16 | 9.90 | 10.39 | 8.57 | 10.77 | 10.22 | 9.52 | 2.05 | 4.16 | 11.79 | 10.10 | 11.12 | 10.25 | 21.02 |
| CaO | 10.12 | 12.90 | 10.28 | 11.05 | 11.30 | 11.05 | 11.56 | 12.37 | 11.64 | 11.70 | 11.39 | 13.39 | 13.09 | 9.90 | 12.10 | 12.04 | 11.94 | 5.59 |
| Na ₂ O | 1.80 | 2.31 | 2.04 | 1.76 | 1.19 | 1.76 | 1.47 | 1.81 | 1.55 | 1.59 | 1.57 | 2.23 | 2.13 | 1.42 | 1.46 | 1.43 | 1.39 | 0.63 |
| K ₂ O | 0.17 | 0.22 | 0.55 | 0.21 | 0.16 | 0.21 | 0.17 | 0.17 | 0.14 | 0.15 | 0.19 | 0.27 | 0.18 | 0.17 | 0.16 | 0.15 | 0.13 | 0.08 |
| H ₂ O ⁻ | 0.19 | 0.18 | 0.18 | 0.18 | 0.15 | 0.16 | 0.20 | 0.20 | 0.20 | 0.20 | 0.16 | 0.18 | 0.20 | 0.23 | 0.30 | 0.19 | 0.29 | |
| LOI | 1.04 | 0.72 | | | 1.00 | 0.84 | 0.84 | 0.63 | 0.68 | 0.97 | 0.62 | 0.46 | 0.99 | 0.84 | 1.36 | 0.72 | 1.38 | |
| P ₂ O ₅ | | | 0.04 | 0.03 | 0.08 | 0.07 | 0.07 | 0.07 | 0.07 | 0.02 | 0.03 | 0.02 | 0.26 | 0.02 | 0.03 | 0.01 | 0.03 | |
| S | | | | | | | | | | | | | | | 0.25 | | | |
| Total | 99.57 | 99.67 | 98.48 | 98.59 | 99.70 | 98.56 | 99.71 | 99.87 | 99.94 | 99.80 | 99.58 | 99.94 | 99.92 | 99.57 | 99.49 | 99.99 | 47.55 | 99.50 |
| ap | | | 0.09 | 0.07 | 0.19 | 0.17 | 0.05 | 0.17 | 0.05 | 0.17 | 0.05 | 0.07 | 0.05 | 0.62 | 0.05 | 0.07 | 0.02 | 0.07 |
| Im | 0.42 | 0.46 | 0.25 | 0.42 | 0.57 | 0.42 | 0.25 | 0.23 | 0.23 | 0.51 | 0.38 | 0.30 | 0.30 | 0.30 | 0.38 | 0.25 | 0.15 | 0.46 |
| Mgt | 1.77 | 0.90 | 0.97 | 1.26 | 1.54 | 1.26 | 1.58 | 1.20 | 1.54 | 1.20 | 1.38 | 1.42 | 1.38 | 1.16 | 1.19 | 1.47 | 0.96 | 2.70 |
| Pr | | | | | | | | | | | | | | | | 0.47 | | |
| Or | 1.00 | 1.30 | 3.25 | 1.24 | 0.95 | 1.24 | 1.00 | 1.00 | 0.83 | 0.89 | 1.12 | 1.60 | 1.06 | 1.00 | 0.95 | 0.89 | 0.77 | 0.47 |
| ab | 15.22 | 19.54 | 17.25 | 14.88 | 10.06 | 14.88 | 12.43 | 15.31 | 13.11 | 13.45 | 13.28 | 18.86 | 18.01 | 12.01 | 12.35 | 12.09 | 11.76 | 5.33 |
| an | 32.02 | 50.87 | 35.42 | 37.87 | 33.12 | 37.87 | 43.71 | 36.56 | 37.53 | 36.57 | 62.16 | 55.89 | 38.06 | 40.97 | 37.45 | 40.69 | 12.79 | |
| En | 22.45 | 7.91 | 18.97 | 20.03 | 21.51 | 19.97 | 20.96 | 15.30 | 20.82 | 19.63 | 18.16 | 4.14 | 8.54 | 26.22 | 18.51 | 21.36 | 20.21 | 47.93 |
| Fs | 10.18 | 4.30 | 7.05 | 8.12 | 8.18 | 8.10 | 7.25 | 6.62 | 6.77 | 6.85 | 6.82 | 2.92 | 5.18 | 8.94 | 6.97 | 7.49 | 6.56 | 13.39 |
| Di | 10.55 | 7.22 | 9.29 | 9.96 | 13.52 | 10.08 | 10.57 | 10.25 | 12.93 | 11.94 | 2.09 | 3.91 | 6.74 | 11.40 | 13.64 | 11.44 | 9.46 | |
| Hd | 4.15 | 3.43 | 3.01 | 3.52 | 4.48 | 3.56 | 3.19 | 3.87 | 3.66 | 3.81 | 1.29 | 2.06 | 2.00 | 3.74 | 4.17 | 3.24 | 2.30 | |
| Qtz | 0.60 | 2.86 | | 1.22 | 4.39 | 1.18 | 1.59 | 2.45 | 2.58 | 4.60 | 4.07 | 2.56 | 1.85 | 0.01 | 0.72 | 97.83 | | |
| Fo | | | 2.07 | | | | | | 0.90 | | | | | | 0.94 | | | |
| Fa | | | 0.85 | | | | | | 0.43 | | | | | | 0.39 | | | |
| Sum(Fsp) | 50.18 | 73.61 | 57.55 | 55.76 | 45.86 | 55.73 | 54.96 | 61.63 | 51.99 | 53.32 | 52.87 | 85.07 | 77.11 | 52.75 | 56.39 | 51.94 | 54.64 | 19.65 |
| f# | 25.64 | 29.29 | 22.05 | 23.58 | 22.45 | 23.58 | 20.84 | 24.78 | 19.84 | 20.98 | 22.23 | 34.96 | 31.55 | 20.60 | 22.27 | 21.07 | 19.81 | 17.53 |
| am(norm) | 66.47 | 71.05 | 66.00 | 71.00 | 76.00 | 75.00 | 73.00 | 72.00 | 72.00 | 76.00 | 75.00 | 75.00 | 76.00 | 74.00 | 77.00 | 74.00 | 76.00 | 69.00 |
| K(hy) | 68.98 | 53.43 | 67.91 | 67.30 | 62.25 | 67.30 | 60.81 | 62.45 | 61.84 | 67.66 | 69.66 | 80.08 | 62.72 | 61.83 | 64.58 | 73.90 | 64.58 | 83.90 |

Table 2. (Contd.)

| Component | 5v/ 101.52 | 5v/ 2906.52 | 5v/ 101.68 | 5v/ 2906.68 | 5v/ 101.86 | 5v/ 2906.86 | 5v/ 102.6 | 5v/ 103.09 | 5v/ 103.33 | 5v/ 103.48 | 5v/ 103.79 | 5v/ 2908.48 | 5v/ 2908.79 | 5v/ 2909 | 5v/ 2916 | 5v/ 2917 | 5v/ 2918 | 5v/ 2920.5 | 5v/ 2927.7 | 5v/ 2941.5 | 5v/ 2961 | 5v/ 156 | 5v/ 122.7 | 5v/ 136.5 | 5v/ 115.5 | 5v/ 122.7 | 5v/ 136.5 | 5v/ 162.1 | | | | |
|--------------------------------|---------------|----------------|---------------|----------------|---------------|----------------|--------------|---------------|---------------|---------------|---------------|----------------|----------------|-------------|-------------|-------------|-------------|---------------|---------------|---------------|-------------|------------|--------------|--------------|--------------|--------------|--------------|--------------|-------|-------|-------|-------|
| SiO ₂ | 51.30 | 49.38 | 49.95 | 48.55 | 49.89 | 53.44 | 47.82 | 47.95 | 51.12 | 52.67 | 51.20 | 51.31 | 51.51 | 50.84 | 51.28 | 50.96 | 50.96 | 51.28 | 50.96 | 51.28 | 50.96 | 50.96 | 51.28 | 50.96 | 51.28 | 50.96 | 51.28 | 50.96 | 51.28 | | | |
| TiO ₂ | 0.11 | 0.16 | 0.17 | 0.15 | 0.16 | 0.25 | 0.10 | 0.15 | 0.16 | 0.20 | 0.12 | 0.19 | 0.14 | 0.08 | 0.23 | 0.16 | 0.16 | 0.23 | 0.16 | 0.23 | 0.16 | 0.16 | 0.23 | 0.16 | 0.23 | 0.16 | 0.16 | 0.23 | 0.16 | 0.15 | | |
| Al ₂ O ₃ | 17.52 | 25.24 | 12.61 | 14.44 | 25.48 | 11.22 | 24.92 | 19.14 | 20.27 | 22.29 | 17.43 | 19.30 | 26.52 | 17.02 | 24.84 | 21.00 | 21.00 | 24.84 | 21.00 | 24.84 | 21.00 | 21.00 | 24.84 | 21.00 | 24.84 | 21.00 | 21.00 | 24.84 | 21.00 | 19.35 | | |
| Fe ₂ O ₃ | 0.61 | 0.36 | 0.78 | 1.93 | 0.38 | 0.52 | 0.97 | 1.08 | 0.64 | 0.34 | 0.59 | 0.45 | 0.67 | 0.67 | 0.67 | 0.61 | 0.19 | 0.92 | 0.92 | 0.92 | 0.92 | 0.92 | 0.92 | 0.92 | 0.92 | 0.92 | 0.92 | 0.92 | 0.92 | 0.92 | 0.92 | 1.66 |
| FeO | 6.06 | 3.38 | 10.00 | 8.77 | 3.27 | 6.85 | 3.88 | 3.58 | 5.31 | 4.83 | 3.98 | 5.76 | 4.15 | 2.07 | 4.31 | 3.04 | 4.03 | 4.03 | 3.04 | 4.31 | 3.04 | 4.03 | 4.03 | 3.04 | 4.03 | 4.03 | 4.03 | 3.84 | 4.03 | 3.84 | | |
| MnO | 0.04 | 0.04 | 0.16 | 0.13 | 0.05 | 0.13 | 0.04 | 0.05 | 0.11 | 0.09 | 0.08 | 0.11 | 0.08 | 0.04 | 0.10 | 0.05 | 0.11 | 0.05 | 0.10 | 0.05 | 0.11 | 0.09 | 0.11 | 0.09 | 0.11 | 0.09 | 0.11 | 0.09 | 0.11 | 0.09 | | |
| MgO | 10.87 | 3.16 | 13.34 | 12.71 | 2.46 | 12.43 | 2.32 | 4.07 | 8.50 | 7.46 | 6.36 | 9.99 | 8.25 | 2.08 | 9.04 | 3.11 | 7.00 | 7.56 | 3.11 | 7.00 | 7.56 | 3.11 | 7.00 | 7.56 | 3.11 | 7.00 | 7.56 | 3.11 | 7.00 | 7.56 | | |
| CaO | 9.76 | 13.42 | 7.14 | 8.22 | 12.50 | 11.89 | 12.90 | 11.83 | 11.46 | 10.69 | 11.66 | 10.59 | 12.64 | 13.99 | 13.02 | 11.06 | 10.53 | 10.75 | 11.06 | 10.53 | 10.75 | 11.06 | 10.53 | 10.75 | 11.06 | 10.53 | 10.75 | 11.06 | 10.53 | 10.75 | | |
| Na ₂ O | 1.62 | 2.46 | 1.35 | 1.11 | 2.81 | 1.25 | 2.27 | 2.52 | 2.02 | 2.09 | 2.25 | 1.86 | 1.85 | 2.63 | 1.69 | 3.00 | 2.79 | 2.02 | 3.00 | 2.79 | 2.02 | 3.00 | 2.79 | 2.02 | 3.00 | 2.79 | 2.02 | 3.00 | 2.79 | 2.02 | | |
| K ₂ O | 0.28 | 0.29 | 0.13 | 0.17 | 0.54 | 0.14 | 0.44 | 0.49 | 0.20 | 0.21 | 0.17 | 0.22 | 0.13 | 0.18 | 0.63 | 1.20 | 0.68 | 0.31 | 1.20 | 0.68 | 0.31 | 1.20 | 0.68 | 0.31 | 1.20 | 0.68 | 0.31 | 1.20 | 0.68 | 0.31 | | |
| H ₂ O ⁻ | 0.33 | 0.26 | 0.28 | 0.17 | 0.29 | 0.17 | 0.29 | 0.22 | 0.17 | 0.17 | 0.12 | 0.14 | 0.23 | 0.31 | 0.36 | 0.36 | 0.18 | 0.18 | 0.36 | 0.36 | 0.18 | 0.36 | 0.36 | 0.18 | 0.36 | 0.36 | 0.18 | 0.36 | 0.36 | 0.18 | | |
| LOI | 0.97 | 1.42 | 0.95 | 1.20 | 1.98 | 1.20 | 1.98 | 1.13 | 0.95 | 1.05 | 0.73 | 0.70 | 1.84 | 2.08 | 2.08 | 2.08 | 1.92 | 1.92 | 2.08 | 2.08 | 1.92 | 2.08 | 2.08 | 1.92 | 2.08 | 2.08 | 1.92 | 2.08 | 2.08 | 1.92 | | |
| P ₂ O ₅ | 0.21 | 0.12 | 0.03 | 0.02 | 0.04 | 0.04 | 0.00 | 0.04 | 0.02 | 0.04 | 0.02 | 0.04 | 0.07 | 0.02 | 0.01 | 0.01 | 0.03 | 0.03 | 0.02 | 0.03 | 0.03 | 0.02 | 0.03 | 0.03 | 0.02 | 0.03 | 0.03 | 0.02 | 0.03 | 0.03 | | |
| S | 0.12 | 0.31 | 2.37 | 0.07 | 0.13 | 1.11 | 0.13 | 0.11 | 0.13 | 0.11 | 0.11 | 0.11 | 0.11 | 0.11 | 0.11 | 0.11 | 0.11 | 0.11 | 0.11 | 0.11 | 0.11 | 0.11 | 0.11 | 0.11 | 0.11 | 0.11 | 0.11 | 0.11 | 0.11 | 0.11 | | |
| Total | 99.68 | 99.69 | 95.66 | 97.43 | 97.58 | 99.53 | 97.93 | 96.69 | 100.03 | 100.01 | 99.94 | 97.93 | 99.60 | 100.04 | 100.10 | 100.08 | 98.23 | 99.77 | 99.77 | 99.77 | 99.77 | 99.77 | 99.77 | 99.77 | 99.77 | 99.77 | 99.77 | 99.77 | 99.77 | 99.77 | 99.77 | 99.77 |
| ap | 0.50 | 0.28 | 0.07 | 0.05 | 0.09 | 0.09 | 0.09 | 0.09 | 0.05 | 0.09 | 0.17 | 0.05 | 0.05 | 0.02 | 0.02 | 0.05 | 0.07 | 0.07 | 0.07 | 0.07 | 0.07 | 0.07 | 0.07 | 0.07 | 0.07 | 0.07 | 0.07 | 0.07 | 0.07 | 0.07 | 0.07 | |
| Im | 0.21 | 0.30 | 0.32 | 0.29 | 0.30 | 0.48 | 0.19 | 0.29 | 0.30 | 0.30 | 0.38 | 0.23 | 0.36 | 0.27 | 0.15 | 0.44 | 0.30 | 0.30 | 0.30 | 0.30 | 0.30 | 0.30 | 0.30 | 0.30 | 0.30 | 0.30 | 0.30 | 0.30 | 0.30 | 0.30 | 0.30 | |
| M _{gt} | 0.88 | 0.52 | 1.13 | 2.80 | 0.55 | 0.75 | 1.41 | 1.57 | 0.93 | 0.49 | 0.86 | 0.86 | 0.65 | 0.97 | 0.97 | 0.88 | 0.88 | 0.88 | 0.88 | 0.88 | 0.88 | 0.88 | 0.88 | 0.88 | 0.88 | 0.88 | 0.88 | 0.88 | 0.88 | 0.88 | 0.88 | |
| Pr | 0.22 | 0.58 | 4.43 | 0.13 | 0.24 | 2.08 | 0.13 | 0.24 | 0.24 | 0.24 | 0.20 | 0.18 | 1.24 | 1.00 | 1.30 | 0.77 | 1.06 | 1.06 | 1.06 | 1.06 | 1.06 | 1.06 | 1.06 | 1.06 | 1.06 | 1.06 | 1.06 | 1.06 | 1.06 | 1.06 | 1.06 | 1.06 |
| Or | 1.65 | 1.71 | 0.77 | 1.00 | 3.19 | 0.83 | 2.60 | 2.89 | 1.18 | 1.24 | 1.00 | 1.30 | 0.77 | 1.06 | 1.06 | 1.06 | 1.06 | 1.06 | 1.06 | 1.06 | 1.06 | 1.06 | 1.06 | 1.06 | 1.06 | 1.06 | 1.06 | 1.06 | 1.06 | 1.06 | 1.06 | |
| ab | 13.70 | 20.80 | 11.42 | 9.39 | 23.76 | 10.57 | 19.20 | 21.31 | 17.08 | 17.68 | 19.03 | 15.73 | 15.65 | 22.24 | 14.29 | 25.37 | 23.60 | 17.08 | 17.08 | 25.37 | 23.60 | 17.08 | 17.08 | 25.37 | 23.60 | 17.08 | 17.08 | 25.37 | 23.60 | 17.08 | | |
| an | 39.71 | 56.97 | 27.97 | 33.92 | 55.32 | 24.59 | 56.51 | 55.27 | 42.57 | 45.31 | 50.22 | 38.56 | 43.98 | 60.03 | 37.00 | 50.77 | 42.77 | 42.77 | 42.77 | 42.77 | 42.77 | 42.77 | 42.77 | 42.77 | 42.77 | 42.77 | 42.77 | 42.77 | 42.77 | 42.77 | 42.77 | 42.77 |
| En | 25.00 | 5.74 | 31.34 | 29.67 | 4.74 | 21.38 | 4.00 | 5.32 | 17.32 | 16.57 | 13.88 | 21.05 | 15.19 | 2.89 | 14.54 | 4.92 | 10.39 | 15.79 | 15.79 | 15.79 | 15.79 | 15.79 | 15.79 | 15.79 | 15.79 | 15.79 | 15.79 | 15.79 | 15.79 | 15.79 | 15.79 | 15.79 |
| F _s | 9.49 | 3.71 | 16.74 | 9.03 | 4.16 | 8.09 | 2.74 | 2.90 | 7.50 | 7.52 | 5.94 | 8.55 | 5.17 | 1.78 | 4.66 | 3.92 | 4.70 | 4.70 | 4.70 | 4.70 | 4.70 | 4.70 | 4.70 | 4.70 | 4.70 | 4.70 | 4.70 | 4.70 | 4.70 | 4.70 | 4.70 | |
| Di | 4.43 | 4.59 | 4.01 | 4.25 | 2.99 | 20.62 | 3.83 | 1.73 | 8.28 | 4.31 | 4.20 | 8.23 | 11.53 | 4.93 | 17.18 | 2.00 | 5.52 | 6.54 | 6.54 | 6.54 | 6.54 | 6.54 | 6.54 | 6.54 | 6.54 | 6.54 | 6.54 | 6.54 | 6.54 | 6.54 | 6.54 | 6.54 |
| Hd | 1.46 | 2.59 | 1.87 | 1.13 | 2.29 | 6.80 | 2.28 | 0.82 | 3.12 | 1.70 | 1.57 | 2.91 | 3.42 | 6.64 | 4.80 | 1.18 | 1.82 | 1.70 | 1.70 | 1.70 | 1.70 | 1.70 | 1.70 | 1.70 | 1.70 | 1.70 | 1.70 | 1.70 | 1.70 | 1.70 | 1.70 | 1.70 |
| Qtz | 1.21 | 0.44 | 0.02 | 2.03 | 0.10 | 3.80 | 1.67 | 0.34 | 3.59 | 1.68 | 0.54 | 1.77 | 2.38 | 0.39 | 1.33 | 3.14 | 3.14 | 3.14 | 3.14 | 3.14 | 3.14 | 3.14 | 3.14 | 3.14 | 3.14 | 3.14 | 3.14 | 3.14 | 3.14 | 3.14 | 3.14 | |
| F _o | | | | | | | | | | | | | | | | | | | | | | | | | | | | | | | | |
| F _a | | | | | | | | | | | | | | | | | | | | | | | | | | | | | | | | |
| No. 3 | 56.96 | 82.32 | 42.65 | 49.01 | 84.36 | 83.88 | 62.46 | 65.59 | 72.04 | 57.39 | 61.96 | 85.07 | 56.96 | 85.82 | 72.96 | 65.05 | 65.05 | 65.05 | 65.05 | 65.05 | 65.05 | 65.05 | 65.05 | 65.05 | 65.05 | 65.05 | 65.05 | 65.05 | 65.05 | 65.05 | 65.05 | |
| f# | 22.41 | 32.95 | 28.89 | 18.80 | 40.04 | 22.36 | 34.22 | 29.33 | 24.78 | 25.66 | 23.60 | 20.56 | 31.91 | 19.61 | 34.05 | 22.32 | 18.46 | 18.46 | 18.46 | 18.46 | 18.46 | 18.46 | 18.46 | 18.46 | 18.46 | 18.46 | 18.46 | 18.46 | 18.46 | 18.46 | 18.46 | 18.46 |
| am(norm) | 73.00 | 72.00 | 70.00 | 77.00 | 69.00 | 74.00 | 71.00 | 70.00 | 71.00 | 70.00 | 73.00 | 72.00 | 71.00 | 72.00 | 71.00 | 72.00 | 71.00 | 72.00 | 71.00 | 72.00 | 71.00 | 72.00 | 71.00 | 72.00 | 71.00 | 72.00 | 71.00 | 72.00 | 71.00 | 72.00 | | |
| K(hy) | 85.41 | 56.80 | 89.10 | 87.80 | 62.72 | 51.80 | 52.46 | 76.30 | 68.52 | 80.02 | 77.46 | 72.66 | 57.65 | 38.19 | 46.63 | 57.65 | 57.65 | 57.65 | 57.65 | 57.65 | 57.65 | 57.65 | 57.65 | 57.65 | 57.65 | 57.65 | 57.65 | 57.65 | 57.65 | 57.65 | 57.65 | |

Table 2. (Contd.)

| Com- | 5v/ 174.9 | 5v/188 | 5v/192 | 5v/ 204.7 | 5v/ 214.3 | 5v/ 230 | 5v/ 230 | ka- 139/20 | ka- 139/21 | ka- 139/22 | ka- 139/23 | ka- 139/25 | ka- 139/28 | ka- 139/29 | ka- 139/31 | 1312/ 4920 | 1350/ 5097 | 3293/ 35 | 3293/ 85.85 | 3293/ 130 |
|--------------------------------|--------------|--------|--------|--------------|--------------|------------|------------|---------------|---------------|---------------|---------------|---------------|---------------|---------------|---------------|---------------|---------------|-------------|----------------|--------------|
| ponent | 2979.9 | 2993 | 2997 | 3009.7 | 3019.3 | 3035 | 3073 | 3086 | 3110.5 | 3141 | 3175 | 3206 | 3228 | 3378 | 3448 | 3948 | 4038 | 4078 | | |
| SiO ₂ | 52.12 | 52.63 | 51.99 | 51.62 | 51.64 | 51.11 | 50.77 | 52.02 | 51.89 | 52.53 | 52.08 | 51.60 | 51.82 | 52.28 | 50.75 | 50.72 | 50.88 | | | |
| TiO ₂ | 0.15 | 0.29 | 0.26 | 0.20 | 0.16 | 0.30 | 0.16 | 0.12 | 0.16 | 0.20 | 0.18 | 0.16 | 0.20 | 0.19 | 0.28 | 0.20 | 0.18 | | | |
| Al ₂ O ₃ | 18.92 | 18.83 | 18.32 | 18.98 | 20.05 | 18.70 | 16.29 | 18.81 | 17.38 | 15.10 | 14.98 | 15.65 | 16.90 | 14.77 | 16.72 | 17.64 | 13.62 | 9.82 | | |
| Fe ₂ O ₃ | 0.49 | 1.69 | 1.07 | 0.62 | 0.37 | 0.36 | 1.01 | 0.26 | 0.13 | 0.30 | 0.70 | 0.48 | 1.00 | 1.09 | 1.98 | 1.40 | 1.52 | | | |
| FeO | 5.58 | 4.25 | 6.03 | 5.81 | 5.08 | 5.73 | 5.58 | 5.40 | 5.84 | 5.38 | 5.30 | 4.87 | 4.70 | 4.20 | 3.79 | 4.88 | 5.38 | 6.99 | | |
| MnO | 0.11 | 0.08 | 0.12 | 0.12 | 0.09 | 0.12 | 0.07 | 0.10 | 0.10 | 0.11 | 0.11 | 0.11 | 0.10 | 0.11 | 0.10 | 0.11 | 0.16 | 0.15 | | |
| MgO | 8.29 | 6.50 | 7.87 | 8.20 | 6.76 | 7.80 | 8.82 | 7.01 | 8.98 | 9.84 | 10.68 | 10.08 | 9.14 | 10.08 | 9.25 | 8.39 | 16.28 | 22.73 | | |
| CaO | 10.62 | 11.49 | 10.84 | 11.17 | 12.57 | 11.75 | 12.96 | 12.60 | 11.83 | 13.63 | 12.66 | 13.30 | 13.70 | 13.63 | 12.79 | 10.71 | 6.29 | 4.45 | | |
| Na ₂ O | 2.33 | 2.06 | 2.01 | 2.19 | 2.23 | 2.14 | 2.23 | 2.04 | 1.99 | 1.71 | 1.66 | 1.86 | 2.17 | 2.12 | 2.25 | 1.21 | 1.25 | | | |
| K ₂ O | 0.21 | 0.21 | 0.20 | 0.20 | 0.16 | 0.18 | 0.20 | 0.14 | 0.14 | 0.14 | 0.17 | 0.14 | 0.17 | 0.19 | 0.24 | 0.47 | 0.99 | 0.25 | | |
| H ₂ O ⁻ | 0.24 | 0.27 | 0.15 | 0.31 | 0.18 | 0.23 | 0.18 | 0.23 | 0.19 | 0.18 | 0.12 | 0.14 | 0.21 | 0.14 | 0.25 | 0.27 | 0.13 | | | |
| LOI | 1.37 | 0.82 | 0.70 | 2.37 | 1.02 | 1.20 | 1.32 | 0.59 | 0.78 | 0.67 | 1.23 | 0.88 | 0.88 | 1.81 | 0.88 | 1.81 | 3.35 | 1.66 | | |
| P ₂ O ₅ | 0.07 | 0.03 | 0.04 | 0.04 | 0.07 | 0.04 | 0.01 | 0.01 | 0.01 | <0.01 | <0.01 | <0.01 | <0.01 | <0.01 | <0.01 | <0.01 | <0.01 | | | |
| S | | | | | | | | | | | | | | | | | | | | |
| Total | 98.89 | 99.67 | 99.84 | 99.15 | 100.03 | 98.23 | 99.78 | 99.75 | 99.85 | 99.78 | 99.81 | 99.78 | 99.81 | 99.67 | 99.62 | 99.61 | 99.59 | 99.87 | 100.01 | |
| ap | 0.17 | 0.07 | 0.09 | 0.09 | 0.17 | 0.09 | 0.02 | 0.02 | 0.02 | 0.02 | 0.02 | 0.02 | 0.02 | 0.02 | 0.34 | 0.30 | 0.36 | 0.53 | 0.38 | |
| Im | 0.29 | 0.55 | 0.49 | 0.38 | 0.30 | 0.57 | 0.30 | 0.30 | 0.23 | 0.30 | 0.38 | 0.30 | 0.38 | 0.30 | 0.38 | 0.38 | 0.38 | 0.34 | | |
| Mgt | 0.71 | 2.45 | 1.55 | 0.90 | 0.54 | 0.52 | 1.47 | 0.38 | 0.19 | 0.44 | 1.02 | 1.02 | 1.02 | 1.02 | 1.46 | 1.46 | 1.58 | 2.03 | 2.20 | |
| Pr | | | | | | | | | | | | | | | | | | | | |
| Or | 1.24 | 1.24 | 1.18 | 1.18 | 0.95 | 1.06 | 1.18 | 0.83 | 0.83 | 0.83 | 1.00 | 0.83 | 1.00 | 1.00 | 1.45 | 1.42 | 2.78 | 5.85 | 1.48 | |
| ab | 19.71 | 17.42 | 17.00 | 18.52 | 18.86 | 18.10 | 15.90 | 17.84 | 16.83 | 15.14 | 14.46 | 14.04 | 15.73 | 18.35 | 17.93 | 19.03 | 10.23 | 10.57 | | |
| an | 40.55 | 41.51 | 40.38 | 41.37 | 44.23 | 40.89 | 35.42 | 41.44 | 38.08 | 32.76 | 32.70 | 34.84 | 37.26 | 30.00 | 35.40 | 36.65 | 28.81 | 20.45 | | |
| En | 17.54 | 11.89 | 16.18 | 16.80 | 12.29 | 14.97 | 14.09 | 12.11 | 16.91 | 14.82 | 17.96 | 16.11 | 14.05 | 11.92 | 14.57 | 16.16 | 36.15 | 39.74 | | |
| Fs | 8.33 | 4.47 | 8.24 | 8.27 | 6.52 | 7.67 | 5.96 | 6.68 | 8.04 | 5.79 | 6.10 | 5.31 | 5.04 | 3.21 | 3.75 | 5.47 | 7.75 | 8.12 | | |
| Di | 6.67 | 9.25 | 7.36 | 7.80 | 9.79 | 9.59 | 16.96 | 11.51 | 11.74 | 20.87 | 18.62 | 19.37 | 18.77 | 24.29 | 18.25 | 10.20 | 1.60 | 1.09 | | |
| Hd | 2.76 | 3.03 | 3.27 | 3.35 | 4.53 | 4.28 | 6.25 | 5.53 | 4.86 | 7.11 | 5.51 | 5.57 | 5.86 | 5.70 | 4.10 | 3.01 | 0.30 | 0.19 | | |
| Qtz | 0.93 | 6.18 | 3.00 | 0.50 | 1.02 | 0.48 | 0.20 | 1.97 | 0.70 | 0.28 | 1.30 | 1.35 | 0.09 | 1.22 | 0.77 | 0.77 | 0.77 | 0.77 | | |
| Fo | | | | | | | | | | | | | | | | | | | | |
| Fa | | | | | | | | | | | | | | | | | | | | |
| Sum(Fsp) | 62.92 | 63.35 | 60.61 | 62.46 | 65.22 | 61.88 | 54.71 | 61.39 | 56.89 | 49.93 | 49.33 | 51.03 | 55.21 | 51.36 | 56.66 | 62.15 | 47.84 | 33.97 | | |
| f# | 26.54 | 22.23 | 27.94 | 27.25 | 28.75 | 28.06 | 24.33 | 29.56 | 26.55 | 22.92 | 20.53 | 20.05 | 21.43 | 17.01 | 20.48 | 20.48 | 14.03 | 13.45 | | |
| an(norm) | 66.00 | 69.00 | 69.00 | 68.00 | 69.00 | 68.00 | 68.00 | 69.00 | 68.00 | 67.00 | 68.00 | 70.00 | 69.00 | 61.00 | 65.00 | 64.00 | 73.00 | 65.00 | | |
| K(hy) | 73.28 | 57.13 | 69.67 | 69.22 | 56.77 | 62.00 | 46.35 | 52.45 | 60.05 | 42.42 | 49.92 | 46.21 | 43.66 | 33.53 | 45.05 | 62.09 | 95.86 | 97.38 | | |

Note: Gabbronite: 1-3, 8, 9, 12, 19, 20, 23-25, 28-34, 36-47, 49, 53-55, 57, 62, 65-69, 71, 73-90; norite: 4, 59, 60, 91, 92; troctolite: 5-7; olivine gabbro: 10, 11, 13; olivine norite: 14, 16, 18; olivine leucogabbro-anorthosite: 15, 17; leucogabbro-anorthosite: 21, 22, 48, 50-52, 58, 61, 63, 64, 70, 72; magnetic gabbro: 26-27, 35; pyroxenite: 56. Sum(Fsp) = Or + ab + an, ar/ar# = 100 × F_{Sp}(Fs + En), K(hy) = 100 × Opx/(Opx + Cpx). Dashes mean not analyzed. All analyses were conducted by atomic adsorption at the Geological Institute, Kola Research Center, Russian Academy of Sciences.

* Sample number, ** Depth, m.

Table 3. Chemical composition (wt %) of plagioclase from rocks of the Western Pansky Tundra intrusion

| Com- ponent | yuk-39* | yuk-40 | yuk-40 | yuk-41 | yuk-41 | yuk-49a | yuk-49a | yuk-48 | yuk-48 | yuk-42 | yuk-42 | yuk-44 | yuk-44 | yuk-43 | yuk-43 | yuk-50 | yuk-50 |
|------------------------------------|---------|------------|---------|---------|-----------|---------|-----------|---------|-----------|-----------|-------------|-------------|-------------|-------------|-------------|------------|------------|
| gn pabC** | n pbCa | n pbCa | t pbCa | t pbCa | t pbCa | t pbCa | t pbCa | t pbCa | t pbCa | gn pabC | gn pabC | gn pabC | gn pabC | gn pabC | gn pabC | ol-gn pabC | ol-gn pabC |
| 475*** | 485 | 485 | 502.5 | 502.5 | 518 | 518 | 528.5 | 528.5 | 539.5 | 539.5 | 562 | 562 | 565.5 | 565.5 | 581 | 581 | |
| $\overline{\text{SiO}_2}$ | 49.46 | 49.24 | 49.58 | 49.11 | 48.57 | 48.50 | 48.90 | 48.92 | 48.74 | 49.34 | 49.60 | 49.75 | 48.85 | 48.75 | 48.53 | 47.94 | |
| $\overline{\text{Al}_2\text{O}_3}$ | 32.99 | 33.08 | 33.05 | 32.78 | 33.51 | 32.29 | 32.10 | 32.37 | 32.25 | 32.04 | 31.96 | 33.16 | 33.61 | 33.27 | 32.35 | 32.20 | |
| FeO | 0.53 | 0.61 | 0.61 | 0.58 | 0.57 | 0.59 | 0.62 | 0.39 | 0.17 | 0.36 | 0.47 | 0.50 | 0.51 | 0.49 | 0.52 | 0.49 | |
| CaO | 15.36 | 15.34 | 15.03 | 15.63 | 15.99 | 15.37 | 15.25 | 15.48 | 15.41 | 15.80 | 15.30 | 15.76 | 15.38 | 15.89 | 14.96 | 16.06 | |
| $\overline{\text{Na}_2\text{O}}$ | 2.38 | 2.50 | 2.92 | 2.47 | 2.35 | 2.80 | 2.74 | 2.92 | 2.70 | 2.54 | 2.88 | 2.67 | 2.55 | 2.15 | 2.76 | 2.47 | |
| $\overline{\text{K}_2\text{O}}$ | 0.07 | 0.15 | 0.12 | 0.14 | 0.10 | 0.12 | 0.17 | 0.04 | 0.04 | 0.09 | 0.07 | 0.10 | 0.13 | 0.14 | 0.10 | 0.06 | |
| Total | 100.79 | 100.92 | 101.30 | 100.70 | 101.08 | 99.67 | 99.78 | 100.17 | 99.49 | 99.77 | 100.02 | 101.78 | 101.42 | 101.12 | 100.79 | 99.15 | |
| Si | 8.967 | 8.931 | 8.958 | 8.935 | 8.814 | 8.928 | 8.984 | 8.957 | 8.988 | 8.961 | 9.032 | 8.927 | 8.971 | 8.845 | 8.861 | 8.956 | |
| Al | 7.050 | 7.071 | 7.038 | 7.030 | 7.168 | 7.005 | 6.951 | 6.979 | 6.985 | 6.944 | 6.896 | 7.035 | 7.033 | 7.173 | 7.128 | 7.037 | |
| Fe | 0.081 | 0.093 | 0.092 | 0.089 | 0.086 | 0.090 | 0.096 | 0.059 | 0.026 | 0.086 | 0.072 | 0.076 | 0.076 | 0.074 | 0.078 | 0.075 | |
| Ca | 2.984 | 2.981 | 2.910 | 3.046 | 3.110 | 3.031 | 3.001 | 3.035 | 3.034 | 3.114 | 3.001 | 3.040 | 2.972 | 3.084 | 3.113 | 2.957 | |
| Na | 0.838 | 0.879 | 1.021 | 0.872 | 0.827 | 1.001 | 0.977 | 1.035 | 0.962 | 0.905 | 1.023 | 0.932 | 0.890 | 0.754 | 0.767 | 0.987 | |
| K | 0.016 | 0.036 | 0.027 | 0.031 | 0.022 | 0.029 | 0.040 | 0.040 | 0.010 | 0.010 | 0.020 | 0.016 | 0.022 | 0.032 | 0.022 | 0.014 | |
| Or | 0.42 | 0.92 | 0.68 | 0.79 | 0.56 | 0.71 | 1.00 | 0.25 | 0.25 | 0.50 | 0.40 | 0.55 | 0.80 | 0.83 | 0.56 | 0.35 | |
| ab | 21.83 | 22.56 | 25.80 | 22.08 | 20.89 | 24.65 | 24.32 | 25.37 | 24.01 | 22.41 | 25.32 | 23.34 | 22.86 | 19.48 | 19.66 | 24.94 | |
| an | 77.75 | 76.51 | 73.52 | 77.13 | 78.56 | 74.64 | 74.69 | 74.39 | 75.74 | 77.10 | 74.28 | 76.11 | 76.34 | 79.69 | 79.78 | 74.71 | |
| Com- ponent | yuk-51 | yuk-51 | yuk-31B | yuk-31B | yuk-31a | yuk-31a | yuk-14a | yuk-14a | yuk-14B | yuk-14B | yuk-45 | yuk-46 | yuk-46 | yuk-70 | yuk-70 | yuk-47 | |
| gn pabC | gn pabC | ol-gn pabC | gn pabC | gn pabC | ol-n pbCa | gn pabC | ol-n pbCa | gn pabC | ol-n pbCa | ol-n pbCa | ol-n pbCoab | ol-n pbCoab | ol-lg pCoab | ol-n pbCoab | ol-n pbCoab | gn pbC | |
| 600 | 600 | 614.5 | 614.5 | 618 | 618 | 631 | 631 | 632 | 632 | 633 | 633 | 633 | 633.5 | 633.5 | 638 | 647 | |
| $\overline{\text{SiO}_2}$ | 50.70 | 51.35 | 48.36 | 48.80 | 48.32 | 49.36 | 49.08 | 49.63 | 48.83 | 48.55 | 49.20 | 49.21 | 48.35 | 48.23 | 48.70 | 49.05 | |
| $\overline{\text{Al}_2\text{O}_3}$ | 31.98 | 31.86 | 32.04 | 32.28 | 31.68 | 32.98 | 32.65 | 33.73 | 33.22 | 32.12 | 31.91 | 33.69 | 33.64 | 33.64 | 31.90 | 31.46 | |
| FeO | 0.42 | 0.47 | 0.51 | 0.40 | 0.55 | 0.48 | 0.58 | 0.58 | 0.63 | 0.40 | 0.60 | 0.47 | 0.59 | 0.59 | 0.63 | 0.51 | |
| CaO | 14.39 | 13.78 | 15.81 | 15.43 | 15.43 | 15.12 | 15.45 | 15.59 | 15.32 | 15.16 | 15.36 | 15.21 | 15.94 | 16.11 | 15.85 | 15.23 | |
| $\overline{\text{Na}_2\text{O}}$ | 3.35 | 3.40 | 2.59 | 2.88 | 3.14 | 2.53 | 2.56 | 2.53 | 2.34 | 3.03 | 2.89 | 2.29 | 2.34 | 2.83 | 2.71 | 2.43 | |
| $\overline{\text{K}_2\text{O}}$ | 0.12 | 0.13 | 0.12 | 0.04 | 0.14 | 0.09 | 0.13 | 0.13 | 0.10 | 0.10 | 0.02 | 0.13 | 0.10 | 0.04 | 0.09 | 0.12 | |
| Total | 100.97 | 100.99 | 99.42 | 99.83 | 99.36 | 99.87 | 100.74 | 101.15 | 101.08 | 99.99 | 100.14 | 99.93 | 100.84 | 100.94 | 99.80 | 99.08 | |
| Si | 9.164 | 9.254 | 8.929 | 8.956 | 8.927 | 9.055 | 8.922 | 8.985 | 8.843 | 8.882 | 9.000 | 9.023 | 8.790 | 8.770 | 8.961 | 9.064 | |
| Al | 6.814 | 6.767 | 6.973 | 6.984 | 6.978 | 6.850 | 7.066 | 6.968 | 7.199 | 7.162 | 6.926 | 6.897 | 7.219 | 7.210 | 6.920 | 6.853 | |
| Fe | 0.064 | 0.071 | 0.790 | 0.061 | 0.084 | 0.073 | 0.087 | 0.088 | 0.087 | 0.096 | 0.061 | 0.091 | 0.072 | 0.090 | 0.970 | 0.078 | |
| Ca | 2.786 | 2.661 | 3.127 | 3.034 | 3.135 | 2.972 | 3.010 | 3.025 | 2.973 | 2.971 | 3.010 | 2.988 | 3.106 | 3.138 | 3.087 | 3.016 | |
| Na | 1.175 | 1.187 | 0.927 | 1.025 | 0.888 | 1.117 | 0.890 | 0.897 | 0.888 | 0.830 | 1.076 | 1.029 | 0.805 | 0.824 | 1.009 | 0.969 | |
| K | 0.027 | 0.030 | 0.270 | 0.010 | 0.032 | 0.022 | 0.029 | 0.031 | 0.024 | 0.023 | 0.005 | 0.029 | 0.024 | 0.024 | 0.020 | 0.029 | |
| Or | 0.68 | 0.77 | 6.24 | 0.25 | 0.79 | 0.54 | 0.74 | 0.78 | 0.62 | 0.60 | 0.12 | 0.72 | 0.61 | 0.20 | 0.49 | 0.72 | |
| ab | 29.46 | 30.61 | 21.44 | 25.19 | 21.90 | 27.17 | 22.65 | 22.86 | 21.71 | 26.30 | 25.43 | 20.46 | 20.76 | 24.51 | 24.14 | 21.98 | |
| an | 69.86 | 68.62 | 72.32 | 74.56 | 77.31 | 72.29 | 76.61 | 76.53 | 77.69 | 73.58 | 73.85 | 78.93 | 79.04 | 75.00 | 75.14 | 77.35 | |

Table 3. (Contd.)

| Com- | yuk-47 | yuk-55 | yuk-54 | yuk-53 | yuk-52 | yuk-51 | yuk-50 | yuk-49 | yuk-48 | yuk-47 | gn pabC | gn pab#mC |
|------------------------------------|-----------|--------|--------|--------|--------|--------|--------|--------|--------|--------|---------|---------|---------|---------|---------|---------|---------|---------|---------|---------|-----------|
| Com- | 647 | 685 | 706 | 730 | 737 | 737 | 737 | 737 | 737 | 737 | an pCab | 894 |
| ponent | | | | | | | | | | | | | | | | | | | | | 894 |
| $\overline{\text{SiO}_2}$ | 48.43 | 49.99 | 50.38 | 50.27 | 51.16 | 50.65 | 49.86 | 50.43 | 50.74 | 51.05 | 52.17 | 52.14 | 54.18 | 54.16 | 54.16 | 54.16 | 54.16 | 54.16 | 54.16 | 54.16 | |
| $\overline{\text{Al}_2\text{O}_3}$ | 33.64 | 30.89 | 30.76 | 33.20 | 33.25 | 32.26 | 33.38 | 32.75 | 32.50 | 30.56 | 30.09 | 29.63 | 28.68 | 28.68 | 28.68 | 28.68 | 28.68 | 28.68 | 28.68 | 28.68 | |
| $\overline{\text{FeO}}$ | 0.59 | 0.38 | 0.68 | 0.41 | 0.41 | 0.29 | 0.10 | 0.32 | 0.39 | 0.55 | 0.58 | 0.67 | 0.61 | 0.76 | 0.68 | 0.68 | 0.68 | 0.68 | 0.68 | 0.68 | |
| $\overline{\text{CaO}}$ | 16.22 | 13.86 | 13.29 | 15.17 | 15.00 | 13.79 | 15.09 | 15.02 | 14.80 | 13.86 | 13.29 | 12.96 | 13.28 | 11.20 | 11.41 | 11.41 | 11.41 | 11.41 | 11.41 | 11.41 | |
| $\overline{\text{Na}_2\text{O}}$ | 2.15 | 3.53 | 3.77 | 2.93 | 2.75 | 3.47 | 3.52 | 2.73 | 3.00 | 3.49 | 3.95 | 3.98 | 4.02 | 5.27 | 5.24 | 5.24 | 5.24 | 5.24 | 5.24 | 5.24 | |
| $\overline{\text{K}_2\text{O}}$ | 0.13 | 0.91 | 0.09 | 0.14 | 0.16 | 0.15 | 0.08 | 0.85 | 0.16 | 0.22 | 0.14 | 0.16 | 0.10 | 0.04 | 0.06 | 0.06 | 0.06 | 0.06 | 0.06 | 0.06 | |
| Total | 101.16 | 98.74 | 98.97 | 102.12 | 101.22 | 101.11 | 102.82 | 100.76 | 101.28 | 99.71 | 99.56 | 100.03 | 99.78 | 100.12 | 99.95 | 99.95 | 99.95 | 99.95 | 99.95 | 99.95 | |
| Si | 8.786 | 9.233 | 9.284 | 8.999 | 8.962 | 9.206 | 9.004 | 9.030 | 9.091 | 9.286 | 9.347 | 9.489 | 9.514 | 9.805 | 9.822 | 9.822 | 9.822 | 9.822 | 9.822 | 9.822 | |
| Al | 7.194 | 6.726 | 6.681 | 7.004 | 7.075 | 6.843 | 6.993 | 6.991 | 6.906 | 6.656 | 6.596 | 6.450 | 6.373 | 6.118 | 6.074 | 6.074 | 6.074 | 6.074 | 6.074 | 6.074 | |
| Fe | 0.089 | 0.059 | 0.104 | 0.062 | 0.062 | 0.044 | 0.015 | 0.048 | 0.058 | 0.084 | 0.088 | 0.101 | 0.093 | 0.115 | 0.103 | 0.103 | 0.103 | 0.103 | 0.103 | 0.103 | |
| Ca | 3.153 | 2.742 | 2.623 | 2.909 | 2.902 | 2.659 | 2.873 | 2.916 | 2.859 | 2.717 | 2.607 | 2.526 | 2.596 | 2.171 | 2.217 | 2.217 | 2.217 | 2.217 | 2.217 | 2.217 | |
| Na | 0.757 | 1.265 | 1.347 | 1.018 | 0.962 | 1.209 | 1.213 | 0.959 | 1.049 | 1.237 | 1.401 | 1.403 | 1.422 | 1.848 | 1.841 | 1.841 | 1.841 | 1.841 | 1.841 | 1.841 | |
| K | 0.030 | 0.021 | 0.020 | 0.032 | 0.032 | 0.036 | 0.033 | 0.017 | 0.020 | 0.036 | 0.050 | 0.032 | 0.038 | 0.024 | 0.009 | 0.013 | 0.013 | 0.013 | 0.013 | 0.013 | |
| Or | 0.76 | 0.52 | 0.50 | 0.81 | 0.92 | 0.85 | 0.41 | 0.51 | 0.91 | 1.25 | 0.79 | 0.96 | 0.59 | 0.22 | 0.32 | 0.32 | 0.32 | 0.32 | 0.32 | 0.32 | |
| ab | 19.21 | 31.41 | 33.76 | 25.71 | 24.67 | 30.99 | 29.56 | 24.62 | 26.60 | 30.89 | 34.68 | 35.37 | 35.18 | 45.88 | 45.22 | 45.22 | 45.22 | 45.22 | 45.22 | 45.22 | |
| an | 80.03 | 68.07 | 65.74 | 73.48 | 74.41 | 68.16 | 70.02 | 74.87 | 72.49 | 67.86 | 64.53 | 63.68 | 64.23 | 53.90 | 54.46 | 54.46 | 54.46 | 54.46 | 54.46 | 54.46 | |
| Com- | yuk-124/3 | yuk-74 | yuk-74 | yuk-75 | yuk-75 | yuk-76 | yuk-76 | yuk-76 | yuk-77 | yuk-77 | yuk-78 | yuk-78 | yuk-79 | yuk-79 | yuk-80 | yuk-80 | yuk-80 | yuk-80 | yuk-80 | yuk-80 | |
| ponent | | | | | | | | | | | | | | | | | | | | | |
| $\overline{\text{SiO}_2}$ | 52.92 | 52.32 | 51.24 | 50.92 | 51.08 | 52.08 | 51.89 | 51.54 | 51.29 | 50.26 | 50.43 | 49.58 | 51.33 | 52.69 | 52.07 | 52.07 | 52.07 | 52.07 | 52.07 | 52.07 | |
| $\overline{\text{Al}_2\text{O}_3}$ | 29.32 | 30.43 | 31.18 | 31.01 | 30.55 | 30.62 | 30.90 | 31.25 | 31.05 | 31.76 | 30.72 | 30.72 | 29.32 | 29.66 | 29.66 | 29.66 | 29.66 | 29.66 | 29.66 | | |
| $\overline{\text{FeO}}$ | 0.76 | 0.53 | 0.62 | 0.40 | 0.23 | 0.11 | 0.55 | 0.43 | 0.59 | 0.56 | 0.50 | 0.53 | 0.53 | 0.70 | 0.59 | 0.59 | 0.59 | 0.59 | 0.59 | 0.59 | |
| $\overline{\text{CaO}}$ | 12.35 | 12.61 | 13.80 | 13.67 | 13.43 | 12.96 | 13.35 | 14.05 | 13.89 | 14.23 | 14.16 | 14.88 | 13.65 | 12.26 | 13.02 | 13.02 | 13.02 | 13.02 | 13.02 | 13.02 | |
| $\overline{\text{Na}_2\text{O}}$ | 4.20 | 4.46 | 3.63 | 3.62 | 3.82 | 4.25 | 3.66 | 3.60 | 3.79 | 3.65 | 3.13 | 4.02 | 4.66 | 4.29 | 4.29 | 4.29 | 4.29 | 4.29 | 4.29 | 4.29 | |
| $\overline{\text{K}_2\text{O}}$ | 0.05 | 0.21 | 0.22 | 0.07 | 0.06 | 0.07 | 0.04 | 0.16 | 0.21 | 0.07 | 0.05 | 0.08 | 0.08 | 0.15 | 0.19 | 0.19 | 0.19 | 0.19 | 0.19 | 0.19 | |
| Total | 99.60 | 99.72 | 99.86 | 100.07 | 99.80 | 100.14 | 100.21 | 100.58 | 100.20 | 99.89 | 99.92 | 100.33 | 99.78 | 99.83 | | | | | | | |
| Si | 2.410 | 9.557 | 9.361 | 9.275 | 9.315 | 9.447 | 9.414 | 9.351 | 9.321 | 9.178 | 9.224 | 9.079 | 9.332 | 9.605 | 9.505 | 9.505 | 9.505 | 9.505 | 9.505 | 9.505 | |
| Al | 1.574 | 6.327 | 6.551 | 6.694 | 6.667 | 6.531 | 6.541 | 6.548 | 6.619 | 6.726 | 6.693 | 6.585 | 6.584 | 6.299 | 6.381 | 6.381 | 6.381 | 6.381 | 6.381 | 6.381 | |
| Fe | 0.029 | 0.114 | 0.082 | 0.095 | 0.061 | 0.034 | 0.016 | 0.084 | 0.066 | 0.091 | 0.086 | 0.076 | 0.081 | 0.106 | 0.090 | 0.090 | 0.090 | 0.090 | 0.090 | 0.090 | |
| Ca | 0.603 | 2.469 | 2.700 | 2.667 | 2.625 | 2.518 | 2.596 | 2.731 | 2.706 | 2.784 | 2.774 | 2.920 | 2.660 | 2.395 | 2.546 | 2.546 | 2.546 | 2.546 | 2.546 | 2.546 | |
| Na | 0.371 | 1.578 | 1.286 | 1.278 | 1.352 | 1.496 | 1.489 | 1.286 | 1.267 | 1.343 | 1.295 | 1.110 | 1.418 | 1.648 | 1.520 | 1.520 | 1.520 | 1.520 | 1.520 | 1.520 | |
| K | 0.003 | 0.048 | 0.052 | 0.015 | 0.014 | 0.017 | 0.010 | 0.037 | 0.048 | 0.017 | 0.011 | 0.018 | 0.017 | 0.034 | 0.045 | 0.045 | 0.045 | 0.045 | 0.045 | 0.045 | |
| Or | 0.31 | 1.17 | 1.29 | 0.38 | 0.35 | 0.42 | 0.4 | 0.91 | 1.19 | 0.41 | 0.27 | 0.44 | 0.42 | 0.83 | 1.09 | 1.09 | 1.09 | 1.09 | 1.09 | 1.09 | |
| ab | 37.97 | 38.53 | 31.85 | 32.27 | 33.88 | 37.11 | 36.36 | 31.72 | 31.51 | 32.41 | 31.74 | 27.42 | 34.63 | 40.42 | 36.97 | 36.97 | 36.97 | 36.97 | 36.97 | 36.97 | |
| an | 61.72 | 60.29 | 66.86 | 67.35 | 65.77 | 62.47 | 63.39 | 67.37 | 67.30 | 67.18 | 67.99 | 72.13 | 64.96 | 58.74 | 61.93 | 61.93 | 61.93 | 61.93 | 61.93 | 61.93 | |

Table 3. (Contd.)

| Com- ponent | yuk-81 | | yuk-81 | | yuk-82 | | yuk-82 | | yuk-83 | | yuk-83 | | yuk-84 | | yuk-84 | | yuk-85 | | yuk-85 | | ma-50 | | yuk-86 | | yuk-86 | | ma-48 | |
|--------------------------------|-----------|---------|---------|---------|---------|---------|---------|---------|---------|---------|---------|---------|---------|---------|---------|---------|---------|---------|---------|---------|---------|---------|---------|---------|---------|---------|-------|--|
| | mg pab#mC | gn pabC | | |
| SiO ₂ | 54.88 | 55.15 | 52.25 | 51.78 | 51.09 | 49.72 | 49.47 | 50.09 | 49.75 | 50.00 | 51.45 | 52.34 | 48.78 | 49.55 | 50.45 | 50.45 | 53.44 | 53.44 | 53.44 | 53.44 | 53.44 | 53.44 | 53.44 | 53.44 | 53.44 | 53.44 | 53.44 | |
| Al ₂ O ₃ | 28.71 | 28.12 | 30.05 | 30.27 | 31.44 | 32.50 | 32.29 | 32.37 | 32.28 | 31.79 | 31.28 | 29.88 | 32.83 | 31.99 | 31.99 | 31.40 | 31.40 | 27.98 | 27.98 | 27.98 | 27.98 | 27.98 | 27.98 | 27.98 | 27.98 | 27.98 | 27.98 | |
| FeO | 0.23 | 0.31 | 0.50 | 0.56 | 0.35 | 0.22 | 0.39 | 0.04 | 0.64 | 0.48 | 0.27 | 0.06 | 0.38 | 0.39 | 0.22 | 0.22 | 0.18 | 0.18 | 0.18 | 0.18 | 0.18 | 0.18 | 0.18 | 0.18 | 0.18 | 0.18 | 0.18 | |
| CaO | 10.93 | 10.53 | 12.90 | 12.85 | 13.95 | 15.07 | 15.24 | 15.18 | 15.00 | 14.84 | 13.65 | 13.45 | 15.78 | 15.09 | 14.56 | 14.56 | 13.13 | 13.13 | 13.13 | 13.13 | 13.13 | 13.13 | 13.13 | 13.13 | 13.13 | 13.13 | | |
| Na ₂ O | 5.59 | 5.74 | 4.32 | 4.26 | 3.69 | 2.92 | 3.18 | 3.03 | 2.95 | 3.16 | 3.53 | 3.72 | 2.48 | 3.08 | 3.65 | 3.65 | 4.15 | 4.15 | 4.15 | 4.15 | 4.15 | 4.15 | 4.15 | 4.15 | 4.15 | 4.15 | 4.15 | |
| K ₂ O | 0.05 | 0.07 | 0.22 | 0.06 | 0.07 | 0.03 | 0.08 | 0.03 | 0.10 | 0.07 | 0.11 | 0.05 | 0.03 | 0.12 | 0.07 | 0.07 | 0.07 | 0.07 | 0.07 | 0.07 | 0.07 | 0.07 | 0.07 | 0.07 | 0.07 | 0.07 | 0.07 | |
| Total | 100.39 | 99.92 | 100.25 | 99.78 | 100.60 | 100.47 | 100.65 | 100.73 | 100.72 | 100.35 | 100.28 | 99.49 | 100.27 | 100.21 | 100.36 | 99.12 | 99.12 | 99.12 | 99.12 | 99.12 | 99.12 | 99.12 | 99.12 | 99.12 | 99.12 | 99.12 | | |
| Si | 9.873 | 9.961 | 9.489 | 9.442 | 9.256 | 9.036 | 9.004 | 9.074 | 9.040 | 9.110 | 2.331 | 2.385 | 8.907 | 9.049 | 2.296 | 2.296 | 2.446 | 2.446 | 2.446 | 2.446 | 2.446 | 2.446 | 2.446 | 2.446 | 2.446 | 2.446 | | |
| Al | 6.089 | 5.986 | 6.433 | 6.507 | 6.714 | 6.962 | 6.910 | 6.914 | 6.828 | 6.828 | 1.671 | 1.604 | 7.066 | 6.886 | 1.684 | 1.684 | 1.510 | 1.510 | 1.510 | 1.510 | 1.510 | 1.510 | 1.510 | 1.510 | 1.510 | 1.510 | | |
| Fe | 0.035 | 0.047 | 0.076 | 0.086 | 0.053 | 0.033 | 0.059 | 0.005 | 0.096 | 0.074 | 0.010 | 0.002 | 0.058 | 0.059 | 0.008 | 0.008 | 0.007 | 0.007 | 0.007 | 0.007 | 0.007 | 0.007 | 0.007 | 0.007 | 0.007 | 0.007 | | |
| Ca | 2.106 | 2.037 | 2.511 | 2.510 | 2.708 | 2.935 | 2.972 | 2.946 | 2.921 | 2.897 | 0.663 | 0.656 | 3.088 | 2.953 | 0.710 | 0.710 | 0.644 | 0.644 | 0.644 | 0.644 | 0.644 | 0.644 | 0.644 | 0.644 | 0.644 | 0.644 | | |
| Na | 1.951 | 2.011 | 1.521 | 1.507 | 1.297 | 1.028 | 1.124 | 1.065 | 1.038 | 1.118 | 0.310 | 0.329 | 0.877 | 1.091 | 0.322 | 0.322 | 0.368 | 0.368 | 0.368 | 0.368 | 0.368 | 0.368 | 0.368 | 0.368 | 0.368 | 0.368 | | |
| K | 0.011 | 0.016 | 0.051 | 0.014 | 0.016 | 0.008 | 0.018 | 0.007 | 0.023 | 0.017 | 0.006 | 0.003 | 0.007 | 0.007 | 0.004 | 0.004 | 0.010 | 0.010 | 0.010 | 0.010 | 0.010 | 0.010 | 0.010 | 0.010 | 0.010 | 0.010 | | |
| Or | 0.7 | 0.39 | 1.25 | 0.35 | 0.40 | 0.20 | 0.44 | 0.17 | 0.58 | 0.42 | 0.61 | 0.30 | 0.30 | 0.18 | 0.69 | 0.39 | 0.39 | 0.98 | 0.98 | 0.98 | 0.98 | 0.98 | 0.98 | 0.98 | 0.98 | 0.98 | 0.98 | |
| ab | 47.96 | 49.48 | 37.25 | 37.39 | 32.26 | 25.89 | 27.32 | 26.51 | 26.07 | 27.73 | 31.66 | 33.30 | 22.08 | 26.79 | 31.08 | 31.08 | 36.01 | 36.01 | 36.01 | 36.01 | 36.01 | 36.01 | 36.01 | 36.01 | 36.01 | 36.01 | | |
| an | 51.77 | 50.12 | 61.50 | 62.27 | 67.35 | 73.91 | 72.24 | 73.32 | 73.36 | 71.85 | 67.72 | 66.40 | 77.74 | 72.52 | 68.53 | 68.53 | 63.01 | 63.01 | 63.01 | 63.01 | 63.01 | 63.01 | 63.01 | 63.01 | 63.01 | 63.01 | | |
| ma-47 | ma-47 | ma-44 | ma-44 | ma-44 | ma-43 | ma-43 | ma-43 | ma-43 | yuk-87 | yuk-87 | ma-24b | ma-24b | yuk-88 | yuk-88 | ma-24g | ma-24g | ma-24a | | |
| Com- ponent | gn pabC | gn pabC | gn pabC | gn pabC | gn pabC | gn pabC | gn pabC | gn pabC | gn pabC | gn pabC | gn pabC | gn pabC | gn pabC | gn pabC | gn pabC | gn pabC | gn pabC | gn pabC | gn pabC | gn pabC | gn pabC | gn pabC | gn pabC | gn pabC | gn pabC | gn pabC | | |
| SiO ₂ | 28.10 | 28.36 | 28.60 | 28.60 | 28.60 | 28.60 | 28.60 | 28.60 | 28.65 | 28.65 | 28.65 | 28.65 | 28.79 | 28.80 | 28.80 | 28.80 | 28.80 | 28.80 | 28.80 | 28.80 | 28.80 | 28.80 | 28.80 | 28.80 | 28.80 | 28.80 | 28.80 | |
| Al ₂ O ₃ | 28.78 | 29.53 | 31.21 | 31.06 | 31.09 | 32.21 | 32.80 | 32.40 | 28.57 | 28.45 | 32.31 | 31.35 | 31.89 | 32.84 | 32.73 | 32.73 | 32.83 | 32.83 | 32.83 | 32.83 | 32.83 | 32.83 | 32.83 | 32.83 | 32.83 | 32.83 | 32.83 | |
| FeO | 0.23 | 0.45 | 0.44 | 0.44 | 0.33 | 0.44 | 0.26 | 0.25 | 0.19 | 0.03 | 0.02 | 0.02 | 0.02 | 0.02 | 0.02 | 0.02 | 0.02 | 0.02 | 0.02 | 0.02 | 0.02 | 0.02 | 0.02 | 0.02 | 0.02 | 0.02 | 0.02 | |
| CaO | 13.71 | 14.44 | 14.34 | 13.93 | 14.49 | 14.93 | 15.49 | 15.04 | 14.25 | 14.47 | 14.86 | 13.77 | 15.58 | 15.20 | 15.74 | 15.74 | 14.86 | 14.86 | 14.86 | 14.86 | 14.86 | 14.86 | 14.86 | 14.86 | 14.86 | 14.86 | | |
| Na ₂ O | 4.41 | 4.00 | 3.35 | 2.50 | 3.48 | 2.99 | 2.53 | 3.20 | 3.90 | 3.93 | 3.31 | 3.81 | 2.97 | 1.77 | 1.38 | 1.38 | 1.84 | 1.84 | 1.84 | 1.84 | 1.84 | 1.84 | 1.84 | 1.84 | 1.84 | 1.84 | | |
| K ₂ O | 0.07 | 0.05 | 0.09 | 0.02 | 0.11 | 0.03 | 0.16 | 0.05 | 0.06 | 0.05 | 0.04 | 0.06 | 0.05 | 0.05 | 0.05 | 0.05 | 0.05 | 0.05 | 0.05 | 0.05 | 0.05 | 0.05 | 0.05 | 0.05 | 0.05 | 0.05 | | |
| Total | 98.16 | 98.71 | 99.08 | 98.99 | 99.90 | 99.12 | 99.81 | 100.92 | 99.47 | 99.05 | 100.60 | 99.96 | 99.92 | 99.37 | 99.27 | 99.04 | 99.04 | 99.04 | 99.04 | 99.04 | 99.04 | 99.04 | 99.04 | 99.04 | 99.04 | | | |
| Si | 2.370 | 2.330 | 2.290 | 2.350 | 2.304 | 2.254 | 2.885 | 9.051 | 2.400 | 2.390 | 9.078 | 9.272 | 2.262 | 2.258 | 2.258 | 2.258 | 2.258 | 2.258 | 2.258 | 2.258 | 2.258 | 2.258 | 2.258 | 2.258 | 2.258 | 2.258 | | |
| Al | 1.578 | 1.615 | 1.696 | 1.671 | 1.675 | 1.747 | 7.098 | 6.916 | 1.543 | 1.543 | 0.007 | 0.005 | 0.003 | 0.003 | 0.003 | 0.003 | 0.003 | 0.003 | 0.003 | 0.003 | 0.003 | 0.003 | 0.003 | 0.003 | 0.003 | | | |
| Fe | 0.009 | 0.017 | 0.017 | 0.013 | 0.013 | 0.068 | 0.039 | 0.010 | 0.289 | 0.289 | 0.715 | 0.699 | 0.699 | 0.699 | 0.699 | 0.699 | 0.699 | 0.699 | 0.699 | 0.699 | 0.699 | 0.699 | 0.699 | 0.699 | 0.699 | | | |
| Ca | 0.683 | 0.718 | 0.708 | 0.681 | 0.710 | 0.736 | 3.047 | 2.917 | 1.124 | 1.124 | 0.346 | 0.351 | 1.163 | 1.346 | 0.263 | 0.263 | 0.157 | 0.157 | 0.157 | 0.157 | 0.157 | 0.157 | 0.157 | 0.157 | 0.157 | 0.157 | | |
| Na | 0.398 | 0.360 | 0.299 | 0.221 | 0.308 | 0.267 | 0.899 | 0.037 | 0.012 | 0.012 | 0.004 | 0.003 | 0.010 | 0.014 | 0.003 | 0.003 | 0.003 | 0.003 | 0.003 | 0.003 | 0.003 | 0.003 | 0.003 | 0.003 | 0.003 | 0.003 | | |
| K | 0.004 | 0.003 | 0.001 | 0.001 | 0.006 | 0.002 | 0.002 | 0.002 | 0.037 | 0.037 | 0.30 | 0.38 | 0.28 | 0.25 | 0.35 | 0.29 | 0.55 | 0.55 | 0.55 | 0.55 | 0.55 | 0.55 | 0.55 | 0.55 | 0.55 | 0.55 | | |
| Or | 0.37 | 0.28 | 0.49 | 0.11 | 0.59 | 0.20 | 0.93 | 0.20 | 0.93 | 0.20 | 0.93 | 0.20 | 0.93 | 0.20 | 0.93 | 0.20 | 0.93 | 0.20 | 0.93 | 0.20 | 0.93 | 0.20 | 0.93 | 0.20 | 0.93 | 0.20 | | |
| ab | 36.68 | 33.30 | 29.55 | 24.47 | 30.08 | 26.57 | 22.57 | 27.73 | 32.98 | 32.83 | 28.63 | 33.28 | 25.56 | 17.33 | 13.56 | 13.56 | 13.56 | 13.56 | 13.56 | 13.56 | 13.56 | 13.56 | 13.56 | 13.56 | 13.56 | 13.56 | 13.56 | |
| an | 62.95 | 66.42 | 69.96 | 75.42 | 69.34 | 73.23 | 76.50 | 71.97 | 66.88 | 66.88 | 71.12 | 66.33 | 66.33 | 66.33 | 66.33 | 66.33 | 66.33 | 66.33 | 66.33 | 66.33 | 66.33 | 66.33 | 66.33 | 66.33 | 66.33 | 66.33 | | |

Table 3. (Contd.)

| Com- ponent | ma-24a an pCab | ma-24a an pCab | ma-24a an pCab | ma-24a an pCab | ma-42 n pbC | ma-42 n pbC | ma-42 n pbC | ma-42 n pbC | ma-15/3 an pCab | ma-15/3 an pCab | ma-15/4 an pCab | ma-15/4 an pCab | ma-14/4 an pCab | ma-14/4 an pCab | ma-19b gn pabC |
|--------------------------------|-------------------|-------------------|-------------------|-------------------|----------------|----------------|----------------|----------------|--------------------|--------------------|--------------------|--------------------|--------------------|--------------------|-------------------|
| | 2881.5 | 2881.5 | 2881.5 | 2881.5 | 2890 | 2890 | 2890 | 2890 | 2897.4 | 2897.4 | 2897.6 | 2897.6 | 2898 | 2898 | 2900.4 |
| SiO ₂ | 49.39 | 49.75 | 49.45 | 50.60 | 50.08 | 51.05 | 48.45 | 49.67 | 48.36 | 49.43 | 49.60 | 47.87 | 50.15 | 50.69 | 50.52 |
| Al ₂ O ₃ | 32.87 | 33.27 | 32.84 | 30.22 | 16.63 | 31.05 | 31.31 | 32.94 | 31.62 | 32.52 | 32.19 | 32.55 | 31.88 | 32.40 | 32.78 |
| FeO | 15.60 | 14.49 | 15.31 | 14.90 | 11.50 | 15.14 | 14.76 | 15.19 | 0.07 | 0.07 | 0.16 | 0.26 | 0.44 | 0.27 | |
| CaO | 1.44 | 2.36 | 1.75 | 3.66 | 2.20 | 2.18 | 2.38 | 3.15 | 3.47 | 2.83 | 14.32 | 14.01 | 14.48 | 13.65 | 14.82 |
| Na ₂ O | 0.10 | 0.13 | 0.16 | 0.11 | 0.04 | 0.10 | 0.02 | 0.06 | <0.05 | 0.07 | 0.06 | 0.08 | 0.08 | 0.11 | 0.10 |
| K ₂ O | Total | 99.39 | 100.01 | 99.50 | 99.61 | 100.16 | 99.36 | 99.51 | 99.86 | 98.03 | 98.10 | 100.90 | 99.30 | 98.24 | 100.19 |
| Si | 2.257 | 2.259 | 2.259 | 2.322 | 2.260 | 2.325 | 2.326 | 2.325 | 2.326 | 2.326 | 2.326 | 2.326 | 2.326 | 2.284 | 2.284 |
| Al | 1.771 | 1.780 | 1.768 | 1.634 | 1.697 | 1.672 | 1.682 | 1.672 | 1.682 | 1.682 | 1.682 | 1.682 | 1.682 | 1.711 | 1.747 |
| Fe | 0.764 | 0.705 | 0.749 | 0.733 | 0.790 | 0.741 | 0.721 | 0.794 | 0.721 | 0.794 | 0.721 | 0.794 | 0.721 | 0.706 | 0.718 |
| Ca | 0.127 | 0.208 | 0.155 | 0.326 | 0.263 | 0.193 | 0.210 | 0.193 | 0.210 | 0.193 | 0.210 | 0.193 | 0.210 | 0.256 | 0.184 |
| Na | 0.006 | 0.008 | 0.010 | 0.006 | 0.003 | 0.006 | 0.001 | 0.006 | 0.014 | 0.014 | 0.014 | 0.014 | 0.014 | 0.005 | 0.005 |
| K | 0.67 | 0.87 | 1.09 | 0.56 | 0.28 | 0.64 | 0.11 | 0.34 | 0.41 | 0.00 | 0.32 | 0.46 | 0.39 | 0.50 | 0.55 |
| Or | 14.16 | 22.58 | 16.96 | 30.61 | 24.91 | 20.53 | 22.53 | 27.18 | 32.21 | 26.35 | 29.76 | 28.86 | 24.70 | 29.32 | 28.96 |
| ab | 85.17 | 76.55 | 81.95 | 68.83 | 74.81 | 78.83 | 77.36 | 72.48 | 67.37 | 73.65 | 69.92 | 70.67 | 74.92 | 70.18 | 70.36 |
| an | ma-19b | ma-19b | ma-14/1 | ma-14/1 | ma-18c | ma-18b | ma-18b | ma-18b | ma-41 | ma-41 | ma-40 | ma-40 | ma-70 | ma-39 | ma-38 |
| Com- ponent | gn pabC | gn pabC | n pbCa | n pbCa | an pCab | gn pabC | gn pabC | gn pabC | an pC | an pC | n pbC | gn pbaC | gn pbaC | gn pbaC | gn pbaC |
| SiO ₂ | 50.43 | 50.30 | 48.15 | 47.86 | 50.21 | 51.71 | 49.97 | 49.82 | 51.54 | 50.37 | 50.90 | 50.37 | 50.52 | 52.62 | 51.72 |
| Al ₂ O ₃ | 32.72 | 31.56 | 32.91 | 33.29 | 30.97 | 29.91 | 30.16 | 30.55 | 30.03 | 30.81 | 30.68 | 29.03 | 29.85 | 30.60 | 29.83 |
| FeO | 15.08 | 14.41 | 15.49 | 15.03 | 14.72 | 13.45 | 14.62 | 14.79 | 0.59 | 0.50 | 0.41 | 0.77 | 0.29 | 0.37 | 0.30 |
| CaO | 1.88 | 3.53 | 2.99 | 2.69 | 3.56 | 3.80 | 3.59 | 3.37 | 4.20 | 4.03 | 13.68 | 14.53 | 14.83 | 13.30 | 13.66 |
| Na ₂ O | 0.10 | 0.09 | 0.07 | <0.05 | 0.06 | 0.11 | 0.14 | 0.16 | 0.19 | 0.12 | 0.10 | 0.14 | 0.16 | 0.09 | 0.02 |
| K ₂ O | Total | 10.20 | 100.17 | 99.84 | 99.06 | 99.57 | 98.97 | 99.07 | 99.02 | 99.46 | 99.41 | 100.47 | 98.38 | 99.34 | 99.77 |
| Si | 2.283 | 2.292 | 8.845 | 8.821 | 2.302 | 2.371 | 2.311 | 2.304 | 2.360 | 2.313 | 2.318 | 2.344 | 2.328 | 2.382 | 2.364 |
| Al | 1.745 | 1.695 | 7.124 | 7.231 | 1.674 | 1.617 | 1.644 | 1.664 | 1.621 | 1.668 | 1.647 | 1.592 | 1.621 | 1.633 | 1.608 |
| Fe | 0.731 | 0.704 | 3.049 | 2.968 | 0.723 | 0.028 | 0.023 | 0.013 | 0.019 | 0.016 | 0.029 | 0.011 | 0.014 | 0.006 | 0.017 |
| Ca | 0.165 | 0.312 | 1.065 | 0.959 | 0.316 | 0.338 | 0.661 | 0.724 | 0.732 | 0.638 | 0.673 | 0.709 | 0.739 | 0.723 | 0.669 |
| Na | 0.006 | 0.005 | 0.015 | 0.003 | 0.007 | 0.008 | 0.011 | 0.011 | 0.007 | 0.006 | 0.008 | 0.010 | 0.005 | 0.001 | 0.340 |
| K | 0.67 | 0.49 | 0.36 | 0.00 | 0.29 | 0.70 | 0.76 | 1.05 | 1.08 | 0.67 | 0.59 | 0.74 | 0.93 | 0.55 | 0.006 |
| Or | 18.29 | 30.56 | 25.79 | 24.42 | 30.33 | 33.60 | 28.90 | 36.50 | 34.55 | 30.11 | 30.96 | 31.56 | 28.81 | 30.44 | 33.50 |
| ab | 81.04 | 68.95 | 73.84 | 75.58 | 69.39 | 65.71 | 68.69 | 70.05 | 62.43 | 64.77 | 69.31 | 68.30 | 70.65 | 69.46 | 65.91 |

Table 3. (Contd.)

| Component | ma-38 | ma-38 | 139/21 | 139/23 | 139/28 | 139/31 | 1300/4880 | 1110/5120 | 3293/35.0 | 3293/85.85 |
|--------------------------------|---------|---------|---------|---------|---------|---------|-----------|-----------|-----------|------------|
| | gn pabC | gn pabC | gn pabC | n pbC |
| SiO ₂ | 51.49 | 50.35 | 49.94 | 51.14 | 52.06 | 50.35 | 52.091 | 50.81 | 50.86 | 51.59 |
| Al ₂ O ₃ | 30.75 | 30.74 | 31.03 | 30.44 | 29.57 | 30.76 | 28.765 | 31.13 | 29.02 | 29.07 |
| FeO | | | 0.55 | 0.34 | 0.34 | 0.39 | 0.372 | 0.39 | 0.24 | 0.38 |
| CaO | 13.35 | 13.87 | 14.88 | 14.05 | 12.65 | 14.27 | 13.476 | 13.45 | 13.28 | 12.6 |
| Na ₂ O | 3.99 | 3.80 | 3.18 | 3.50 | 4.30 | 3.44 | 4.154 | 3.60 | 4.99 | 5.38 |
| K ₂ O | 0.19 | 0.18 | 0.08 | 0.07 | 0.10 | 0.11 | 0.212 | 0.22 | 0.04 | 0.04 |
| Total | 99.78 | 98.95 | 99.66 | 99.54 | 99.02 | 99.32 | 99.10 | 99.60 | 98.48 | 99.06 |
| Si | 2.345 | 2.319 | 2.292 | 2.339 | 2.387 | 2.314 | 2.395 | 2.322 | 9.443 | 2.377 |
| Al | 1.651 | 1.669 | 1.679 | 1.641 | 1.598 | 1.666 | 1.559 | 1.677 | 6.350 | 1.579 |
| Fe | | | 0.021 | 0.013 | 0.013 | 0.015 | 0.014 | 0.015 | 0.037 | 0.015 |
| Ca | 0.652 | 0.684 | 0.732 | 0.689 | 0.621 | 0.703 | 0.664 | 0.659 | 2.641 | 0.622 |
| Na | 0.352 | 0.340 | 0.283 | 0.311 | 0.382 | 0.307 | 0.370 | 0.319 | 1.797 | 0.481 |
| K | 0.011 | 0.011 | 0.005 | 0.004 | 0.006 | 0.006 | 0.012 | 0.013 | 0.009 | 0.002 |
| Or | 1.08 | 1.06 | 0.49 | 0.40 | 0.59 | 0.59 | 1.15 | 1.31 | 0.20 | 0.18 |
| ab | 34.68 | 32.85 | 27.75 | 30.98 | 37.86 | 30.22 | 35.37 | 32.19 | 40.41 | 43.53 |
| an | 64.24 | 66.09 | 71.76 | 68.63 | 61.55 | 69.19 | 63.48 | 66.50 | 59.39 | 56.29 |

Note: Rocks: gn – gabbronorite, n – norite, t – troctolite, ol-gn – olivine gabbro, ol-n – olivine norite, ol-lg – olivine leucogabbro-anorthosite, mg – magnetite gabbro, p – pyroxene; C – cumulate; C – pyroxene; b# – orthopyroxene, a – clinopyroxene, b – plagioclase; symbols before C denote cumulus phases, symbols after C are intercumulus phases; dashes mean not detected. Cation numbers are normalized to 32 or 8 oxygens. Microprobe analyses of minerals in Tables 2, 3, and 4 were conducted on a Cameca MS-46 X-ray microprobe at the Geological Institute, Kola Research Center, Russian Academy of Sciences, and on an Jeol JGX-a 733 electron microscope at the Institute of Electron Optics, University of Oulu. Here and in Tables 4, 5, * sample number; ** rock depth, m.

Table 4. Chemical composition (wt %) of orthopyroxene from rocks of the Western Pansky Tundra intrusion

| Component | yuk-39 gn pabC | yuk-40 n pbCa | yuk-41 t poCab | yuk-44 gn pabC | yuk-43 ol-gn paboC | yuk-50 ol-gn paboC | yuk-51 gn pabC | yuk-31B ol-gn paboC | yuk-31a gn pabC | yuk-4a ol-n pboC | yuk-45 ol-n pboC | yuk-70 yuk-47 gn pabC |
|--------------------------------|-------------------|------------------|-------------------|-------------------|-----------------------|-----------------------|-------------------|------------------------|--------------------|---------------------|---------------------|-----------------------------|
| SiO ₂ | 56.3 | 55.72 | 55.58 | 55.64 | 56.41 | 55.45 | 56.24 | 55.38 | 55.41 | 56.30 | 55.85 | 54.98 |
| TiO ₂ | 0.14 | 0.11 | 0.19 | 0.20 | 0.12 | 0.09 | 0.16 | 0.12 | 0.11 | 0.13 | 0.12 | 0.11 |
| Al ₂ O ₃ | 1.02 | 0.98 | 1.15 | 0.97 | 1.09 | 1.02 | 0.95 | 1.07 | 1.09 | 1.16 | 1.08 | 0.98 |
| FeO | 10.83 | 13.56 | 11.85 | 12.37 | 11.49 | 11.20 | 11.81 | 11.29 | 11.71 | 11.20 | 11.27 | 12.52 |
| MnO | 0.28 | 0.22 | 0.28 | 0.28 | 0.23 | 0.23 | 0.17 | 0.21 | 0.25 | 0.29 | 0.30 | 0.28 |
| MgO | 29.89 | 28.66 | 29.90 | 28.86 | 30.80 | 29.30 | 29.62 | 29.26 | 29.45 | 30.35 | 29.87 | 28.38 |
| CaO | 2.22 | 2.30 | 1.93 | 2.09 | 2.18 | 2.25 | 2.30 | 2.25 | 2.34 | 2.41 | 2.12 | 2.36 |
| Na ₂ O | 0.03 | 0.02 | 0.02 | 0.03 | 0.01 | 0.04 | 0.04 | 0.04 | 0.05 | 0.05 | 0.03 | 0.02 |
| K ₂ O | | | | | | | | | | 0.01 | 0.02 | 0.02 |
| V ₂ O ₃ | 0.02 | 0.01 | 0.01 | 0.01 | 0.03 | 0.01 | 0.09 | 0.01 | 0.01 | 0.03 | 0.07 | 0.01 |
| Cr ₂ O ₃ | 0.02 | 0.06 | 0.03 | | | | | | | 0.02 | 0.02 | 0.09 |
| CoO | | | | | | | | | | | | 0.06 |
| NiO | 0.22 | 0.02 | 0.07 | 0.19 | 0.03 | 0.02 | 0.14 | 0.05 | 0.05 | 0.16 | 0.04 | 0.09 |
| ZnO | 0.12 | | 0.09 | 0.09 | 0.03 | 0.02 | 0.02 | 0.06 | | 0.02 | 0.10 | |
| Total | 100.48 | 101.97 | 100.97 | 100.50 | 102.65 | 99.83 | 101.30 | 99.74 | 100.41 | 101.99 | 100.91 | 99.81 |
| Si | 1.973 | 1.962 | 1.957 | 1.973 | 1.953 | 1.971 | 1.972 | 1.971 | 1.963 | 1.959 | 1.965 | 1.968 |
| Ti | 0.004 | 0.003 | 0.005 | 0.005 | 0.003 | 0.002 | 0.004 | 0.003 | 0.003 | 0.003 | 0.003 | 0.003 |
| Al | 0.042 | 0.040 | 0.048 | 0.040 | 0.044 | 0.043 | 0.039 | 0.045 | 0.046 | 0.047 | 0.045 | 0.041 |
| Fe | 0.319 | 0.399 | 0.349 | 0.367 | 0.333 | 0.333 | 0.346 | 0.336 | 0.347 | 0.347 | 0.326 | 0.332 |
| Mn | 0.008 | 0.006 | 0.008 | 0.008 | 0.007 | 0.007 | 0.005 | 0.006 | 0.007 | 0.008 | 0.009 | 0.008 |
| Mg | 1.569 | 1.504 | 1.570 | 1.525 | 1.590 | 1.553 | 1.549 | 1.552 | 1.555 | 1.574 | 1.567 | 1.515 |
| Ca | 0.084 | 0.087 | 0.073 | 0.079 | 0.081 | 0.086 | 0.086 | 0.086 | 0.089 | 0.090 | 0.080 | 0.091 |
| Na | 0.002 | 0.001 | 0.002 | 0.002 | | | | | 0.003 | 0.003 | 0.002 | 0.001 |
| K | | | | | | | | | 0.001 | 0.001 | 0.001 | 0.002 |
| V | | | | | | 0.001 | 0.003 | | 0.001 | 0.001 | 0.001 | 0.002 |
| Cr | 0.001 | 0.002 | 0.001 | | | 0.001 | 0.001 | | 0.001 | 0.001 | 0.003 | 0.002 |
| Co | | | | | | | | | | | | 0.001 |
| Ni | 0.006 | | | | | 0.005 | 0.004 | | 0.001 | | 0.005 | 0.001 |
| Zn | | 0.003 | | | | 0.002 | 0.001 | | 0.002 | | 0.001 | 0.003 |
| Fs | 16.18 | 20.05 | 17.52 | 18.62 | 16.62 | 16.89 | 17.47 | 17.02 | 17.43 | 16.38 | 16.78 | 18.93 |
| En | 79.56 | 75.58 | 78.82 | 77.37 | 79.34 | 78.75 | 78.19 | 78.62 | 78.10 | 79.10 | 79.18 | 76.48 |
| Wo | 4.26 | 4.37 | 3.66 | 4.01 | 4.04 | 4.36 | 4.34 | 4.36 | 4.47 | 4.52 | 4.04 | 4.59 |
| f# | 16.90 | 20.97 | 18.19 | 19.40 | 17.32 | 17.66 | 18.26 | 17.80 | 18.24 | 17.16 | 17.48 | 19.84 |

Table 4. (Contd.)

| Component | yuk-55 gn pabC | yuk-71 gn pabC | yuk-72 gn pabC | yuk-73 mg pab#mC | yuk-74 gn pabC | yuk-75 gn pabC | yuk-76 gn pabC | yuk-77 gn pabC | yuk-78 gn pabC | yuk-79 gn pabC | yuk-80 mg pab#mC | yuk-81 gn pabC | yuk-82 gn pabC | yuk-83 gn pabC |
|--------------------------------|-------------------|-------------------|-------------------|---------------------|-------------------|-------------------|-------------------|-------------------|-------------------|-------------------|---------------------|-------------------|-------------------|-------------------|
| SiO ₂ | 54.62 | 54.81 | 54.59 | 52.34 | 54.48 | 0.00 | 54.20 | 55.19 | 54.63 | 54.75 | 53.93 | 51.25 | 52.44 | 53.44 |
| TiO ₂ | 0.11 | 0.15 | 0.12 | 0.19 | 0.14 | 0.18 | 0.12 | 0.16 | 0.15 | 0.06 | 0.21 | 0.24 | 0.28 | 0.12 |
| Al ₂ O ₃ | 0.91 | 0.88 | 0.91 | 0.79 | 0.94 | 0.99 | 0.99 | 0.81 | 0.96 | 0.85 | 0.93 | 0.39 | 0.64 | 0.86 |
| FeO | 13.93 | 15.8 | 15.28 | 22.75 | 17.24 | 19.52 | 16.51 | 15.72 | 15.67 | 16.81 | 17.82 | 29.46 | 23.78 | 20.11 |
| MnO | 0.30 | 0.38 | 0.22 | 0.45 | 0.35 | 0.40 | 0.24 | 0.25 | 0.19 | 0.32 | 0.28 | 0.72 | 0.45 | 0.50 |
| MgO | 27.72 | 26.29 | 26.66 | 21.88 | 25.41 | 23.19 | 25.65 | 26.77 | 26.47 | 25.57 | 25.12 | 15.64 | 20.85 | 22.62 |
| CaO | 2.21 | 2.12 | 2.32 | 1.04 | 2.25 | 2.13 | 2.15 | 1.82 | 1.76 | 2.42 | 1.92 | 2.28 | 1.36 | 2.13 |
| Na ₂ O | 0.01 | 0.04 | 0.02 | 0.03 | 0.01 | 0.01 | 0.02 | 0.03 | 0.02 | 0.02 | 0.01 | 0.01 | 0.01 | 0.02 |
| K ₂ O | 0.01 | 0.01 | 0.01 | 0.01 | 0.01 | 0.01 | 0.02 | 0.02 | 0.02 | 0.01 | 0.01 | 0.01 | 0.01 | 0.01 |
| V ₂ O ₃ | 0.03 | 0.11 | 0.02 | 0.04 | 0.03 | 0.03 | 0.02 | 0.02 | 0.02 | 0.03 | 0.03 | 0.01 | 0.08 | 0.07 |
| Cr ₂ O ₃ | 0.02 | 0.02 | 0.04 | 0.02 | 0.08 | 0.02 | 0.01 | 0.01 | 0.01 | 0.01 | 0.05 | 0.01 | 0.01 | 0.02 |
| CoO | NiO | 0.20 | 0.02 | 0.02 | 0.08 | 0.02 | 0.08 | 0.10 | 0.29 | 0.07 | 0.08 | 0.16 | 0.01 | 0.04 |
| ZnO | Total | 100.07 | 100.59 | 100.26 | 99.45 | 100.98 | 99.85 | 100.25 | 100.86 | 99.97 | 101.05 | 100.35 | 100.04 | 99.81 |
| Si | 1.964 | 1.974 | 1.969 | 1.973 | 1.969 | 1.971 | 1.969 | 1.978 | 1.975 | 1.974 | 1.966 | 1.989 | 1.974 | 1.980 |
| Ti | 0.003 | 0.004 | 0.003 | 0.005 | 0.004 | 0.005 | 0.005 | 0.003 | 0.004 | 0.004 | 0.006 | 0.007 | 0.008 | 0.03 |
| Al | 0.039 | 0.038 | 0.038 | 0.035 | 0.040 | 0.043 | 0.042 | 0.034 | 0.041 | 0.041 | 0.036 | 0.040 | 0.018 | 0.028 |
| Fe | 0.419 | 0.475 | 0.461 | 0.713 | 0.521 | 0.604 | 0.502 | 0.471 | 0.474 | 0.507 | 0.543 | 0.956 | 0.749 | 0.623 |
| Mn | 0.009 | 0.012 | 0.007 | 0.014 | 0.011 | 0.013 | 0.007 | 0.008 | 0.006 | 0.010 | 0.009 | 0.024 | 0.014 | 0.016 |
| Mg | 1.486 | 1.412 | 1.434 | 1.222 | 1.369 | 1.278 | 1.389 | 1.430 | 1.427 | 1.374 | 1.365 | 0.905 | 1.170 | 1.250 |
| Ca | 0.085 | 0.082 | 0.090 | 0.042 | 0.087 | 0.084 | 0.084 | 0.070 | 0.068 | 0.093 | 0.075 | 0.095 | 0.055 | 0.085 |
| Na | K | 0.003 | 0.002 | 0.001 | 0.002 | 0.001 | 0.001 | 0.002 | 0.001 | 0.001 | 0.001 | 0.001 | 0.001 | 0.001 |
| V | Cr | 0.001 | 0.003 | 0.001 | 0.001 | 0.001 | 0.001 | 0.001 | 0.001 | 0.001 | 0.001 | 0.001 | 0.001 | 0.001 |
| Co | Ni | 0.006 | 0.002 | 0.001 | 0.001 | 0.003 | 0.009 | 0.002 | 0.002 | 0.002 | 0.005 | 0.003 | 0.002 | 0.002 |
| Zn | Fs | 21.06 | 24.12 | 23.22 | 36.06 | 26.35 | 30.72 | 25.42 | 23.90 | 24.07 | 25.68 | 27.38 | 48.88 | 37.94 |
| En | 74.67 | 71.71 | 72.24 | 61.81 | 69.25 | 65.01 | 70.33 | 72.55 | 69.60 | 68.84 | 46.27 | 59.27 | 63.84 | 31.82 |
| Wo | f# | 4.27 | 4.16 | 4.53 | 2.12 | 4.40 | 4.27 | 4.55 | 3.55 | 4.71 | 3.78 | 4.86 | 2.79 | 4.34 |
| | | 21.99 | 25.17 | 24.33 | 36.85 | 27.57 | 32.09 | 26.55 | 24.78 | 24.93 | 26.95 | 28.48 | 51.37 | 33.26 |

Table 4. (Contd.)

| Com- ponent | yuk-85 gn pabC | yuk-50 gn pabC | yuk-86 gn pabC | ma-48 gn pabC | ma-47 gn pabC | ma-44 gn pabC | ma-43 gn pabC | yuk-87 gn pabC | ma-24b gn pabC | ma-42 gn pabC | ma-21-I gn pabC | ma-15/6 gn pabC | ma-19b gn pabC | ma-19b gn pabC |
|--------------------------------|-------------------|-------------------|-------------------|------------------|------------------|------------------|------------------|-------------------|-------------------|------------------|--------------------|--------------------|-------------------|-------------------|
| 2512 | 2741 | 2750 | 2781 | 2810 | 2836 | 2860 | 2865 | 2879.8 | 2890 | 2894.5 | 2897.4 | 2900.4 | 2900.4 | 2900.4 |
| SiO ₂ | 54.61 | 57.25 | 53.61 | 55.23 | 55.16 | 54.58 | 54.42 | 54.89 | 55.27 | 54.47 | 55.75 | 54.79 | 54.94 | 53.17 |
| TiO ₂ | 0.21 | 0.18 | 0.25 | 0.12 | 0.10 | 0.15 | 0.16 | 0.13 | 0.27 | 0.06 | 0.04 | 0.11 | 0.13 | 0.13 |
| Al ₂ O ₃ | 0.75 | 0.95 | 0.87 | 0.79 | 0.36 | 0.79 | 0.93 | 0.80 | 1.01 | 0.61 | 0.52 | 0.62 | 1.00 | 0.74 |
| FeO | 18.53 | 9.68 | 19.76 | 12.92 | 13.05 | 15.38 | 16.53 | 16.31 | 13.22 | 15.05 | 8.68 | 9.37 | 14.51 | 15.17 |
| MnO | 0.32 | 0.36 | 0.35 | 0.33 | 0.33 | 0.03 | 0.33 | 0.33 | 0.44 | 0.29 | 0.25 | 0.27 | 0.30 | 0.43 |
| MgO | 24.66 | 28.53 | 23.83 | 28.29 | 29.02 | 26.98 | 26.01 | 26.27 | 28.23 | 27.25 | 17.65 | 17.26 | 27.72 | 27.52 |
| CaO | 1.61 | 2.07 | 1.59 | 1.82 | 1.20 | 2.44 | 1.32 | 1.63 | 1.25 | 2.30 | 1.53 | 1.16 | 1.28 | 1.86 |
| Na ₂ O | 0.01 | 0.01 | 0.01 | 0.01 | | | 0.14 | | | | | | | 0.09 |
| K ₂ O | 0.05 | 0.05 | 0.01 | 0.03 | 0.12 | 0.09 | 0.04 | 0.06 | 0.01 | 0.03 | 0.01 | 0.07 | | |
| V ₂ O ₃ | 0.008 | 0.05 | 0.01 | 0.03 | | | | | | | | | | |
| Cr ₂ O ₃ | | | | | | | | | | | | | | |
| CoO | | | | | | | | | | | | | | |
| NiO | 0.11 | 0.05 | | 0.09 | | | | | | | | | | |
| ZnO | 0.05 | | | | | | | | | | | | | |
| Total | 100.95 | 99.12 | 100.39 | 99.49 | 99.31 | 100.34 | 99.88 | 100.63 | 99.62 | 100.24 | 54.43 | 54.52 | 99.86 | 99.10 |
| Si | 1.982 | 2.024 | 1.970 | 1.982 | 1.982 | 1.964 | 1.978 | 1.980 | 1.965 | 1.972 | 1.979 | 1.975 | 1.945 | 1.945 |
| Ti | 0.006 | 0.005 | 0.007 | 0.033 | 0.003 | 0.003 | 0.004 | 0.003 | 0.007 | 0.003 | 0.002 | 0.003 | 0.004 | 0.004 |
| Al | 0.032 | 0.040 | 0.038 | 0.033 | 0.015 | 0.034 | 0.040 | 0.034 | 0.043 | 0.026 | 0.041 | 0.050 | 0.042 | 0.032 |
| Fe | 0.562 | 0.286 | 0.607 | 0.388 | 0.392 | 0.463 | 0.502 | 0.492 | 0.396 | 0.454 | 0.334 | 0.361 | 0.436 | 0.464 |
| Mn | 0.010 | 0.011 | 0.011 | 0.010 | 0.010 | 0.010 | 0.010 | 0.010 | 0.013 | 0.009 | 0.010 | 0.011 | 0.009 | 0.013 |
| Mg | 1.334 | 1.504 | 1.305 | 1.513 | 1.555 | 1.447 | 1.408 | 1.412 | 1.508 | 1.465 | 1.562 | 1.530 | 1.486 | 1.501 |
| Ca | 0.063 | 0.078 | 0.063 | 0.070 | 0.046 | 0.094 | 0.051 | 0.063 | 0.048 | 0.089 | 0.082 | 0.062 | 0.049 | 0.073 |
| Na | | | 0.001 | | | | 0.010 | | | | | | | 0.006 |
| K | 0.002 | 0.001 | 0.001 | 0.003 | 0.002 | 0.001 | 0.002 | 0.001 | 0.001 | 0.002 | | | | |
| V | 0.002 | | | | | | | | | | | | | |
| Cr | | | | | | | | | | | | | | |
| Co | | | | | | | | | | | | | | |
| Ni | 0.003 | | | | | | | | | | | | | |
| Zn | 0.001 | | | | | | | | | | | | | |
| F _s | 28.69 | 15.31 | 30.73 | 19.69 | 19.67 | 23.10 | 25.60 | 25.01 | 20.29 | 22.61 | 16.89 | 18.48 | 22.12 | 22.77 |
| E _n | 68.10 | 80.51 | 66.08 | 76.76 | 78.02 | 72.21 | 71.80 | 71.78 | 77.25 | 72.96 | 78.97 | 78.34 | 75.39 | 73.65 |
| W _o | 3.22 | 4.18 | 3.19 | 3.55 | 2.31 | 4.69 | 2.60 | 3.20 | 2.46 | 4.43 | 4.15 | 3.17 | 2.49 | 3.58 |
| f# | 29.64 | 15.98 | 31.75 | 20.41 | 20.15 | 24.64 | 26.67 | 25.84 | 20.80 | 24.00 | 17.61 | 19.09 | 23.05 | 23.61 |

Table 4. (Contd.)

| Com- ponent | ma-19b gn pabC | ma-14/1 gn pabC | ma-18b gn pabC | ma-70 gn pabC | ma-38 gn pabC | 139/21 gn pabC | 139/23 gn pabC | 139/28 gn pabC | 139/31 gn pabC | 1300/4880 gn pabC | 1110/5120 gn pabC | 3293/35.0 gn pabC | 3293/85.85 n pbC |
|--------------------------------|-------------------|--------------------|-------------------|------------------|------------------|-------------------|-------------------|-------------------|-------------------|----------------------|----------------------|----------------------|---------------------|
| 2900.4 | 2902 | 2903.5 | 2905 | 2915 | 2942.4 | 3086 | 3110.5 | 3175 | 3228 | 3338 | 3478 | 3948 | 4038 |
| SiO ₂ | 53.45 | 55.08 | 54.29 | 54.24 | 55.70 | 54.58 | 54.24 | 54.59 | 54.51 | 55.46 | 53.39 | 54.95 | 54.34 |
| TiO ₂ | 0.10 | 0.13 | 0.10 | 0.12 | 0.11 | 0.29 | 0.26 | 0.16 | 0.07 | 0.20 | 0.11 | 0.89 | 0.51 |
| Al ₂ O ₃ | 0.95 | 0.86 | 0.99 | 1.04 | 1.07 | 0.77 | 0.90 | 0.66 | 1.03 | 0.71 | 0.85 | 12.22 | 16.57 |
| FeO | 14.13 | 13.95 | 13.81 | 12.87 | 12.26 | 15.93 | 16.65 | 14.65 | 13.08 | 12.53 | 15.16 | 0.27 | 0.35 |
| MnO | 0.39 | 0.30 | 0.31 | 0.36 | 0.38 | 0.41 | 0.41 | 0.33 | 0.30 | 0.32 | 0.42 | 0.27 | 0.29 |
| MgO | 29.02 | 31.90 | 31.06 | 27.81 | 28.81 | 25.93 | 25.42 | 27.61 | 28.37 | 28.61 | 28.02 | 25.99 | 28.73 |
| CaO | 1.57 | 1.22 | 2.04 | 2.12 | 1.60 | 1.82 | 1.68 | 2.12 | 1.51 | 1.78 | 2.53 | 2.11 | 1.64 |
| Na ₂ O | 0.08 | | | 0.22 | 0.15 | | | | | 0.12 | | | |
| K ₂ O | | | | | | | | | | 0.06 | | | |
| V ₂ O ₃ | | | | | | | | | | | | 0.06 | |
| Cr ₂ O ₃ | | | | | | | | | | | | 0.07 | |
| CoO | | | | | | | | | | | | | |
| NiO | | | | | | | | | | | | | |
| ZnO | | | | | | | | | | | | | |
| Total | 99.68 | 103.59 | 102.80 | 98.80 | 100.11 | 99.69 | 99.61 | 99.39 | 99.61 | 99.48 | 99.68 | 99.70 | 99.81 |
| Si | 1.933 | 1.912 | 1.905 | 1.966 | 1.979 | 1.982 | 1.979 | 1.976 | 1.961 | 1.985 | 1.940 | 1.967 | 1.967 |
| Ti | 0.003 | 0.003 | 0.003 | 0.003 | 0.003 | 0.008 | 0.008 | 0.007 | 0.004 | 0.002 | 0.005 | 0.003 | 0.037 |
| Al | 0.040 | 0.035 | 0.041 | 0.044 | 0.045 | 0.033 | 0.039 | 0.028 | 0.044 | 0.030 | 0.036 | 0.037 | 0.373 |
| Fe | 0.427 | 0.405 | 0.405 | 0.390 | 0.364 | 0.484 | 0.508 | 0.444 | 0.394 | 0.375 | 0.461 | 0.366 | 0.505 |
| Mn | 0.012 | 0.009 | 0.009 | 0.011 | 0.011 | 0.012 | 0.013 | 0.010 | 0.009 | 0.010 | 0.013 | 0.008 | 0.009 |
| Mg | 1.565 | 1.651 | 1.624 | 1.503 | 1.526 | 1.404 | 1.382 | 1.490 | 1.521 | 1.527 | 1.517 | 1.528 | 1.513 |
| Ca | 0.061 | 0.045 | 0.077 | 0.082 | 0.061 | 0.071 | 0.065 | 0.049 | 0.082 | 0.058 | 0.069 | 0.097 | 0.082 |
| Na | 0.005 | | | 0.015 | 0.010 | | | | | 0.008 | 0.008 | 0.003 | 0.062 |
| K | | | | | | | | | | | | | |
| V | | | | | | | | | | | | | |
| Cr | | | | | | | | | | | | | |
| Co | | | | | | | | | | | | | |
| Ni | 0.004 | 0.003 | | | | | | | 0.001 | 0.001 | 0.002 | 0.002 | 0.002 |
| Zn | | | | | | | | | 0.001 | 0.001 | 0.002 | 0.002 | 0.002 |
| Fs | 20.80 | 19.28 | 19.23 | 19.75 | 18.66 | 24.71 | 70.69 | 75.14 | 76.16 | 77.91 | 22.52 | 18.38 | 19.15 |
| En | 76.23 | 78.58 | 77.11 | 76.10 | 78.22 | 71.67 | 25.98 | 22.39 | 19.73 | 19.13 | 74.11 | 76.75 | 77.67 |
| Wo | 2.97 | 2.14 | 3.66 | 4.15 | 3.13 | 3.62 | 3.32 | 2.47 | 4.11 | 2.96 | 3.37 | 4.87 | 3.18 |
| f# | 21.44 | 20.05 | 20.31 | 20.60 | 19.26 | 26.10 | 26.88 | 22.96 | 20.57 | 19.72 | 23.29 | 19.32 | 19.80 |

Note: Cation numbers are normalized to 6 oxygens, f# = 100 × Fe/(Fe + Mg), other symbols are as in Table 3.

Table 5. Chemical composition (wt %) of clinopyroxene from rocks of the Western Pansky Tundra intrusion

| Component | yuk-39 | yuk-40 | yuk-41 | yuk-44 | yuk-43 | yuk-50 | yuk-51 | yuk-31B | yuk-31A | yuk-14A | yuk-70 | yuk-47 |
|--------------------------------|---------|--------|---------|---------|-------------|---------|-------------|---------|-----------|-----------|-----------|---------|
| | gn pabc | n pbCa | t poCab | gn pabc | ol-gn paboC | gn pabc | ol-gn paboC | gn pabc | ol-n pboc | ol-n pboc | ol-n pboc | gn pabc |
| SiO ₂ | 54.39 | 53.12 | 53.23 | 53.49 | 53.38 | 52.65 | 53.33 | 52.72 | 53.01 | 53.40 | 52.50 | 53.62 |
| TiO ₂ | 0.24 | 0.35 | 0.26 | 0.26 | 0.21 | 0.22 | 0.19 | 0.22 | 0.20 | 0.33 | 0.24 | 0.22 |
| Al ₂ O ₃ | 1.53 | 1.78 | 1.90 | 1.79 | 1.98 | 1.75 | 1.66 | 1.79 | 1.66 | 1.78 | 1.78 | 1.91 |
| FeO | 6.79 | 6.03 | 5.63 | 5.16 | 5.18 | 4.94 | 5.83 | 5.03 | 5.63 | 6.19 | 5.88 | 5.38 |
| MnO | 0.21 | 0.19 | 0.12 | 0.20 | 0.16 | 0.16 | 0.20 | 0.22 | 0.20 | 0.18 | 0.23 | 0.17 |
| MgO | 18.92 | 16.34 | 16.70 | 16.72 | 17.24 | 16.29 | 17.05 | 16.25 | 16.58 | 18.02 | 16.26 | 16.38 |
| CaO | 19.78 | 22.56 | 22.63 | 22.77 | 22.24 | 22.62 | 21.96 | 22.50 | 22.60 | 20.70 | 22.60 | 22.69 |
| Na ₂ O | 0.14 | 0.22 | 0.18 | 0.22 | 0.23 | 0.24 | 0.24 | 0.26 | 0.25 | 0.18 | 0.19 | 0.18 |
| K ₂ O | 0.01 | 0.01 | 0.01 | 0.01 | 0.01 | 0.01 | 0.01 | 0.01 | 0.01 | 0.01 | 0.01 | 0.00 |
| V ₂ O ₃ | 0.01 | 0.10 | 0.10 | 0.10 | 0.02 | 0.02 | 0.09 | 0.05 | 0.11 | 0.04 | 0.04 | 0.07 |
| Cr ₂ O ₃ | 0.00 | 0.06 | 0.05 | 0.07 | 0.03 | 0.04 | 0.04 | 0.07 | 0.04 | 0.01 | 0.01 | 0.06 |
| NiO | 0.11 | 0.01 | 0.06 | 0.01 | 0.02 | 0.01 | 0.03 | 0.02 | 0.19 | 0.04 | 0.12 | 0.02 |
| ZnO | 0.03 | 0.02 | 0.01 | 0.08 | 0.08 | 0.03 | 0.03 | 0.02 | 0.04 | 0.01 | 0.08 | 0.43 |
| Total | 102.02 | 100.89 | 100.85 | 100.75 | 100.75 | 99.07 | 100.65 | 99.11 | 100.49 | 100.89 | 99.89 | 101.15 |
| Si | 1.951 | 1.942 | 1.941 | 1.949 | 1.942 | 1.950 | 1.948 | 1.952 | 1.944 | 1.941 | 1.939 | 1.953 |
| Ti | 0.007 | 0.010 | 0.007 | 0.007 | 0.006 | 0.006 | 0.005 | 0.006 | 0.006 | 0.009 | 0.007 | 0.006 |
| Al | 0.065 | 0.077 | 0.082 | 0.077 | 0.085 | 0.077 | 0.077 | 0.078 | 0.072 | 0.076 | 0.077 | 0.082 |
| Fe | 0.204 | 0.184 | 0.172 | 0.157 | 0.158 | 0.153 | 0.178 | 0.156 | 0.173 | 0.188 | 0.182 | 0.164 |
| Mn | 0.006 | 0.006 | 0.004 | 0.006 | 0.005 | 0.005 | 0.005 | 0.006 | 0.007 | 0.006 | 0.007 | 0.005 |
| Mg | 1.012 | 0.890 | 0.908 | 0.908 | 0.935 | 0.899 | 0.928 | 0.897 | 0.906 | 0.976 | 0.896 | 0.890 |
| Ca | 0.760 | 0.884 | 0.884 | 0.889 | 0.867 | 0.898 | 0.859 | 0.893 | 0.880 | 0.806 | 0.895 | 0.886 |
| Na | 0.010 | 0.015 | 0.013 | 0.015 | 0.016 | 0.016 | 0.017 | 0.017 | 0.018 | 0.013 | 0.014 | 0.013 |
| K | | | | | | | 0.001 | 0.003 | 0.002 | 0.003 | 0.001 | 0.001 |
| V | 0.003 | 0.003 | 0.002 | 0.002 | 0.002 | 0.001 | 0.001 | 0.002 | 0.002 | 0.003 | 0.002 | 0.002 |
| Cr | 0.002 | 0.002 | 0.002 | 0.002 | 0.001 | 0.001 | 0.001 | 0.002 | 0.001 | 0.001 | 0.002 | 0.002 |
| Ni | 0.003 | 0.001 | 0.001 | 0.001 | 0.001 | 0.001 | 0.001 | 0.006 | 0.006 | 0.001 | 0.003 | 0.001 |
| Zn | 0.001 | 0.001 | 0.001 | 0.002 | 0.002 | 0.001 | 0.001 | 0.001 | 0.001 | 0.001 | 0.002 | 0.001 |
| Fs | 10.32 | 9.40 | 8.76 | 8.03 | 8.06 | 7.85 | 9.06 | 8.02 | 8.83 | 9.54 | 9.22 | 8.45 |
| En | 51.21 | 45.45 | 46.23 | 46.47 | 47.70 | 46.10 | 47.23 | 46.09 | 46.25 | 49.54 | 45.41 | 45.88 |
| Wo | 38.46 | 45.15 | 45.01 | 45.50 | 44.23 | 46.05 | 43.72 | 45.89 | 44.92 | 40.91 | 45.36 | 45.67 |
| f# | 16.78 | 17.13 | 15.93 | 14.74 | 14.46 | 14.54 | 16.09 | 14.81 | 16.03 | 16.15 | 16.88 | 15.56 |

Table 5. (Contd.)

| Component | yuk-55 | yuk-71 | yuk-72 | yuk-73 | yuk-74 | yuk-75 | yuk-76 | yuk-77 | yuk-78 | yuk-79 | yuk-80 |
|--------------------------------|---------|---------|---------|-----------|---------|---------|---------|---------|---------|---------|---------|
| | gn pabC | gn pabC | gn pabC | mg pab#mC | gn pabC |
| SiO ₂ | 52.81 | 52.68 | 52.80 | 51.36 | 52.21 | 51.57 | 52.20 | 52.74 | 52.30 | 52.60 | 52.19 |
| TiO ₂ | 0.25 | 0.32 | 0.27 | 0.46 | 0.51 | 0.52 | 0.42 | 0.35 | 0.44 | 0.47 | 0.37 |
| Al ₂ O ₃ | 1.65 | 1.81 | 1.74 | 2.39 | 1.64 | 1.99 | 1.66 | 1.29 | 1.53 | 1.53 | 1.75 |
| FeO | 6.75 | 6.74 | 6.94 | 11.35 | 8.50 | 9.82 | 8.72 | 7.67 | 7.43 | 7.91 | 8.74 |
| MnO | 0.16 | 0.16 | 0.19 | 0.30 | 0.23 | 0.24 | 0.15 | 0.20 | 0.21 | 0.20 | 0.31 |
| MgO | 16.13 | 15.60 | 15.92 | 14.13 | 14.94 | 14.31 | 14.71 | 15.84 | 15.48 | 15.07 | 14.98 |
| CaO | 20.97 | 22.05 | 22.21 | 19.58 | 22.14 | 21.01 | 21.71 | 21.37 | 22.33 | 21.94 | 21.02 |
| Na ₂ O | 0.20 | 0.32 | 0.21 | 0.30 | 0.23 | 0.22 | 0.28 | 0.25 | 0.24 | 0.26 | 0.26 |
| K ₂ O | 0.01 | 0.05 | 0.01 | 0.02 | 0.01 | 0.04 | 0.09 | 0.03 | 0.10 | 0.06 | 0.13 |
| V ₂ O ₃ | 0.15 | 0.05 | 0.04 | 0.04 | 0.01 | 0.01 | 0.01 | 0.01 | 0.01 | 0.02 | 0.04 |
| Cr ₂ O ₃ | 0.13 | 0.02 | 0.17 | | | | | | 0.12 | 0.05 | 0.05 |
| NiO | | | | | | | | | 0.12 | 0.05 | 0.13 |
| ZnO | | | | | | | | | 0.12 | 0.01 | |
| Total | 99.20 | 99.76 | 100.50 | 99.90 | 100.44 | 99.76 | 99.98 | 99.97 | 100.13 | 100.06 | 99.97 |
| Si | 1.960 | 1.950 | 1.944 | 1.929 | 1.938 | 1.934 | 1.946 | 1.955 | 1.940 | 1.952 | 1.944 |
| Ti | 0.007 | 0.009 | 0.008 | 0.013 | 0.014 | 0.015 | 0.012 | 0.010 | 0.012 | 0.013 | 0.010 |
| Al | 0.072 | 0.079 | 0.075 | 0.106 | 0.072 | 0.088 | 0.073 | 0.056 | 0.067 | 0.067 | 0.077 |
| Fe | 0.209 | 0.209 | 0.214 | 0.356 | 0.264 | 0.308 | 0.272 | 0.234 | 0.230 | 0.245 | 0.272 |
| Mn | 0.005 | 0.005 | 0.006 | 0.009 | 0.007 | 0.007 | 0.005 | 0.005 | 0.007 | 0.006 | 0.010 |
| Mg | 0.892 | 0.861 | 0.874 | 0.791 | 0.827 | 0.800 | 0.818 | 0.876 | 0.856 | 0.833 | 0.832 |
| Ca | 0.834 | 0.874 | 0.876 | 0.788 | 0.880 | 0.844 | 0.867 | 0.849 | 0.887 | 0.872 | 0.839 |
| Na | 0.014 | 0.023 | 0.015 | 0.022 | 0.016 | 0.016 | 0.020 | 0.018 | 0.017 | 0.019 | 0.019 |
| K | | | | 0.001 | 0.003 | 0.001 | 0.001 | 0.001 | 0.001 | 0.003 | 0.004 |
| V | 0.004 | 0.002 | 0.001 | 0.005 | | | 0.003 | 0.003 | 0.006 | 0.002 | 0.001 |
| Cr | | | | | | | | 0.003 | 0.003 | 0.002 | 0.001 |
| Ni | 0.004 | | | | | | | | | | 0.001 |
| Zn | | | | | | | | | | | 0.003 |
| F _s | 10.80 | 10.75 | 10.90 | 18.40 | 13.39 | 15.78 | 13.90 | 0.23 | 11.66 | 12.56 | 14.00 |
| E _n | 46.10 | 44.29 | 44.50 | 40.88 | 41.96 | 40.98 | 41.80 | 50.67 | 43.39 | 42.72 | 42.82 |
| W _o | 43.10 | 44.96 | 44.60 | 40.72 | 44.65 | 43.24 | 44.30 | 49.10 | 44.96 | 44.72 | 43.18 |
| f# | 18.98 | 19.53 | 19.67 | 31.04 | 24.20 | 27.80 | 24.95 | 0.45 | 21.18 | 22.73 | 24.64 |

Table 5. (Contd.)

| Component | yuk-81 | yuk-82 | yuk-83 | yuk-84 | yuk-85 | yuk-86 | yuk-87 | ma-44 | ma-43 | yuk-87 | ma-24b | ma-19b |
|--------------------------------|-----------|---------|---------|---------|---------|---------|---------|---------|---------|---------|---------|---------|
| | mg pab#mC | gn pabC |
| 2190 | 2334 | 2384 | 2434 | 2512 | 2750 | 2781 | 2836 | 2860 | 2865 | 2879.8 | 2900.4 | |
| SiO ₂ | 50.57 | 51.24 | 52.36 | 51.28 | 52.69 | 52.12 | 52.82 | 52.78 | 52.67 | 52.43 | 53.01 | 52.86 |
| TiO ₂ | 0.44 | 0.46 | 0.37 | 0.73 | 0.51 | 0.55 | 1.72 | 1.79 | 1.73 | 0.31 | 0.56 | 0.41 |
| Al ₂ O ₃ | 1.46 | 1.43 | 1.86 | 1.82 | 1.54 | 1.72 | 8.75 | 7.03 | 1.28 | 1.42 | 1.64 | 1.63 |
| FeO | 14.53 | 10.42 | 8.82 | 9.11 | 8.54 | 8.75 | 0.12 | 0.16 | 0.16 | 7.41 | 6.98 | 6.52 |
| MnO | 0.33 | 0.27 | 0.16 | 0.16 | 0.12 | 0.16 | 14.54 | 16.87 | 0.18 | 0.20 | 0.13 | 0.39 |
| MgO | 11.36 | 13.50 | 14.22 | 13.88 | 15.08 | 22.16 | 21.90 | 19.93 | 16.07 | 15.79 | 15.46 | 15.37 |
| CaO | 20.56 | 21.27 | 21.38 | 22.16 | 22.23 | 21.64 | 21.66 | 21.64 | 21.66 | 22.19 | 21.73 | 22.32 |
| Na ₂ O | 0.22 | 0.28 | 0.28 | 0.29 | 0.26 | 0.29 | 0.29 | 0.29 | 0.24 | 0.15 | 0.25 | 0.14 |
| K ₂ O | 0.00 | | 0.01 | | 0.01 | | 0.02 | | | | | |
| V ₂ O ₃ | | 0.03 | 0.04 | 0.13 | 0.04 | 0.15 | | | | | | |
| Cr ₂ O ₃ | 0.02 | 0.03 | 0.03 | 0.01 | 0.09 | 0.05 | 0.15 | 0.08 | 0.08 | 0.11 | 0.05 | 0.09 |
| NiO | | 0.12 | 0.07 | 0.01 | 0.05 | 0.14 | | | | | | |
| ZnO | | 0.09 | | 0.03 | 0.02 | | | | | 0.11 | 0.11 | |
| Total | 99.48 | 99.14 | 99.60 | 99.61 | 101.19 | 100.33 | 99.04 | 100.09 | 99.55 | 99.68 | 99.25 | 100.04 |
| Si | 1.945 | 1.945 | 1.956 | 1.928 | 1.941 | 1.939 | 1.959 | 1.946 | 1.958 | 1.948 | 1.967 | 1.950 |
| Ti | 0.013 | 0.013 | 0.010 | 0.021 | 0.014 | 0.015 | 0.014 | 0.014 | 0.009 | 0.016 | 0.010 | 0.011 |
| Al | 0.066 | 0.064 | 0.082 | 0.080 | 0.067 | 0.076 | 0.078 | 0.075 | 0.056 | 0.062 | 0.072 | 0.071 |
| Fe | 0.467 | 0.331 | 0.276 | 0.286 | 0.263 | 0.272 | 0.218 | 0.211 | 0.230 | 0.217 | 0.202 | 0.201 |
| Mn | 0.011 | 0.009 | 0.005 | 0.005 | 0.004 | 0.005 | 0.005 | 0.005 | 0.006 | 0.004 | 0.012 | 0.005 |
| Mg | 0.651 | 0.764 | 0.792 | 0.778 | 0.828 | 0.806 | 0.933 | 0.883 | 0.875 | 0.856 | 0.850 | 0.860 |
| Ca | 0.847 | 0.865 | 0.856 | 0.893 | 0.877 | 0.873 | 0.792 | 0.855 | 0.863 | 0.883 | 0.864 | 0.883 |
| Na | 0.017 | 0.021 | 0.020 | 0.021 | 0.019 | 0.021 | 0.021 | 0.017 | 0.017 | 0.018 | 0.010 | 0.039 |
| K | | | | | 0.001 | 0.001 | 0.005 | 0.004 | 0.002 | 0.002 | 0.003 | |
| V | 0.001 | 0.001 | 0.001 | 0.004 | 0.001 | 0.003 | 0.001 | 0.005 | 0.004 | 0.002 | 0.001 | 0.003 |
| Cr | 0.001 | 0.001 | 0.001 | 0.002 | 0.001 | 0.001 | 0.004 | 0.004 | 0.002 | 0.002 | 0.003 | |
| Ni | | 0.004 | | | | | | | | | | |
| Zn | | 0.003 | | 0.001 | | | | | | | | |
| Fs | 23.77 | 16.89 | 14.35 | 14.61 | 13.36 | 13.94 | 11.22 | 10.83 | 11.69 | 11.09 | 10.54 | 10.34 |
| En | 33.13 | 38.98 | 41.16 | 39.75 | 42.07 | 41.31 | 48.02 | 45.31 | 44.46 | 43.76 | 44.36 | 44.24 |
| Wo | 43.10 | 44.13 | 44.49 | 45.63 | 44.56 | 44.75 | 40.76 | 43.87 | 43.85 | 45.14 | 45.09 | 45.42 |
| f# | 41.77 | 30.23 | 25.84 | 26.88 | 24.11 | 25.23 | 18.94 | 19.29 | 20.81 | 20.22 | 19.20 | 18.94 |

Table 5. (Contd.)

| Component | ma-14/1 | ma-18c | ma-70 | ma-38 | 139/21 | 139/23 | 139/28 | 139/31 | 1300/4880 | 3293/35.0 | 3293/85.85 |
|--------------------------------|---------|---------|---------|---------|---------|---------|---------|---------|-----------|-----------|------------|
| | gn pabC | an pCab | gn pabC | gn pbaC | gn pbC |
| | 2902 | 2903.5 | 2915 | 2942.4 | 3086 | 3110.5 | 3130 | 3228 | 3338 | 3948 | 4038 |
| SiO ₂ | 52.72 | 56.02 | 53.80 | 52.54 | 51.91 | 51.93 | 51.85 | 52.33 | 53.77 | 53.33 | 51.91 |
| TiO ₂ | 0.17 | 0.08 | 0.43 | 0.47 | 0.56 | 0.49 | 0.42 | 0.39 | 1.29 | 1.29 | 1.89 |
| Al ₂ O ₃ | 1.71 | 2.54 | 1.57 | 1.63 | 1.54 | 1.51 | 1.29 | 1.34 | 6.72 | 8.95 | 6.71 |
| FeO | 5.46 | 7.73 | 5.15 | 7.22 | 7.75 | 7.34 | 6.02 | 6.72 | 0.28 | 0.27 | 0.19 |
| MnO | 0.23 | 0.23 | 0.16 | 0.23 | 0.22 | 0.20 | 0.22 | 0.23 | 16.67 | 17.37 | 17.15 |
| MgO | 18.27 | 18.43 | 17.72 | 14.94 | 15.20 | 16.11 | 22.11 | 21.42 | 22.22 | 21.24 | 21.59 |
| CaO | 21.23 | 12.68 | 20.54 | 22.04 | 0.31 | 0.26 | 0.34 | 0.24 | 0.25 | 0.29 | 0.51 |
| Na ₂ O | 0.20 | 0.18 | 0.31 | 0.26 | 0.34 | 0.24 | 0.25 | 0.25 | 0.34 | 0.51 | 0.20 |
| K ₂ O | 0.05 | | | | | | | | 0.08 | 0.01 | 0.01 |
| V ₂ O ₃ | 0.06 | | | | | | | | | | |
| Cr ₂ O ₃ | 0.08 | | | | | | | | | | |
| NiO | 0.28 | | | | | | | | | | |
| ZnO | | | | | | | | | | | |
| Total | 100.41 | 97.92 | 99.72 | 99.32 | 99.70 | 99.37 | 99.07 | 100.08 | 99.69 | 99.92 | 99.65 |
| Si | 1.928 | 2.043 | 1.966 | 1.958 | 1.937 | 1.937 | 1.934 | 1.932 | 1.977 | 1.972 | 1.925 |
| Ti | 0.005 | 0.002 | 0.012 | 0.013 | 0.016 | 0.014 | 0.012 | 0.011 | | | |
| Al | 0.074 | 0.109 | 0.068 | 0.072 | 0.068 | 0.066 | 0.057 | 0.058 | | | |
| Fe | 0.167 | 0.236 | 0.157 | 0.225 | 0.242 | 0.229 | 0.188 | 0.207 | | | |
| Mn | 0.007 | 0.007 | 0.005 | 0.007 | 0.007 | 0.006 | 0.007 | 0.007 | | | |
| Mg | 0.996 | 1.002 | 0.965 | 0.830 | 0.845 | 0.896 | 0.927 | 0.956 | | | |
| Ca | 0.832 | 0.495 | 0.804 | 0.880 | 0.884 | 0.856 | 0.888 | 0.840 | | | |
| Na | 0.014 | 0.012 | 0.022 | 0.019 | 0.025 | 0.017 | 0.018 | 0.021 | | | |
| K | 0.002 | | | | | | | | | | |
| V | 0.002 | | | | | | | | | | |
| Cr | 0.002 | | | | | | | | | | |
| Ni | 0.008 | | | | | | | | | | |
| Zn | | | | | | | | | | | |
| <i>Fs</i> | 8.37 | 13.62 | 8.15 | 11.63 | 2.64 | 2.41 | 3.38 | 3.11 | 10.76 | 14.25 | 10.33 |
| <i>En</i> | 49.92 | 57.82 | 50.10 | 42.89 | 12.28 | 11.56 | 9.39 | 10.33 | 48.34 | 47.12 | 47.07 |
| <i>Wo</i> | 41.70 | 28.56 | 41.74 | 45.48 | 44.85 | 43.21 | 44.33 | 41.94 | 40.90 | 38.63 | 42.60 |
| <i>f</i> # | 14.36 | 19.06 | 13.99 | 21.33 | 22.26 | 20.36 | 16.86 | 17.80 | 18.21 | 23.22 | 17.99 |

Note: Cation numbers are normalized to 6 oxygens, # = 100 × Fe/(Fe + Mg), other symbols are as in Table 3.

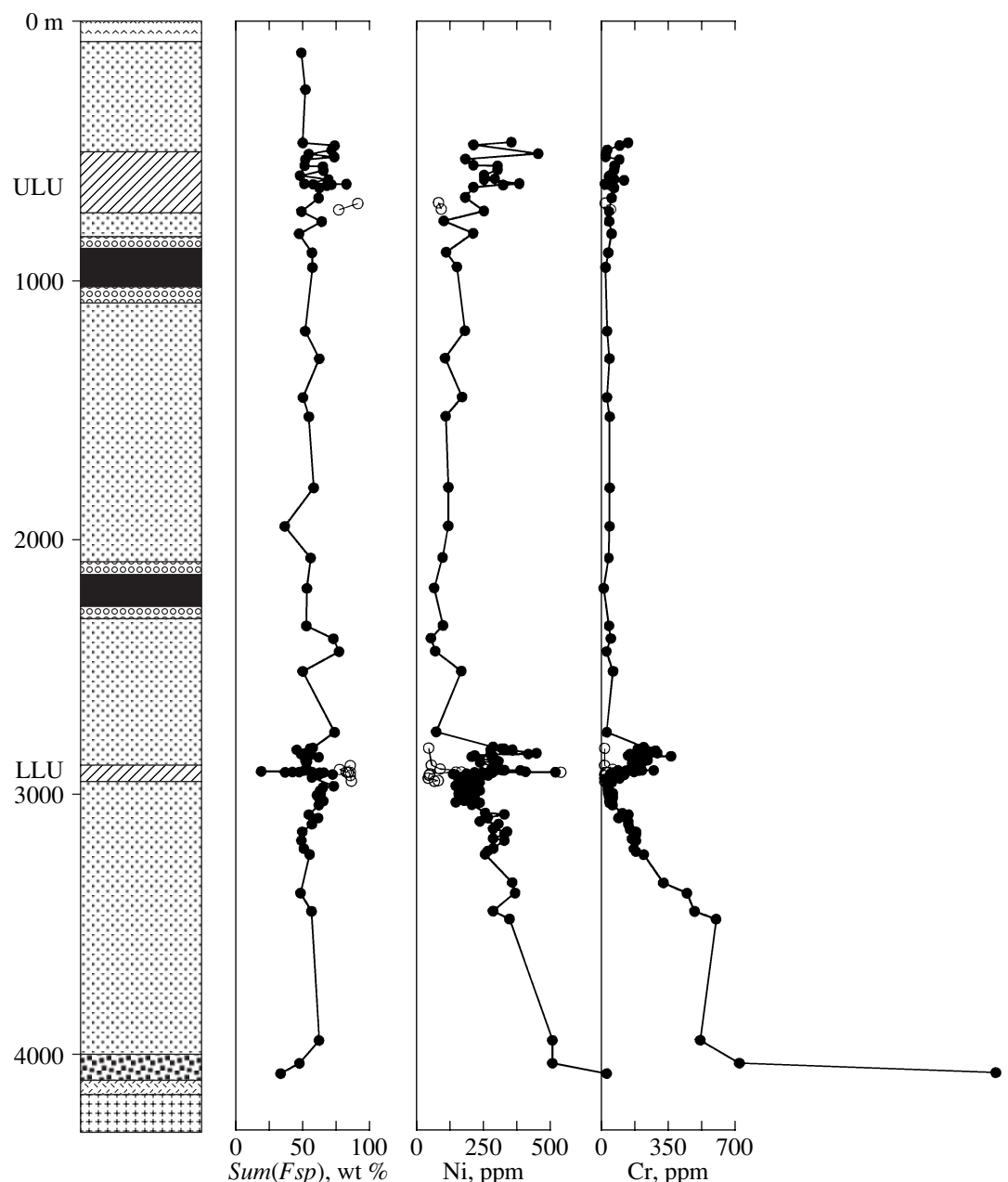


Fig. 5. Variations in the concentrations of minor elements over the vertical section of the intrusion (Fig. 1, line I-I). See Fig. 3 for symbol explanations. Open circles are leucogabbro and anorthosite, other mafic rocks are shown with solid circles. The chart is based on data from Table 6.

The viewpoint that there is a single, Fedorovo-Pansky, massif (Dokuchaeva, 1994) occurs in conflict with the fact that the surmised parts of this massif reveal different directions of the advance of their solidification fronts. The magmatic sequences of the Eastern Pansky Tundra and Fedorovo Tundra massifs were built up predominantly from bottom to top, as is inferred from the direction of the cryptic layering (Alapieti and Lahtinen, 1989) and macrolayering (Alapieti and Lahtinen, 1989; Odinets, 1971). The latter type of layering is pronounced as a systematic upward alteration of norite,

gabbronorite, gabbro, and magnetite gabbro zones (the latter is present only in the Fedorovo Tundra intrusion). The situation is different in the Western Pansky Tundra intrusion, which is located between the two massifs (Fig. 1). It does not have pronounced macrolayering, which would permit one to reliably identify the bottom and roof of the pluton (Fig. 3). The massif does not exhibit any evolutionary trend in the compositions of pyroxenes and plagioclase, with such trends commonly recognized as an inherent feature of layered massifs. The sinusoidal character of variations in the chemistry

Table 6. Concentrations (ppm) of Cr and Ni in rocks of the Western Pansky Tundra intrusion

| Sample | Rock | Depth | Cr | Ni | Sample | Rock | Depth | Cr | Ni |
|-----------|-------------|--------|-----|-----|-----------|---------|--------|-----|------|
| yuk-39 | gn pabC | 475 | 120 | 340 | 5v/95.63 | gn pabC | 2900.6 | 180 | 3100 |
| yuk-40 | n pbC | 485 | 77 | 200 | 5v/95.76 | gn pabC | 2900.8 | 260 | 560 |
| yuk-41 | t poCab | 502.5 | 14 | 640 | 5v/95.83 | gn pabC | 2900.8 | 200 | 8100 |
| yuk-49a | t poCab | 518 | 7 | 440 | 5v/95.9 | gn pabC | 2900.9 | 190 | 1000 |
| yuk-48 | t poCab | 528.5 | 6 | 540 | 5v/96.08 | gn pabC | 2901.1 | 180 | 310 |
| yuk-42 | gn pabC | 539.5 | 75 | 170 | 5v/96.23 | gn pabC | 2901.2 | 170 | 290 |
| yuk-44 | gn pabC | 562 | 51 | 200 | 5v/96.44 | gn pabC | 2901.4 | 160 | 320 |
| yuk-43 | ol-gn paboC | 565.5 | 52 | 290 | 5v/96.66 | gn pabC | 2901.7 | 120 | 320 |
| yuk-50 | ol-gn paboC | 581 | 48 | 290 | 5v/96.71 | gn pabC | 2901.7 | 150 | 380 |
| yuk-51 | gn pabC | 600 | 25 | 240 | 5v/96.78 | gn pabC | 2901.8 | 180 | 270 |
| yuk-31v | ol-gn paboC | 614.5 | 50 | 280 | 5v/97.5 | gn pabC | 2902.5 | 150 | 270 |
| yuk-31a | gn pabC | 618 | 100 | 240 | 5v/99.0a | an pCab | 2904.0 | 91 | 360 |
| yuk-14v | ol-lg pCoab | 632 | 2 | 370 | 5v/101.53 | gn pabC | 2906.5 | 110 | 400 |
| yuk-45 | ol-n pboC | 633 | 31 | 600 | 5v/101.7 | an pCab | 2906.7 | 120 | 1500 |
| yuk-46 | ol-lg pCoab | 634 | 3 | 630 | 5v/101.87 | n pbC | 2906.9 | 160 | 9200 |
| yuk-70 | ol-n pboC | 638 | 34 | 310 | 5v/102.09 | an pCab | 2907.1 | 16 | 280 |
| yuk-47 | gn pabC | 647 | 48 | 200 | 5v/102.36 | n pbC | 2907.4 | 75 | 670 |
| yuk-55 | gn pabC | 685 | 36 | 170 | 5v/102.44 | n pbC | 2907.4 | 120 | 630 |
| yuk-54 | an pCab | 706 | 4 | 70 | 5v/102.54 | n pbC | 2907.5 | 78 | 5100 |
| yuk-53 | an pCab | 730 | 31 | 80 | 5v/122.7 | gn pabC | 2927.7 | 67 | 190 |
| yuk-52 | gn pabC | 737 | 23 | 240 | 5v/124.9 | gn pabC | 2929.9 | 84 | 210 |
| yuk-71 | gn pabC | 775 | 24 | 90 | 5v/127 | gn pabC | 2932.0 | 85 | 220 |
| yuk-72 | gn pabC | 822 | 37 | 200 | 5v/128 | an pCab | 2933.0 | 10 | 37 |
| yuk-73 | mg pab#mC | 894 | 21 | 99 | 5v/130.2 | an pCab | 2935.2 | 14 | 150 |
| yuk-121/5 | mg pab#mC | 950 | 8 | 140 | 5v/136.5 | an pCab | 2941.5 | 10 | 74 |
| yuk-74 | gn pabC | 1194 | 15 | 170 | 5v/139.8 | an pCab | 2944.8 | 10 | 60 |
| yuk-75 | gn pabC | 1300 | 28 | 96 | 5v/142.9 | gn pabC | 2947.9 | 46 | 230 |
| yuk-76 | gn pabC | 1450 | 16 | 160 | 5v/151.4 | gn pabC | 2956.4 | 30 | 170 |
| yuk-76 | gn pabC | 1450 | 16 | 160 | 5v/156 | gn pabC | 2961.0 | 20 | 140 |
| yuk-77 | gn pabC | 1525 | 29 | 99 | 5v/162.1 | gn pabC | 2967.1 | 30 | 200 |
| yuk-78 | gn pabC | 1800 | 32 | 110 | 5v/169.6a | gn pabC | 2974.6 | 20 | 170 |
| yuk-79 | gn pabC | 1950 | 32 | 110 | 5v/174.9 | gn pabC | 2979.9 | 30 | 230 |
| yuk-80 | gn pabC | 2072 | 26 | 89 | 5v/178.8 | gn pabC | 2983.8 | 30 | 190 |
| yuk-81 | mg pab#mC | 2190 | 3 | 59 | 5v/183.7 | gn pabC | 2988.7 | 50 | 210 |
| yuk-82 | gn pabC | 2334 | 30 | 92 | 5v/188 | gn pabC | 2993.0 | 30 | 150 |
| yuk-83 | gn pabC | 2384 | 40 | 47 | 5v/192 | gn pabC | 2997.0 | 30 | 180 |
| yuk-84 | gn pabC | 2434 | 18 | 63 | 5v/197.3 | gn pabC | 3002.3 | 50 | 210 |
| yuk-85 | gn pabC | 2512 | 52 | 160 | 5v/204.7 | gn pabC | 3009.7 | 50 | 210 |
| yuk-86 | gn pabC | 2750 | 20 | 67 | 5v/211.9 | gn pabC | 3016.9 | 40 | 190 |
| 5v/5.2 | gn pabC | 2810.2 | 210 | 280 | 5v/214.3 | gn pabC | 3019.3 | 40 | 170 |
| 5v/9.91 | gn pabC | 2814.9 | 10 | 39 | 5v/220.4 | gn pabC | 3025.4 | 30 | 140 |
| 5v/11 | gn pabC | 2816 | 210 | 310 | 5v/223 | gn pabC | 3028 | 40 | 230 |
| 5v/12.01 | an pCab | 2817 | 180 | 320 | 5v/230 | gn pabC | 3035 | 50 | 200 |
| 5v/13.2 | gn pabC | 2818.2 | 180 | 320 | ka-139/19 | gn pabC | 3067 | 100 | 250 |
| 5v/15 | gn pabC | 2820 | 220 | 350 | ka-139/20 | gn pabC | 3073 | 130 | 320 |

Table 6. (Contd.)

| Sample | Rock | Depth | Cr | Ni | Sample | Rock | Depth | Cr | Ni |
|----------|-------------|--------|-----|-----|------------|---------|-------|------|-----|
| 5v/17.3 | gn pabC | 2822.3 | 190 | 270 | ka-139/21 | gn pabC | 3086 | 81 | 260 |
| 5v/18.6a | gn pabC | 2823.6 | 270 | 350 | ka-139/22 | gn pabC | 3101 | 130 | 230 |
| 5v/23 | gn pabC | 2828 | 250 | 930 | ka-139/23 | gn pabC | 3111 | 130 | 300 |
| 5v/28.8 | gn pabC | 2833.8 | 280 | 440 | ka-139/24 | gn pabC | 3130 | 140 | 280 |
| 5v/32.1I | an pCab | 2837.1 | 140 | 410 | ka-139/25 | gn pabC | 3141 | 170 | 330 |
| 5v/34.7 | gn pabC | 2839.7 | 230 | 270 | ka-139/26 | gn pabC | 3151 | 170 | 320 |
| 5v/38.4 | gn pabC | 2843.4 | 130 | 210 | ka-139/27 | gn pabC | 3168 | 150 | 280 |
| 5v/40.8 | gn pabC | 2845.8 | 350 | 280 | ka-139/28 | gn pabC | 3175 | 170 | 320 |
| 5v/43.6 | gn pabC | 2848.6 | 150 | 200 | ka-139/29 | gn pabC | 3206 | 160 | 280 |
| 5v/52.7 | gn pabC | 2857.7 | 220 | 230 | ka-139/30 | gn pabC | 3216 | 170 | 260 |
| 5v/56.4 | gn pabC | 2861.4 | 230 | 280 | ka-139/31 | gn pabC | 3228 | 210 | 250 |
| 5v/61.3 | gn pabC | 2866.3 | 180 | 300 | 1300/4880 | gn pabC | 3338 | 310 | 350 |
| 5v/61.8 | an pCab | 2866.8 | 210 | 280 | 1312/4920 | gn pabC | 3378 | 430 | 360 |
| 5v/65.9 | gn pabC | 2870.9 | 150 | 230 | 1350/5097 | gn pabC | 3448 | 470 | 280 |
| 5v/76.5 | an pCab | 2881.5 | 10 | 49 | 1110/5120 | gn pabC | 3478 | 580 | 340 |
| 5v/91.3 | an pCab | 2896.3 | 50 | 81 | 3293/35 | gn pabC | 3948 | 500 | 500 |
| 5v/95.1 | an pCab | 2900.1 | 200 | 320 | 3293/85.85 | n pbC | 4038 | 700 | 500 |
| 5v/95.55 | ol-gn paboC | 2900.6 | 78 | 800 | 3293/130 | n pbC | 4078 | 2000 | 700 |

Note: See Table 3 for symbol explanations.

of minerals (as is inferred from both petrochemical parameters of the rocks and microprobe analyses of minerals) leaves uncertain the main direction of the advance of the solidification front during the development of the massif.

It follows that materials available nowadays on the massif provide no valid reasons to interpret the Eastern Pansky Tundra, Western Pansky Tundra, and Fedorovo Tundra intrusions as tectonically separated blocks of the single Fedorovo-Pansky Massif. This problem requires further investigation. Currently, following Odinets (1971) and Kozlov (1973), we believe it is justified to consider the evolutionary history of the Western Pansky Tundra intrusion as that of an independent individual geologic body.

Magnetite Gabbro Bodies as the Crystallization Products of the Residual Melt

The genesis of the magnetite gabbro is a principal problem, because its interpretation is strongly related to the interpretation of all other genetic issues. The two alternative, mutually exclusive interpretations of these rocks are as follows. First, they are syngenetic rocks of the intrusion, which were produced by in-chamber differentiation (Proskuryakov, 1967; Odinets, 1971; Kozlov, 1973). Second, the rocks are foreign and compose sills (Osokin, personal communication) or strongly altered xenoliths. The latter interpretation allows three variants: these are metavolcanics of the

Kuksha suite of the Imandra-Varzuga zone (Borisova *et al.*, 1999), they are gneisses of the Archean basement (Konnikov, personal communication), or the gabbro belongs to a hypothetical prototintrusion, which supposedly existed at the site of the Western Pansky Tundra Massif (Korchagin, personal communication).

In order to resolve this problem, we examined the petrography of the rocks and all details of the compositional variations in rocks and minerals across the strikes of several magnetite gabbro bodies. The analysis of these data convincingly demonstrates that there are no reasons to regard magnetite gabbro bodies in the Western Pansky Tundra layered intrusion as foreign (sills or xenoliths) (Latypov and Chistyakova, 2001a, 2001b). The magnetite gabbro reveals no unsystematic deviations from the surrounding rocks either in their mineralogy or chemistry, and it contains no relict mineral assemblages of the "original" rocks, such as gneisses or metabasalts, whose profound transformations could have produced the magnetite gabbro. At the same time, the original nature of transformed xenoliths from the Archean gneiss basement or metabasalts xenoliths, which do occur in both the Western Pansky Tundra and the Fedorovo Tundra Massif, can be readily distinguished.

A direct indication of the syngenetic nature of magnetite gabbro bodies is the discovered gradual and systematic transitions between the gabbronorite of the massif and magnetite gabbro, because of which the latter rock looks like as an inherent constituent of the plu-

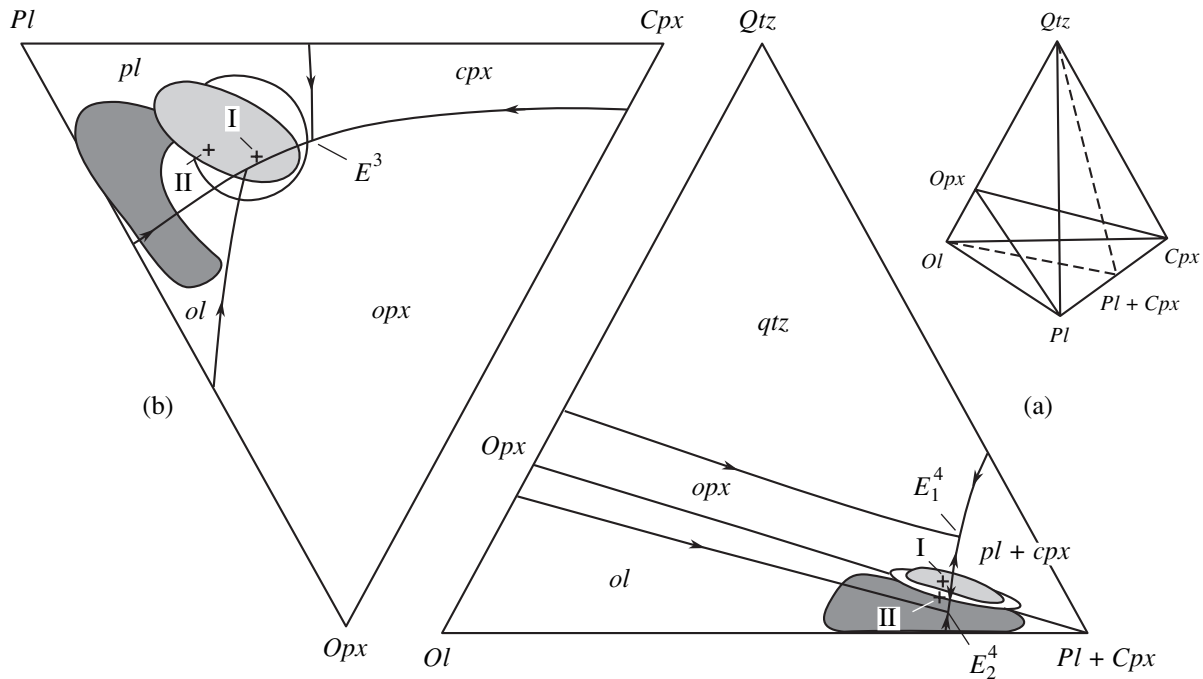


Fig. 6. Compositional fields for the rocks of the intrusion in projection planes of the $Ol^{25-50}-Cpx-Pl^{60-70}-Qtz-H_2O$ isobaric isopleth (projection after Dubrovskii, 1998).

The position of the projection planes in the phase diagram is indicated in the inset. The unshaded field is the gabbronorite of the first intrusive phase, the gray field is the gabbronorite of the second intrusive phase, and the dark field is the olivine-bearing rocks of the ULU. I and II are the parental melt compositions for the first and second intrusive phases, respectively. $E_1^4: Opx + Cpx + Pl + Qtz = L$, $E_2^4: Ol + Opx + Cpx + Pl = L$, $E^3: Opx + Cpx + Pl = L$.

ton (Figs. 3, 4). These transitions are characterized by (1) phase layering, which is pronounced as the replacement of $Pl-Opx-Cpx$ cumulates (gabbronorite), first, by $Pl-Opx-Pig\#-Cpx$ cumulates (gabbronorite with inverted pigeonite) and, then, by $Pl-Opx-Pig\#-Cpx-Mgt$ cumulates (magnetite gabbro with inverted pigeonite); (2) modal layering, which is recognizable by a decrease in the percentage of orthopyroxene (pigeonite) at an increase in the content of clinopyroxene; (3) cryptic layering in the form of a systematic increase in the Fe# of orthopyroxene [from $f(hy) = 22-25\%$ to $40-45\%$], a systematic decrease in the normative plagioclase Ca# [from $An(\text{norm}) = 65-70\%$ to $48-50\%$], and a regular decrease in the concentrations of Cr (from 150–200 to 3–15 ppm) and Ni (from 350 to 90–100 ppm) at a simultaneous increase in the Sr concentration (from 220–250 to 350–400 ppm).

Another argument for the syngenetic origin of the magnetite gabbro is the extremely low Cr concentrations of the rocks (<3 ppm; Latypov and Chistyakova, 2001b), which is absolutely atypical not only of the Kuksha metavolcanics but also of all basaltic volcanics in the Pechenga and Imandra–Varzuga zones (Fedotov, 1985). At the same time, similarly low Cr concentrations serve as a distinguishing feature of ferrogabbro, magnetite gabbro, and gabbronorite in layered intru-

sions, such as the Skaergaard intrusion, Bushveld Complex, and Imandra lopolith, in which these rocks are reportedly the inherent final differentiation products (Wager and Brown, 1967; Zhangurov *et al.*, 1994).

Hence, a complex of data provides convincing evidence that magnetite gabbro bodies are the final products in the in-chamber Fenner differentiation trend of the parental melt of the Western Pansky Tundra intrusion.

Upward Build-up of the Intrusive Succession and Later Dividing of the Chamber into a Series of Smaller Reservoirs

Usually, the build-up direction of the igneous successions in layered mafite–ultramafite plutons can be readily derived from the character of their phase, modal, and cryptic layering (Wager and Brown, 1967). However, these three types of layering are poorly pronounced in the Western Pansky Tundra intrusion (except in its Lower and the Upper Layered Unit). Hence, it is hard to reproduce the direction of the solidification front advance based solely on the chemistry of rocks and minerals (Fig. 3). None of the previously described variants can be directly applied to this intrusion, be it an upward advance, as at Bushveld or Still-

water, or that from the margins to center, as at Skaergaard. The situation is further complicated by the occurrence of olivine-bearing rocks with the least evolved compositions of minerals in the upper, but not lower (as in layered massifs), portion of the intrusion. This fact was many times invoked as an argument for the overturned setting of rocks in the massif. Apparently, these complications were the main reason for a wide spectrum of explanations proposed for the solidification order of the intrusion (Table 1).

This problem was significantly clarified by newly obtained data on the Cr and Ni distribution over the cross section of the intrusion. It is known that the concentrations of these compatible elements in residual liquids should notably decrease because of the incorporation of the elements in early cumulus minerals. In terms of Cr and Ni concentrations, the intrusion is divided into clearly distinct lower and upper parts (Fig. 5). The lower part, which spans the interval from the intrusion floor to LLU, is characterized by a regular upward decrease in the contents of both elements (from 2000 to 50–100 ppm for Cr and from 500 to 125 ppm for Ni), whereas the upper part (from LLU to ULU) displays nearly unvarying Cr and Ni concentrations (Cr = 50–100 ppm and Ni = 100–125 ppm). However, a closer consideration of the distribution of these element revealed a systematic decrease in their concentrations from the inner contact to the center of magnetite gabbro bodies (Fig. 4; see also Latypov and Chistyakova, 2001a, 2001b). The Cr concentration decreases in this direction from 150–200 to 3–15 ppm, and the corresponding values for Ni are 350 and 90–100 ppm.

The data presented above led us to the following conclusions. First, the contacts between the intrusion and Archean gneisses corresponds to the pluton bottom, and, hence, it is reasonable to state that the pluton occurs in a normal setting. Second, it is evident that the magmatic succession was built up in an exact upward direction up to the LLU level. Third, the transition to the upper part of the intrusion should have been marked by some changes in the character of in-chamber differentiation. In our opinion, this was closely related to the crystallization of magnetite gabbro. Attempts to resolve the problem as to where the residual melt was localized that could have produced the magnetite gabbro at different stratigraphic levels of the gabbronorite zone inevitably lead to the idea that the intrusion was connected with several chambers. According to this viewpoint, which was first expressed by Proskuryakov (1967), at this period of time, the chamber should have been divided into a series of smaller subchambers, and the crystallization of their melt has a systematically directed character with a tendency of ending at the central parts of the reservoirs (Latypov and Chistyakova, 2001a, 2001b).

The division mechanism of the chamber into a number of smaller reservoirs remains unclear. As a working hypothesis, it can be proposed that the gradual increase

in the system viscosity due to a temperature decrease in the process of crystallization and the relative enrichment of the system in crystalline phases should have hampered the settling of crystals (in accordance with the Stokes equation). An important role was played therewith by the bonding forces between the crystallizing particles and the surface through which the heat was removed, i.e., the roof and walls of the chamber, as well as its already-solid bottom. A further temperature decrease resulted in the cessation of the settling of crystals, which built a peculiar framework with cells filled by isolated residual melt portions. The resultant cells (subchambers) were oriented in accordance with the overall structural pattern of the massif.

Two Intrusive Phases and the Composition of Their Parental Melts

The scenario proposed above for the evolution of the gabbronorite zone puts forth a very important problem. The origin of the central subzone of the gabbronorite zone by the directed crystallization of melt from the walls to centers of some chambers suggests that the melt had fully disappeared from the vicinity of the intrusion roof. However, it remains unclear as to what melt had produced the upper subzone, which includes the ULU and its gabbronorite succession. In our opinion, a realistic settling of this contradiction can be achieved by admitting that the upper subzone is an individual intrusive phase. It should have been produced by a large fresh magma batch, which was intruded along the contact zone between the rocks of the first intrusive phase and the volcanic-sedimentary rocks of the Imandra-Varzuga zone. No geologic contact was detected as yet between the hypothetical intrusive phases, a fact suggesting that one was emplaced shortly after the other. During the intrusion of the phase-II melt, the phase-I rocks were likely still hot enough to be susceptible to recrystallization, which obscured the contacts between the phases.

The composition of the parental melts of both phases of the pluton corresponded, according to the systematics (Yoder and Tilley, 1962), to saturated tholeiite. This is implied by the predominantly gabbronitic composition of both intrusive phases and the arrangement of the rock data points along the *Opx-Cpx-Pl* join on the projection of the *Ol-Cpx-Pl-Qtz-H₂O* isopleth (Fig. 6a). Judging from the mineralogical composition of the earliest cumulates of the first intrusive phase (norite, *Pl-Opx* cumulates) and the second intrusive phase (gabbronorite, *Pl-Opx-Cpx* cumulates), the composition point of the parental melt for the first phase should lie on the *Opx + Pl + L* cotectic line, whereas the composition point of the second intrusive phase falls exactly on the E³ eutectic: *Opx + Cpx + Pl + L*. It is difficult to compare the compositions of the parental melts more precisely, because it is impossible to correctly evaluate the composition of the second-phase parental melt. The point is that the crystallization

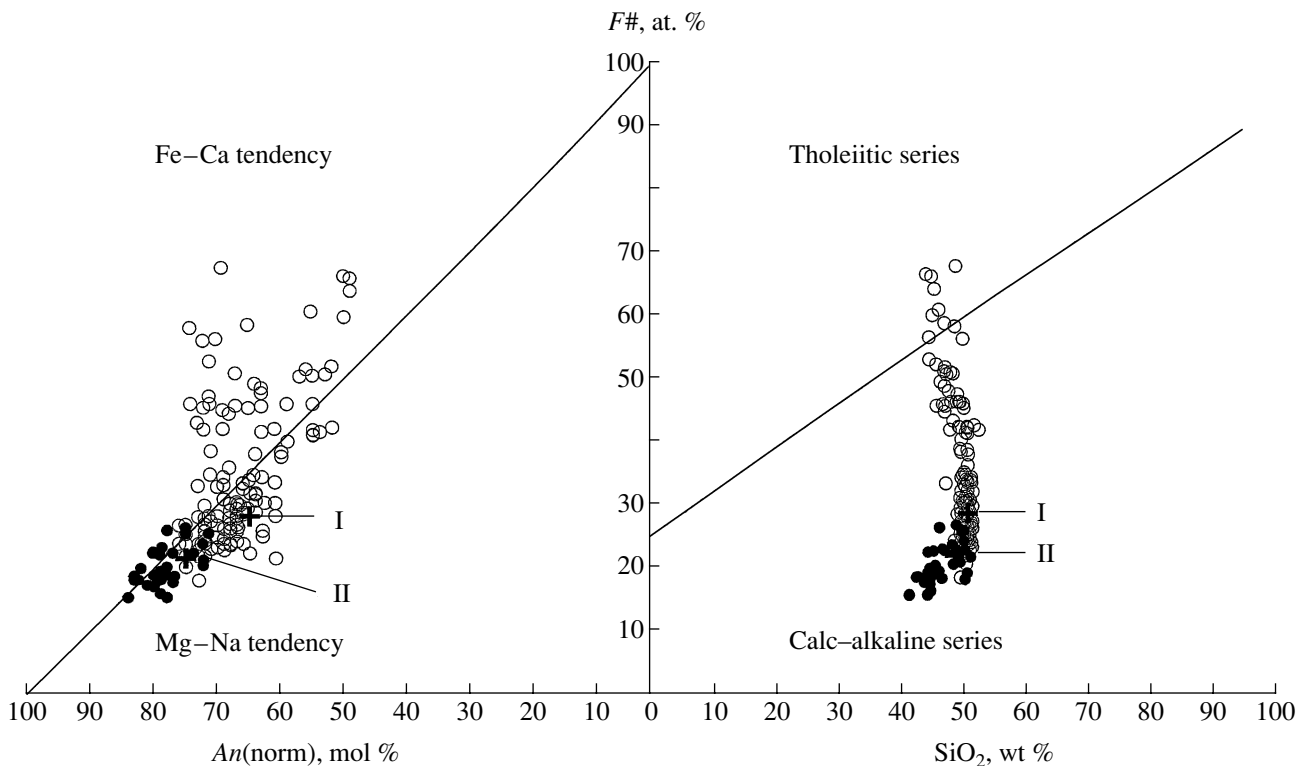


Fig. 7. Composition points of rocks from the intrusion in an $An(\text{norm})$ - $F\#$ - SiO_2 plot (after Dubrovskii, 1998).

Open circles show the rocks of the first intrusive phase; solid circles are the gabbro-norite of the second intrusive phase and the olivine-bearing rocks of the ULU. I and II are the parental melt compositions for the first and second intrusive phases, respectively. $An(\text{norm}) = 100 \times An/(An + Ab)$, $F\# = 100 \times (\text{Fe}^{2+} + \text{Fe}^{3+})/(\text{Fe}^{2+} + \text{Fe}^{3+} + \text{Mg})$.

The $F\#$ vs. SiO_2 diagram is a modification of the Osborn (1959) diagram, which also shows the boundary line between the tholeiitic and calc-alkaline series, after Miyashiro (1974).

of this phase proceeded in a not fully closed system, and, as will be demonstrated below, its composition was affected by multiple magma replenishments in the chamber, as follows, for example, from olivine-bearing layers in the ULU. Thus, the weighted mean composition of the second-phase rocks reflects, in fact, an integral mixing effect of significantly different melt compositions but not the composition of the parental melt. Taking this into account, it can be stated that the tholeiitic melt of the second phase contained more calcic normative plagioclase than that of the first-phase melt and was characterized by Fe-poorer mafic minerals ($an^L = 65\%$, $f^L = 23\%$ for phase I and $an^L = 75\%$, $f^L = 19\%$ for phase II, Table 7). These differences are clearly pronounced in $An(\text{norm})$ vs. $F\#$ petrochemical plots (Fig. 7). The first-phase rocks compose an elongated trend directed at a small angle to the boundary line between the Fe-Ca and Mg-Na fields, whereas the second-phase rocks compose a more compact swarm on the boundary line and are characterized by the lowest $An(\text{norm})$ and $F\#$ values. It is worth noting the inconsistency in the determination of the parental melt type for the intrusive phases of the pluton with the use of the Tilley and Yoder (1962) and Miyashiro (1974) systematics. The two compositions are saturated tholeiite

(Fig. 6a) according to the former, or belong to the calc-alkaline series, according to the latter (Fig. 7, $F\#$ - SiO_2). This apparently demonstrates the ambiguity of such names as *tholeiite*, *tholeiitic*, or *calc-alkaline series*, as was previously noticed in several papers (Miyashiro, 1974; Borodin, 1987; Dubrovskii, 1998).

It is pertinent to mention that the attribution of the Western Pansky Tundra parental melt to the saturated basalt type (tholeiite), as was first done by Dokuchaeva (1994) and later supported by us, is not unanimously acknowledged. For instance, Dolin *et al.* (1994) argue that the composition of the Western Pansky Tundra parental melt was close to boninite-marianite. A similar conclusion was arrived at by Sharkov *et al.* (1997), who ascribed all Early Proterozoic layered intrusions in the northeastern Baltic Shield (Moncha Tundra, Fedorovo-Pansky, Mount General'skaya, and Burakovskii) to the crystallization products of a boninite-like (high in Si and Mg) magma. We do not share this opinion because of the following. When certain rocks are classed with boninite, it is often overlooked that boninite is always a quartz-normative rock, even in spite of the fact that it contains olivine phenocrysts (Ohnenstetter and Brown, 1996; Dubrovskii, 1998). Depending on a boninite subtype, the content of normative quartz may

vary from 3 to 15 wt % (Dubrovskii, 1998), averaging >9 wt %. At the same time, none of the weighted mean compositions of Early Proterozoic layered mafite-ultramafite intrusions of the Baltic Shield satisfy this condition, and all of them contain normative olivine. For example, the concentration of normative olivine is 18 wt % in the weighted mean composition of the Kivakka intrusion, 9 wt % in the Lukkulaisvaara Massif, 14 wt % in the Tsipringa Massif, 55 wt % in the Burakovskii Massif [recalculated data from (Bychkova and Koptev-Dvornikov, 1999)], and 10 wt % in the Monchegorsk Massif (Kozlov, 1973). The weighted mean compositions of the two intrusive phases of the Western Pansky Tundra intrusion are plotted close to the boundary line between olivine- and quartz-normative groups (Fig. 6a; phase I contains 0.81 wt % *Qtz*, and phase II contains 2.89 wt % *Ol*), away from boninite. These very significant differences between the compositions of typical boninite and the weighted mean composition of Early Proterozoic layered mafite-ultramafite massifs suggest that the parental melts of the latter (including the Western Pansky Tundra intrusion) cannot be classified with boninite or boninite-like rocks.

The Nature of the Two Critical Zones of the Massif: Its Lower and Upper Layered Units

Two distinctive features of the LLU and ULU provide a clue to the process responsible for their genesis. First, it is a change in the crystallization order of minerals, which is expressed as the disappearance of cumulus clinopyroxene (Latypov *et al.*, 1999a) in the LLU and the appearance of cumulus olivine in the ULU (Latypov *et al.*, 1999b). Second, these are the reversing trends in the chemistry of minerals toward the high-temperature end-members of the solid solutions (Fig. 3). Compared with the subjacent rocks, the Ca# of plagioclase increases: from 60–70 to 70–80% *An* in the LLU and from 65–70 to 75–80% *An* in the ULU. Simultaneously, the Fe# of the pyroxenes decreases: from *f*# = 25–30 to 23–26% in the LLU and from *f*# = 22–28 to 17–19% in the ULU. Moreover, the LLU rocks display a dramatic, three- to fourfold increase in the concentration of Cr (from 30–40 to 150–200 ppm; Fig. 5).

The changes in the crystallization trend and the chemistry of the crystallizing minerals suggest that the genesis of the critical zones was related to a notable change in the melt composition in the chamber. Most researchers currently admit that this phenomenon was caused by injections of melt (of the original or any other composition) into the chamber (Campbell *et al.*, 1983; Naldrett *et al.*, 1986a, 1986b; Sharkov, 1994). It follows that the development of the two critical zones (LLU and ULU) most probably marked the transient opening of the magma chamber and its replenishment with fresh melt.

Table 7. Weighted mean compositions of rocks of the first and second intrusive phases of the Western Pansky Tundra intrusion, which are assumed to approximate the composition of the parental melts

| Major oxide, wt % | I (283) | II (36) |
|--------------------------------|---------|---------|
| SiO ₂ | 52.00 | 49.80 |
| TiO ₂ | 0.23 | 0.10 |
| Al ₂ O ₃ | 15.09 | 19.40 |
| Fe ₂ O ₃ | 1.14 | 0.75 |
| FeO | 5.93 | 4.22 |
| MnO | 0.15 | 0.09 |
| MgO | 9.86 | 9.39 |
| CaO | 12.15 | 12.82 |
| Na ₂ O | 1.91 | 1.68 |
| K ₂ O | 0.27 | 0.13 |
| H ₂ O | 0.43 | 0.31 |
| LOI | 0.84 | 1.31 |
| Total | 100.00 | 100.00 |
| CIPW norm | | |
| <i>Ilm</i> | 0.44 | 0.19 |
| <i>Mgt</i> | 1.65 | 1.09 |
| <i>Or</i> | 1.60 | 0.77 |
| <i>ab</i> | 16.15 | 14.21 |
| <i>an</i> | 31.81 | 45.01 |
| <i>En</i> | 16.68 | 14.82 |
| <i>Fs</i> | 6.69 | 4.52 |
| <i>Di</i> | 16.97 | 11.73 |
| <i>Hd</i> | 5.93 | 3.12 |
| <i>Qtz</i> | 0.81 | |
| <i>Fo</i> | | 2.18 |
| <i>Fa</i> | | 0.73 |
| Petrochemical coefficients | | |
| <i>an</i> (norm) | 65.00 | 75.00 |
| <i>F</i> # | 28.36 | 21.70 |
| <i>Sum(Fsp)</i> | 51.28 | 61.78 |
| <i>K</i> (hy) | 50.50 | 56.57 |
| <i>f</i> # | 23.38 | 18.84 |

Note: Numbers in parentheses denote the number of analyzed samples used in the calculations; *An*(norm) = 100 × *An*/*An* + *Ab*, *F*# = 100 × (*Fe*²⁺ + *Fe*³⁺)/(*Fe*²⁺ + *Fe*³⁺ + Mg), *Sum(Fsp)* = *Or* + *Ab* + *An*, *K*(hy) = 100 × *Opx*/*Opx* + *Cpx*, *f*# = 100 × *Fs*/*(Fs* + *En*).

Observations lead us to conclude that the fresh melt batches were compositionally close to the parental melt of the intrusion. First, the composition of plagioclase and pyroxenes from LLU rocks is close to the composition of these minerals in the very first crystallization products of the parental melts, the bottom norite zone of the pluton (Odinets, 1971). Second, no significant

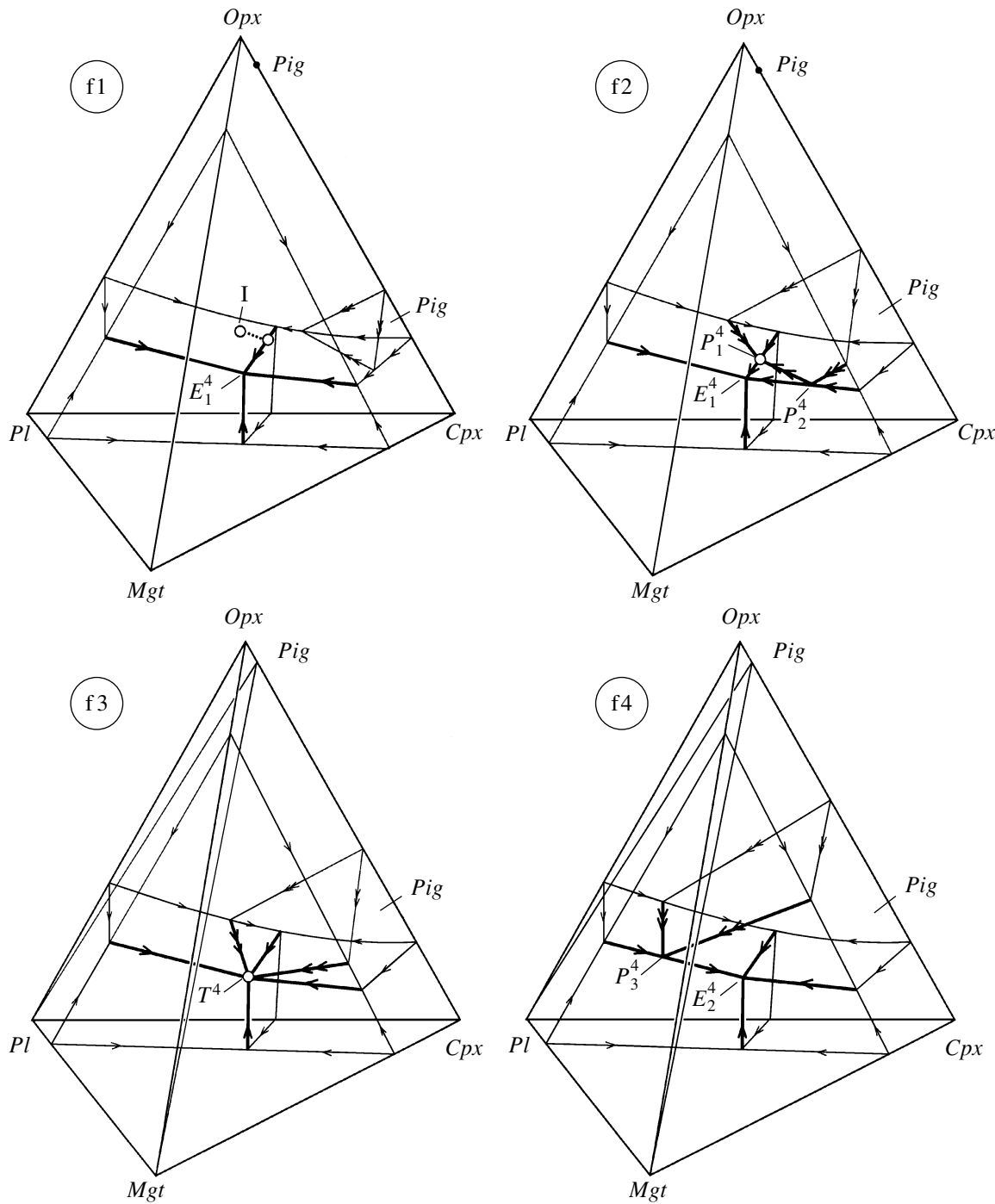


Fig. 8. Hypothetical crystallization trend for the parental melt of the first intrusive phase (point I) in schematic phase diagrams with the isoplethic sections $Opx-Cpx-Pl-Mgt$ (+H₂O) at $P_{H_2O} < 1000$ bar (Latypov and Chistyakova, 2001a). Variations in phase equilibria with increasing Fe# of the melt in the direction from f1 to f4 isoplethic sections involves gradual expansion of the pigeonite crystallization volume. Heavy liquidus lines are located inside the tetrahedron, light lines are in its faces. Single and doubled arrowheads denote, respectively, cotectic and peritectic lines. Arrows are directed toward lower temperatures. E_1^4 : $Opx + Cpx + Pl + Mgt = L$, E_2^4 : $Pig + Cpx + Pl + Mgt = L$, P_1^4 : $Opx + Cpx + Pl = L + Pig$, P_2^4 : $Opx + Cpx = L + Pig + Mgt$, P_3^4 : $Pig + Pl + Mgt = L + Opx$, T^4 : $Opx + Cpx + Pig + Pl + L$. The crystallization succession of phases during the crystallization of the parental melt of the first intrusive phase (point I) corresponds to the scheme $Pl + Opx \longrightarrow Pl + Opx + Cpx \longrightarrow Pl + Opx + Cpx + Pig \longrightarrow Pl + Opx + Cpx + Pig + Mgt$.

deviations can be observed in the crystallization trend of the parental melt (for example, the appearance of such high-temperature minerals as olivine or chromite). Second, the initial $^{87}\text{Sr}/^{86}\text{Sr}$ ratios of LLU rocks vary from 0.7024 to 0.7031 and are close to those in the underlying and overlying gabbro-norites (Latypov *et al.*, 2000).

In contrast to the LLU, the ULU was produced by magma batches whose composition was significantly different from that of the parental melt of the second intrusive phase. This is evident, first of all, from the appearance of rocks with cumulus olivine, which could crystallize from the second-phase tholeiite melt during its equilibrium differentiation. The differences between the rocks of the second phase and ULU are clearly pronounced in projection planes of the $\text{Ol}-\text{Cpx}-\text{Pl}-\text{Qtz}-\text{H}_2\text{O}$ isopleth (Fig. 6). The compositional field of the second-phase rocks extends along the $\text{Ol}-\text{Cpx}-\text{Opx}-\text{Pl}$ boundary plane (Fig. 6a) not far from the "eutectic" E^3 of the $\text{Opx}-\text{Cpx}-\text{Pl}$ isopleth, whereas the points of the ULU rocks are plotted closer to the $\text{Opx}-\text{Pl}$ tie line (Fig. 6b). In accordance with the systematics of Yoder and Tilley (1962), this arrangement of the composition points led us to determine the composition of the fresh magma batches as olivine tholeiite, whereas the parental melt of the second phase was saturated tholeiite. Judging from the position of the compositional field of the ULU rocks in sections of a $\text{Ol}-\text{Pl}-\text{Cpx}-\text{Qtz}-\text{H}_2\text{O}$ diagram (Fig. 6) and from the mineralogical composition of these rocks, the olivine tholeiite melt either was situated immediately on the cotectic surface $\text{Pl} + \text{Ol} + \text{L}$ or was shifted to it shortly after the fractionation onset within the volume of primary plagioclase crystallization. At the same time, the second-phase saturated tholeiite melt was originally situated immediately at the E^3 eutectic $\text{Opx} + \text{Cpx} + \text{Pl} + \text{L}$.

The genesis of the complex cyclic layering observed in both critical zones was discussed in detail elsewhere (Latypov *et al.*, 1999a, 1999b). The leading role in the origin of the contrasting anorthosite–norite–pyroxenite layering of the LLU is ascribed to the discontinuous character of volumetric crystallization that ensured the gravitational separation of plagioclase and pyroxenes during their sinking to the chamber floor. The diverse layering types of the ULU are related to the simultaneous action of a wide spectrum of processes, with the decisive role of continuous or discontinuous volumetric crystallization and directed crystallization with or without the enrichment in low-melting eutectic components at the front.

Crystallization Trends of the Parental Melts of the Intrusive Phases

As is seen from Table 1, the crystallization trends of the Western Pansky Tundra intrusion are notably different from one another and, in fact, reflect the models proposed for the solidification sequence of the pluton. For example, the recognition of the $\text{Pl} \rightarrow \text{Pl} + \text{Ol}$

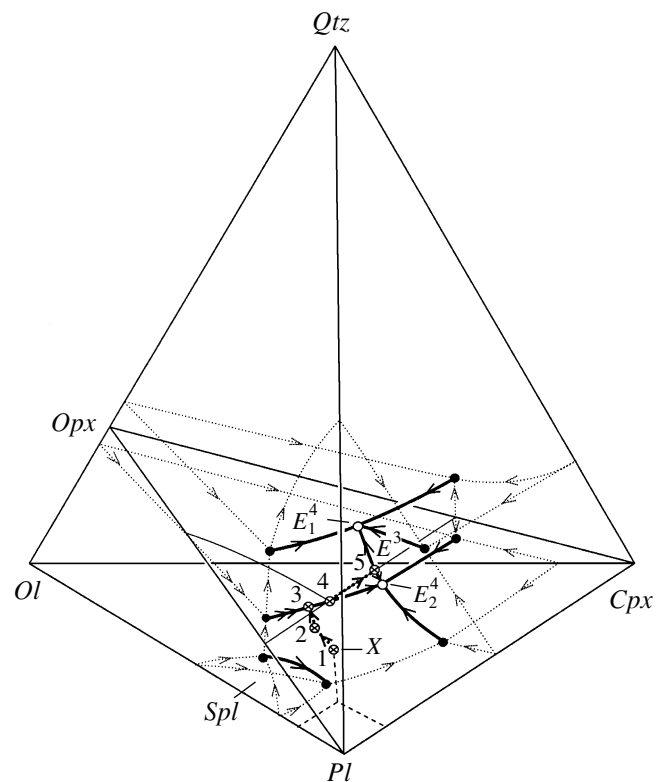


Fig. 9. Hypothetical crystallization trend for one of the hybrid melts X , which was produced by the mixing of the in-chamber tholeiite melt of the second phase with fresh batches of olivine tholeiite magma. The trend passes along the $\text{Ol}^{25-50}-\text{Cpx}-\text{Pl}^{60-70}-\text{Qtz} (+\text{H}_2\text{O})$ isopleth at $P_{\text{H}_2\text{O}} < 1000$ bar (Latypov and Chistyakova, 1999b). Heavy liquidus lines are within the tetrahedron, and dashed lines are in its faces. Single and doubled arrowheads denote, respectively, cotectic and peritectic lines. Thin lines indicate the intersection trace of the surfaces $\text{Ol} + \text{Opx} + \text{L}$, $\text{Ol} + \text{Pl} + \text{L}$, $\text{Opx} + \text{Pl} + \text{L}$, and $\text{Opx} + \text{Cpx} + \text{L}$ and the plane $\text{Opx}-\text{Cpx}-\text{Pl}$. $E_1^4: \text{Opx} + \text{Cpx} + \text{Pl} + \text{Qtz} = \text{L}$, $E_2^4: \text{Ol} + \text{Opx} + \text{Cpx} + \text{Pl} = \text{L}$, $E_3: \text{Opx} + \text{Cpx} + \text{Pl} = \text{L}$. Arrows are directed toward lower temperatures. The crystallization succession of phases from melt X was as follows: $\text{Pl} (\pm \text{Ol})$ (1–2) \rightarrow $\text{Pl} + \text{Ol}$ (2–3) \rightarrow $\text{Pl} + \text{Ol} + \text{Opx}$ (3–4) \rightarrow $\text{Pl} + \text{Opx}$ (4–5) \rightarrow $\text{Pl} + \text{Opx} + \text{Cpx}$ (5).

crystallization stages means that it is assumed that the ULU rocks were the first to crystallize in the massif (Proskuryakov, 1967; Kozlov, 1973). The absence of *Pig* and *Mgt* among the phases crystallizing during the final stage means that the researchers consider the magnetite gabbro to be a foreign rock (Dokuchaev, 1994; Borisova *et al.*, 1999). The most complicated crystallization trend was presented by Dokuchaeva (1994). We believe that it reproduces the crystallization trend of some hypothetical melt rather than the observed succession of mineral assemblages in the intrusion. In any event, we are not aware of any reliable indications that the Western Pansky Tundra intrusion started to crystallize with dunite ($\text{Ol} + \text{Spl}$) and harzburgite ($\text{Ol} + \text{Opx}$)

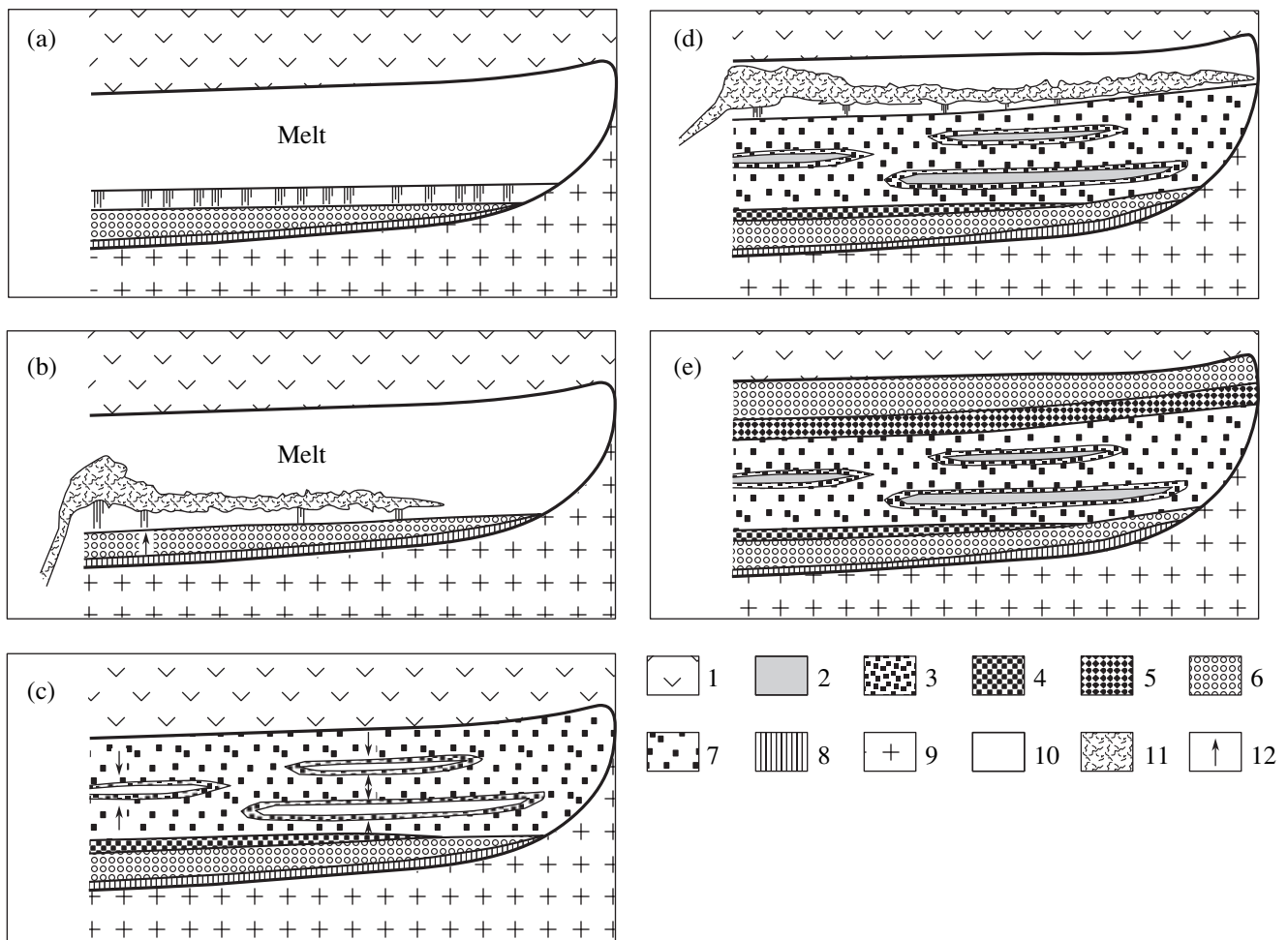


Fig. 10. Hypothetical solidification succession of the Western Pansky Tundra intrusion.

(1) Lower Proterozoic volcano-sedimentary rocks of the Strelna Formation in the Imandra–Varzuga zone; (2–8) rocks of the intrusion: (2) magnetite gabbro with inverted pigeonite ($Pl-Cpx-Opx-Pig\#-Mgt$ cumulates), (3) gabbronorite with inverted pigeonite ($Pl-Cpx-Opx-Pig\#$ cumulates), (4) Lower Layered Unit (LLU), (5) Upper Layered Unit (ULU), (6) trachytoid gabbronorite, (7) massive gabbronorite ($Pl-Cpx-Opx$ cumulates), (8) norite ($Pl-Opx$ cumulates); (9) Archean granitoids of the Keivy block; (10) melt; (11) injections of fresh magma batches; (12) direction of the solidification front advance. Vertical lines show the settling of crystals in the crystallization zone.

or the massif contains rocks with magmatic amphibole and quartz ($Opx + Cpx + Pl + Am + Qtz$).

According to our concept of the intrusion solidification succession, a clear distinction should be drawn between the crystallization trends for the first and second intrusive phases. The inferred crystallization trend of the first-phase parental melt can be conveniently illustrated in the $Opx-Cpx-Pl-Mgt$ isoplethic section, which were constructed geometrically based on the $Opx-Cpx-Pl$ boundary isopleth by adding the Mgt component (Latypov and Chistyakova, 2001a). The isoplethic sections in Fig. 8 demonstrate the changes in the diagram topology with an increase in the Fe# of the melt: mainly a gradual increase in the crystallization volume of pigeonite at the sacrifice of that of orthopyroxene.

The first-phase parental melt seems to have started to crystallize at the $Pl + Opx + L$ cotectic surface (Fig. 8, point I) with the development of the norite-zone rocks ($Pl-Opx$ cumulates). After a brief period of its differentiation, the melt occurred at the $Opx + Cpx + Pl + L$ cotectic line (Fig. 8, f1). The crystallization products of this stage were $Pl-Cpx-Opx$ cumulates, i.e., gabbronorite with gabbroic or gabbro-ophitic textures in the lower and central subzones of the gabbronorite zone (Figs. 1, 2). Fractional crystallization was coupled with a prograde increase in the Fe# of the residual melt. The pigeonite crystallization volume in the plot expanded at the cost of the orthopyroxene volume. Because of this, the melt eventually attained the point P_1^4 (Fig. 8, f2), and this resulted in the crystallization of $Pl-Cpx-Opx-Pig\#$ cumulates (gabbronorite with inverted pigeonite), which are characterized by

relatively rare assemblage of three coexisting pyroxenes. Finally, the crystallization of magnetite gabbro, i.e., $Pl-Cpx-Opx-Pig\#-Mgt$ cumulates, corresponded to the moment when the Fe# further increased and the composition point of the melt arrived at the T^4 invariant point, $Opx + Cpx + Pig + Pl + Mgt + L$, at which the settling phases were joined by magnetite (Fig. 8, f3). The further evolution of the melt should theoretically lead to the consumption of orthopyroxene and its replacement by pigeonite (Fig. 8, f4). However, this was not observed in our rocks, and, hence, the melt ended its crystallization at the aforementioned invariant point.

The crystallization trend of the parental melt of the second phase (which comprises the upper subzone of the gabbronorite zone, Fig. 2) is relatively simple. It involves a single, gabbronorite, crystallization stage ($Pl + Opx + Cpx$). However, the differentiation was significantly complicated at the level of the olivine-bearing subunits of the ULU because of the injection of fresh batches of olivine tholeiite into the chamber. The olivine-bearing subunits of the ULU commonly show the following crystallization succession of minerals: $Pl(\pm Ol)$ (olivine leucogabbro) $\rightarrow Pl + Ol$ (troctolite) $\rightarrow Pl + Ol + Opx$ (olivine norite) $\rightarrow Pl + Opx$ (norite) $\rightarrow Pl + Opx + Cpx$ (gabbronorite). This crystallization trend corresponds to one of the theoretically possible crystallization successions in the diagram $Ol^{25-50}-Cpx-Pl^{60-70}-Qtz$ (see also Latypov *et al.*, 1999b). However, it should be mentioned that these disturbances were not long-lasting, because the thicknesses of the olivine-bearing subunits usually do not exceed 15–30 m. The melt rapidly returned to the gabbronorite cotectic ($Pl + Opx + Cpx + L$). In this connection, we believe that these temporary disturbances in the crystallization trend cannot be identified with the crystallization trend of the whole intrusion (Proskuryakov, 1967).

The Overall Solidification Succession of the Intrusion

The following successive stages of the Western Pansky Tundra intrusion solidification were inferred from the aforementioned data and considerations (Fig. 10):

Stage A. The magmatic chamber is filled with tholeiitic melt, which gives rise to the norite zone and the lower subzone of the gabbronorite zone. The front of the magmatic succession build-up generally advances from the bottom to top.

Stage B. Development of LLU in response to the temporary opening of the magma chamber and its replenishment with small amounts of fresh melt, whose composition is close to that of the parental melt.

Stage C. Division of the chamber into a series of smaller reservoirs (subchambers). The directed crystallization of the residual melt from the walls to centers of the subchambers and the crystallization of magnetite gabbro. The origin of the central subzone of the first-phase gabbro zone.

Stage D. Second-phase tholeiitic melt arrives, and the rocks of the upper subzone of the gabbronorite zone are formed. ULU is produced as a consequence of temporary complications in the in-chamber crystallization trend because of olivine tholeiite melt replenishment in the chamber.

Stage E. The Western Pansky Tundra intrusion is formed in its final form and with its modern inner geologic structure.

CONCLUSION

The Western Pansky Tundra intrusion is an individual, geologically independent layered Early Proterozoic pluton, whose cryptic and modal layering have no analogues among other layered intrusions worldwide. The pluton is composed of two intrusive phases: the first phase comprises the lower part of the massif, from its bottom to the ULU, and the second phase includes the ULU and the overlying rocks. The composition of the parental melt of the first intrusive phase corresponded to saturated tholeiite, its crystallization was predominantly volumetric and was accompanied by the gravitational settling of solid phases to the chamber bottom. The overall build-up direction of the magmatic sequence of this phase was from bottom to top. This mechanism and the direction of the crystallization front advance did not change to approximately the LLU level. Its origin was caused by the introduction of insignificant melt amounts into the chamber, with the composition of this melt roughly corresponding to the composition of the parental melt. Later, the continuous increase in the viscosity of the system because of the settling of the crystallizing phases resulted in the division of the chamber into a series of smaller reservoirs (subchambers) with isolated portions of residual melt. The formation of the first phase of the pluton ended with the directed crystallization of the residual melt in subchambers from their walls to centers and the crystallization of magnetite gabbro. The origin of the second phase was triggered by the addition of a new batch of tholeiitic melt, which had a less evolved composition than the first-phase melt. The crystallization of this melt was complicated by the recurrent introduction of small batches of olivine tholeiite melt into the chamber. This melt produced the ULU.

It should be mentioned that the key points of this scenario proposed for the origin of the intrusion were expressed, in various forms, in earlier papers by other researchers. In particular, the idea that the Western Pansky Tundra intrusion is an independent geologic body was first set up by Odinets (1971) and Kozlov (1973). The concept of the polyphase structure of the intrusion was also advanced by Kozlov (1973). The mechanism of chamber division into a series of smaller reservoirs, which ended their crystallization with magnetite gabbro, was first considered by Proskuryakov (1967). Hence, this paper may be regarded as a natural contin-

uation of these researches at new petrochemical and physicochemical levels.

ACKNOWLEDGMENTS

The authors thank M.I. Dubrovskii (Geological Institute, Kola Research Center, Russian Academy of Sciences) for constructive criticism of and vivid interest in our research. The manuscript was improved after its reviewing by E.V. Sharkov (Institute of the Geology of Ore Deposits, Petrography, Mineralogy, and Geochemistry, Russian Academy of Sciences) and E.V. Koptev-Dvornikov (Moscow State University), who are also thanked by the authors. This study was partially financially supported by grants from the Thule Institute, University of Oulu, Finland, and the Center of International Mobility (CIMO), Helsinki, to R.M. Latypov.

REFERENCES

- Abzalov, M.Z., Veselovskii, N.N., Korchagin, A.U., *et al.*, Silver Minerals from the Intrusive Layered Complex of the Fedorovo–Pansky Tundras, *Dokl. Ross. Akad. Nauk*, 1993, vol. 329, no. 4, pp. 497–499.
- Alapieti, T.T. and Lahtinen, J.J., Proterozoic Layered Intrusions in the Northeastern Part of the Fennoscandian Shield, *5th Int. Platinum Symp. Guide to the Postsymposium Field Trip*, Alapieti, T.T., Ed., *Geol. Surv. Finland Guide*, 1989, vol. 29, pp. 3–41.
- Amelin, Yu.V., Heaman, L.M., and Semenov, V.S., U–Pb Geochronology of Layered Mafic Intrusions in the Eastern Baltic Shield: Implications for the Timing and Duration of Paleoproterozoic Continental Rifting, *Precambrian Res.*, 1995, vol. 75, pp. 31–46.
- Balabonin, N.N., Korchagin, A.U., Latypov, R.M., and Subbotin, V.V., Fedorovo–Pansky Intrusion, in *The Kola Belt of Layered Intrusions: Guide to Pre-Symposium Field Trip*, 7th Int. Platinum Symp., Mitrofanov, F. and Torokhov, M., Eds., Apatity, 1994, pp. 9–41.
- Balashov, Y.A., Bayanova, T.B., and Mitrofanov, F.P., Isotope Data on the Age and Genesis of Layered Basic–Ultrabasic Intrusions in the Korea Peninsula and Northern Karelia, Northeastern Baltic Shield, *Precambrian Res.*, 1993, vol. 64, pp. 197–205.
- Batieva, I.D., *Petrologiya shchelochnykh granitov Kol'skogo poluostrova* (The Petrology of Alkaline Granites of the Kola Peninsula), Leningrad: Nauka, 1976.
- Bayanova, T.B., Levkovich, N.V., and Ivanova, L.V., Zircon–Baddeleyite Geochronological System in the Precambrian Rocks of the Kola Region, 9 molodezhnaya nauchn. konf. “Geologiya Baltiiskogo shchita i drugikh dokembriiskikh oblastei Rossii” (Geology of the Baltic Shield and Other Precambrian Areas of Russia, Proc. 9th Youth Sci. Conf.), Apatity, 1995, pp. 25–33.
- Bayanova, T.B., Mitrofanov, F.P., Korchagin, A.U., and Pavlichenko, L.V., The Age of Gabbronorites from the Lower Layered Horizon (Reef) of the Fedorovo–Pansky Massif (Kola Peninsula), *Dokl. Ross. Akad. Nauk*, 1994, vol. 337, no. 1, pp. 95–97.
- Borisova, V.V., Dubrovskii, M.I., Karpov, S.M., *et al.*, The Petrology of the Pansky Layered Massif (Kola Peninsula) from the Position of Paragenetic Analysis, *Zap. Vseross. Miner. O-va*, 1999, no. 3, pp. 31–48.
- Borodin, L.S., *Petrokhimiya magmicheskikh serii* (Petrochemistry of Igneous Series), Moscow: Nauka, 1987.
- Bychkova, Ya.V. and Koptev-Dvornikov, E.V., Types of Parental Magmas of the Fennoscandian Mafic–Ultramafic Layered Intrusions as a Classification Guide, *Materialy mezdunar. konf. “Riftogenet. magmatizm, metallogeniya dokembriya. Korrelyatsiya geologicheskikh kompleksov Fennoskandii”* (Proc. Int. Conf. on Riftogenesis, Magmatism, and Metallogeny of the Precambrian, and Correlation of Fennoscandian Geologic Complexes), Petrozavodsk, 1999, pp. 20–21.
- Campbell, I.H., Naldrett, A.J., and Barnes, S.J., A Model for the Origin of Platinum-Rich Sulfide Horizons in the Bushveld and Stillwater Complexes, *J. Petrol.*, 1983, vol. 24, pp. 133–165.
- Dodin, D.A., Chernyshov, N.M., Polferov, D.V., and Tarnovetskii, L.L., *Platinometal'nye mestorozhdeniya mira. Tom 1. Platinometal'nye malosul'fidnye mestorozhdeniya v ritmichno-rassloennykh kompleksakh* (Platinum-Metal Deposits of the World), Moscow: Geoinformmark, 1994, vol. 1.
- Dokuchaeva, V.S., Petrology and Conditions of Ore Mineralization in the Fedorovo–Pansky Intrusion, in *Geologiya i genezis mestorozhdenii platinovykh metallov* (Geology and Genesis of Platinum-Metal Deposits), Moscow: Nauka, 1994, pp. 87–100.
- Dubrovskii, M.I., *Trendy differentsiatii olivinnormativnykh bazitovykh i ul'trabazitovykh magm normal'noi shchelochnosti i sootvetstvuyushchie im porodnye serii* (Differentiation Trends of Olivine-Normative Mafic and Ultramafic Magmas of Normal Alkalinity and Corresponding Rock Series), Apatity: Ross. Akad. Nauk, Kol'skii Nauchn. Tsentr, 1998.
- Fedotov, Zh.A., *Evolyutsiya proterozoiskogo vulkanizma vostochnoi chasti Pechengsko-Varzugskogo poyas* (petrogeokhimicheskii aspekt) (Evolution of Proterozoic Volcanism in the Eastern Part of the Pechenga–Varzuga Belt: A Petrochemical Aspect), Apatity: Akad. Nauk SSSR, Kol'skii Filial, 1985.
- Halkoaho, T., Abzalov, M., and Papunen, H., Platinum Group Minerals in the Lower Layered Unit of the Pana Tundra Layered Intrusion of the Kola Peninsula, *International Platinum*, Laverov, N. and Distler, V., Eds., St. Petersburg and Athens: Theophrastus, 1998, pp. 54–61.
- Korchagin, A.U., Bakushkin, E.M., Vinogradov, L.A., *et al.*, Geologic Structure of the Lower Margin Zone of the Pansky Tundra Massif and Its Platinum-Metal Mineralization, in *Geologiya i genezis mestorozhdenii platinovykh metallov* (Geology and Genesis of Platinum Metal Deposits), Moscow: Nauka, 1994, pp. 100–106.
- Kozlov, E.K., *Estestvennye ryady porod nikelenosnykh intruzii i ikh metallogeniya* (Natural Series of Rocks in Nickel-bearing Intrusions and Their Metallogeny), Lenin-grad: Nauka, 1973.
- Krivenko, A.P., Lavrent'ev, Yu.G., Maiorova, O.N., and Tolstykh, N.D., Platinum and Palladium Tellurides in the Pansky Gabbro–Norite Massif, Kola Peninsula, *Dokl. Akad. Nauk SSSR*, 1989, vol. 308, no. 4, pp. 950–954.

- Latypov, R.M., On the Origin of Anorthosites in the Layered Intrusion of the Pansky Tundra, Kola Peninsula: Geological Data, *Geol. Geofiz.*, 1995, vol. 36, no. 3, pp. 55–63.
- Latypov, R.M., The Nature of Rhythmic Layering in the Intrusion of the Western Pansky Tundra, Kola Peninsula, *Dokl. Ross. Akad. Nauk*, 1994, vol. 336, no. 5, pp. 643–647.
- Latypov, R.M. and Chistyakova, S.Yu., Physicochemical Aspects of the Genesis of Magnetite Gabbros with Inverted Pigeonite in the Layered Intrusion of the Western Pansky Tundra, Kola Peninsula, *Petrologiya*, 2001a, no. 1, pp. 1–23.
- Latypov, R.M. and Chistyakova, S.Yu., The Origin of Magnetite Gabbro Bodies in the Layered Intrusion of the Western Pansky Tundra, Kola Peninsula: A Petrogeochemical Analysis, *Geol. Geofiz.*, 2001b (in press).
- Latypov, R.M., Bayanova, T.B., Delenitsyn, A.A., and Sherstobitova, G.M., Isotopic Constraints on the Origin of the Lower Layered Horizon in the Intrusion of the Western Pansky Tundra, Baltic Shield, *Vtoroe Vserossiiskoe soveshchanie: Petrografiya na rubezhe XXI veka (itogi i perspektivy)* (Proc. 2nd All-Russia Conf. Petrography at the Border of the XXI Century: Results and Prospects), Syktyvkar, 2000, vol. 4, pp. 278–279.
- Latypov, R.M., Mitrofanov, F.P., Alapieti, T.T., and Halkoaho, T.A., Petrology of the Lower Layered Horizon of the Western Pansky Tundra Intrusion, Kola Peninsula, *Petrologiya*, 1999a, vol. 7, no. 5, pp. 509–538.
- Latypov, R.M., Mitrofanov, F.P., Alapieti, T.T., and Kaukonen, R.J., Petrology of the Upper Layered Horizon of the Western Pansky Tundra Intrusion, Kola Peninsula, Russia, *Geol. Geofiz.*, 1999b, vol. 40, no. 10, pp. 1434–1456.
- Mitrofanov, F.P., Yakovlev, Yu.N., Distler, V.V., et al., The Kola Region: A New Platinum Metal Province, in *Geologiya i genezis mestorozhdenii platinovykh metallov* (Geology and Genesis of Platinum Metal Deposits), Moscow: Nauka, 1994, pp. 65–79.
- Miyashiro, A., Volcanic Rock Series in Island Area and Active Continental Margins, *Am. J. Sci.*, 1974, vol. 274, pp. 321–355.
- Naldrett, A.J., Gasparini, E.C., Barnes, S.J., et al., The Upper Critical Zone of the Bushveld Complex and the Origin of Merensky-Type Ores, *Econ. Geol.*, 1986a, vol. 8, pp. 1105–1117.
- Naldrett, A.J., Cameron, G., von Gruenewaldt, G., and Sharpe, M.R., The Formation of Stratiform PGE Deposits in Layered Intrusions, in *Origins of Igneous Layering*, Parsons, I., Ed., Boston: Reidel, 1986b, pp. 313–398.
- Odinets, A.Yu., The Petrology of the Pansky Massif of Mafic Rocks, Kola Peninsula, *Cand. Sci. (Geol.–Min.) Dissertation*, Leningrad, 1971.
- Ohnenstetter, D. and Brown, W.L., Boninites: A Review, in *Petrology and Geochemistry of Magmatic Suites of Rocks in the Continental and Oceanic Crusts. A Volume Dedicated to Prof. Jean Michot*, Demaiffe, D., Ed., Bruxelles: Univ. Libre de Bruxelles, 1996, pp. 307–320.
- Orsoev, D.A., Konnikov, E.G., Glotov, A.I., and Kislov, E.V., The Lower Layered Horizon of the Fedorovo–Pansky Gabbroid Massif, Kola Peninsula: Structure, Composition, Distribution of Fluid Phase, *Geol. Geofiz.*, 1997, vol. 38, no. 11, pp. 1782–1791.
- Osborn, E.F., Role of Oxygen Pressure in the Crystallization and Differentiation of Basaltic Magma, *Am. J. Sci.*, 1959, vol. 257, pp. 609–647.
- Proskuryakov, V.V., Geologic Structure and Differentiation Peculiarities of the Mafic Intrusion in the Pansky Vysoty, Kola Peninsula, in *Osnovnye i ul'traosnovnye porody Kol'skogo poluostrova* (Mafic and Ultramafic Rocks of the Kola Peninsula), Leningrad: Nauka, 1967, pp. 40–54.
- Sharkov, E.V., Origin of Critical Zones in Large Layered Intrusions, in *Geologiya i genezis mestorozhdenii platinovykh metallov* (Geology and Genesis of Platinum Metal Deposits), Moscow: Nauka, 1994, pp. 35–48.
- Sharkov, E.V., Smol'kin, V.F., and Krasivskaya, I.S., The Early Proterozoic Magmatic Province of High-Magnesium Boninite-like Rocks in the Eastern Part of the Baltic Shield, *Petrologiya*, 1997, vol. 5, no. 5, pp. 503–522.
- Turchenko, A., Bogomolov, E., and Turchenko, S., Petrologic and Isotope–Geochemical Features of the PGE-bearing Horizons in the Pansky Tundra Layered Intrusion (2.5 Ga), Fennoscandian Shield, Russia, *International Platinum*, Laverov, N. and Distler, V., Eds., St. Petersburg and Athens: Theophrastus, 1998, pp. 71–78.
- Wager, L.R. and Brown, G.M., *Layered Igneous Rocks*, San Francisco: Freeman, 1967. Translated under the title *Rassloennye izverzhennye gornye porody*, Moscow: Mir, 1970.
- Yoder, H.S. and Tilley, C.E., Origin of Basalt Magmas: An Experimental Study of Natural and Synthetic Rock Systems, *J. Petrol.*, 1962, vol. 3, pp. 342–532.
- Zhangurov, A.A., Sholokhnev, V.V., Fedotov, Zh.A., et al., Imandra Layered Intrusion, in *Kola Belt of Layered Intrusions. Guide to Presymposium Field Trip. 7th Int. Platinum Symp.*, Mitrofanov, F., Torokhov, M., Eds., Apatity, 1994, pp. 42–70.